The liver is a dynamic organ shaped by reproduction with implications for young women's breast cancer

Alexandra Q. Bartlett

A THESIS/DISSERTATION

Presented to the Cancer Biology Program
& the Oregon Health & Science University
School of Medicine
in partial fulfillment of
the requirements for the degree of

Doctor of Philosophy

May 2021

School of Medicine

Oregon Health & Science University

CERTIFICATE OF APPROVAL

This is to certify that the PhD dissertation of

Alexandra Quackenbush Bartlett

has been approved

_____
Pepper J. Schedin, PhD, Mentor/Advisor

_____
Philip Streeter, PhD, Oral Exam Committee Chair

_____
Pamela Cassidy, PhD, Member

_____
Daniel Marks, MD, PhD, Member

_____
Skye Mayo, MD, MPH, FACS, Member

_____
Mara Sherman, PhD, Member

_____
Jim Korkola, PhD, Member

Table of Contents

List of Figures

List of Tables

List of Abbreviations

ADPH	Adipophilin
APC	Antigen presenting cell
AQP1	Aquaporin 1
BCLM	Breast cancer liver metastasis
COLIV	Collagen four
COX	Cyclooxygenase
ECM	Extracellualr matrix
EGP	Endogenous glucose production
EMT	Epithelial to mesenchymal transition
ER	Estrogen receptor
FFPE	Formalin fixed paraffin embedded
FN	Fibronectin
GFP	Green fluorescent protein
H&E	Hematoxylin and eosin
HETE	Hydroxyicosatetraenoic acid
IBU	Ibuprofen
ICI	Immune checkpoint inhibitor
IHC	Immunohistochemistry
InvD2	Involution day 2
IRB	Institutional review board
mIHC	Multiplex immunohistochemistry
NK	Natural killer
Nullip	Nulliparous
OHSU	Oregon Health & Science University
PGE2	Prostaglandin E_2
PGF2a	Prostaglandin F_2-
PPBC	Postpartum breast cancer
PR	Progesterone receptor
R	Regressed
Rd	Glucose disposal rate
RT	Room temperature
TBX2	Thromboxane B_2
TGM2	Tissue transglutaminase 2
Th1	T helper 1
Th2	T helper 2
Th17	T helper 17
TNC	Tenascin-c
TNFα	Tumor necrosis factor alpha
Treg	T regulatory
YWBC	Young women’s breast cancer

Acknowledgements

I'd like to thank my mentor Dr. Pepper Schedin for *everything*. Through example and dedicated teaching, Pepper has shown me how to be a scientist. Her commitment to my personal and professional growth was always apparent, for which I feel immense privilege. Maybe best of all - through the past 5 and a half years - our relationship has blossomed: it is collaborative, fun, and trusting. I am grateful for Pepper, and for the opportunity to bring her spirit of mentorship into my future scientific endeavors.

A key tenet in the Schedin laboratory is the power of *team-science,* where we work together to advance our goals and support one another. As such, I am thankful for all Schedin lab members, past and present, with whom I have worked. We were a great team. I owe special thanks to three senior graduate students (Erica Goddard, Courtney Betts, and Qiuchen Guo) who mentored me when I was a very "green" student. They led by example, serving as fantastic role models. Addition thanks go out to two postdoctoral fellows, Nathan Pennock and Edie Mitchell, for all their teaching and advice.

On a personal note, I must thank my parents and my husband for being my anchors in the world. My parents have provided tangible support in the form of dinners, baked goods, and puppy sitting, as well as invaluable intangible support. My husband has been the best partner I could dream of, and is always "in my corner". He reminds me there is more to life than science. Finally, thank you to my "pandemic puppy", Bella, who shows me the power of play.

Abstract

Women diagnosed with breast cancer within 10 years of a completed pregnancy are 2~3x more likely to develop liver metastases than never-pregnant (nulliparous) patients, even after controlling for prognostic variables. This finding suggests a unique biology in the postpartum liver, a putative pre-metastatic niche, which makes postpartum patients more susceptible to liver metastases. In rodents, we identified a postpartum liver biology that supports liver metastasis in mouse models. This biology is weaning-induced liver involution and is characterized by a transient period of hepatocyte death, catabolic metabolism, immune influx, and stromal remodeling.

Here, we investigated the mechanism of metastatic promotion in the involuting liver. Compared to nulliparous mice, involution mice had increased incidence and multiplicity of liver metastasis; however, there was no group differences in tumor size or proliferation index. These data are consistent with the involution liver providing an environment that promotes tumor cell establishment, not proliferation. To further investigate, we assessed tumor cell abundance in the liver after intra-portal injection of mammary tumor cells over a 14 day time course. The metastatic advantage in the involution group emerged by 14 days, but not earlier. Next, we tested the hypothesis that the involution liver is immune suppressed, thereby permitting tumor escape from immune surveillance. To this end, we performed an *in vivo* T cell activation assay and found diminished T cell activation in the normal involution host liver. These data raise the possibility that impaired adaptive immunity could be responsible for increased liver metastasis in the involution group. In support, depletion of CD8+ cytotoxic immune cells in nulliparous hosts recapitulated the involution metastatic advantage. These findings suggest the normal postpartum

liver is immune suppressed, which can provide a pro-metastatic advantage to circulating breast cancer cells.

Next, to increase our understanding of breast cancer liver metastasis (BCLM) and the liver metastatic niche in women, we developed a new IRB-approved protocol to study tissues from women with BCLM. We utilized histological assessment and multiplex immunohistochemistry to characterize the basic features and extracellular matrix (ECM) composition of breast cancer liver metastases. Preliminary observations suggest that BCLMS are luminal-like, have abundant ECM proteins, and are enriched in young women with breast cancer. Data collection and analyses are ongoing.

Neither weaning induced liver involution nor increased liver size with pregnancy have been described in women. To investigate, we conducted a prospective, non-interventional clinical trial in healthy pregnant women. Participants underwent magnetic resonance imaging (MRI) of their livers, provided blood samples, and completed body metric analyses. The majority of women (~70%) had increased liver size and evidence of increased liver function at third trimester compared to first trimester of pregnancy, with liver size returning to pre-pregnancy size post-wean, consistent with rodent models of weaning-induced liver involution. This study provides the first description of human liver size dependency on reproductive state. Moreover, these data are consistent with the hypothesis that reproductive alterations to the liver, in particular weaning-induced involution, contributes to the increased risk for liver metastases in women diagnosed with breast cancer postpartum.

Chapter 1 : Background and Introduction

Young Women's Breast Cancer

Young women's breast cancer is variously defined as a breast cancer diagnosis in women less than or equal to 35-45 years of age. This definition is based on the inflection point in death rates, which are higher in women women until ~45 years of age – after which death rate plateaus [1,2]. Perhaps in part because the definition is nebulous, young women's breast cancer is an under-appreciated clinical problem. This lack of recognition stems somewhat from the notion that young women's breast cancer is rare. A 2019 population-level assessment found that 10-year probability of diagnosis with invasive breast cancer was 0.5% for women at age 30 and 1.5% for women at age 40 [3]. Such data may lead to the conclusion that young women's breast cancer is not a cause for concern. However, these data are misleading as they don't describe the *number* of breast cancer cases in young women. In 2019, there were 49,000 cases of invasive breast cancer in the U.S. in women under age 50, representing ~20% of all invasive breast cancers [3]. Further, the probability of developing breast cancer from birth to 49 years of age is 1 in 49[4]. Thus, it is apparent that young women's breast cancers are not uncommon.

While incidence is one metric to assess cancer's impact on a population, death from cancer is another. Death due to breast cancer occurs when the cancer metastasizes, or spreads to distant organs. Metastatic breast cancer has disproportionally increased in young women over the past several decades. Specifically, between 1976-2006, cases of metastatic breast cancer in the U.S. increased by 2% per year in women less than 40 years of age and by 0.6% per year in women ages 40-54 [5]. In comparison, cases of metastatic breast cancer in women over the age of 55 decreased slightly or remained constant [5].

Further, among women whose cancer progressed to metastatic disease, young women were at higher risk of dying than older women [6,7].

Some attribute the increased risk of death in young women to the observation that young women are at increased risk of being diagnosed with poor prognostic HER2+ and triple negative (ER-PR-HER2-) breast cancers [7,8]. However, even for hormone receptor positive disease, which is typically a good prognostic subtype [2], research shows that young breast cancer patients have worse outcomes compared to older peers [9]. Another study in women with stage 1 or 2 breast cancer investigated whether high tumor grade, lymphatic vessel invasion, or necrosis could account for the poor prognosis of young women's breast cancer [10]. The authors demonstrated that while these poor prognostic variables were more common in young women's breast cancer, young age was an independent poor prognostic factor in breast cancer [10]. Additional recent studies have corroborated that young age is an independent poor prognostic using multivariate models that controlled for tumor size, nodal status, and estrogen receptor expression [7,11]. These findings are suggestive that tumor-extrinsic factors contribute to increased metastasis observed in young women. However, it is possible that differences in tumor mutations between younger- and older-onset breast cancer also impact risk of metastasis.

Germline mutations in *BRCA* genes are associated with increased risk of early onset breast cancer [12], yet only ~10% of breast cancers in young women have detectable *BRCA* mutations [13,14]. As with breast cancer overall, a protective effect of pregnancy has been reported in *BRCA* carriers [15]. However, whether a recent pregnancy increases poor prognosis in *BRCA* carriers remains to be determined, as studies to date have not evaluated risk of breast cancer and/or breast cancer prognosis from the perspective of

proximity to recent pregnancy. Furthermore, because *BRCA* mutations do not associate with worse disease outcome [13,16], *BRCA* mutations are not thought to contribute to the poor prognoses of young women's breast cancer. Alternatively, somatic mutations could be different between younger- and older- onset breast cancers. A recent study examined the somatic mutational profiles of breast cancer arising in younger (<40 years, n=89) and older (>40 years, n=949) women. Somatic mutations in *GATA3* and *CTNNB1* were elevated in younger women, whereas somatic mutations in *PIK3CA, CDH1, MAP3K1* were increased in older women [17]. An additional study showed higher rates of mutation in *TP53* in younger women with breast cancer [18]. As with *BRCA* germline mutations, the somatic found at higher prevalence in young women are not known to confer metastatic advantage, and thus are unlikely to be responsible for metastasis in young women's breast cancer [19,20]. Rather, a further understanding of patterns of metastasis in younger- and older-onset breast cancer may yield insight into the worse prognosis of young women's breast cancer.

Metastatic breast cancer is most commonly found in the bone, lung, brain, and/or liver. One question is whether the pattern of metastatic site differs between women by age, as different sites of metastasis have differing length of overall survival. Brain and liver metastases are consistently found to have the worst survival outcomes. Considering patients with only one site of metastasis, patients with bone or lung metastases had ~32% risk of death within a year, whereas brain-only had 62% risk of death and liver-only had 43% risk of death within a year [21]. 5-year survival rates are 8.5% for liver metastasis [22,23], 17.8% for lung metastasis [24], and less than 10% for brain metastases [25]. Together, these survival data demonstrate that brain and liver metastases are especially deadly.

Data on single-site incidence of metastasis provides further evidence that liver metastases are prevalent in young women with breast cancer. Upon assessment of the average age of patients with Stage IV breast cancer, it was observed that patients with liver metastases had the lowest age of any single-site metastatic group (59.0 vs 61.1 [brain] vs 62.5 [bone] vs 66.2 [lung], $p<0.001$) [26]. Further, aside from bone metastases, liver metastases were identified as the most common single site of metastases in women <49 years of age in a U.S. cohort [27] and <60 years of age in a Danish cohort [21]. In an additional study that focused solely on breast cancer patients who progressed to liver metastasis, 40% of women were pre-menopausal at time of initial diagnosis [22]. These data are striking as pre-menopausal women comprise about 20% of invasive breast cancer cases [3]. Thus, the incidence of liver metastasis in pre-menopausal women is two-fold higher than would be expected if liver metastases were distributed equally amongst age groups.

A study of 197 women who died from metastatic spread of their breast cancer found a statistically significant association between young age at diagnosis and increased incidence of liver metastasis. Specifically, 83% of women <49 years of age at initial breast cancer diagnosis progressed to liver metastasis [28]. In contrast, among women who died from metastatic breast cancer, 72% of women 50-64 years of age and 44% of women over 65 progressed to liver metastasis. This single study found liver metastasis is a major concern for all breast cancers, and suggest liver metastases may be a particular problem in young women's breast cancer.

Taken together, the data on breast cancer incidence and metastasis in young women raise the question of what is unique about young women that makes them more

susceptible to liver metastasis than older women. One defining factor of young women's breast cancer is that it overlaps with the period when reproduction occurs. Pregnancy involves significant whole-body changes; given this, researchers have investigated the relationship between a recent pregnancy and breast cancer.

Postpartum breast cancer

Over the past several decades, the relationship between pregnancy and breast cancer has advanced to a dominant model referred to as "the dual effect of pregnancy". The dual effect of pregnancy describes the phenomenon in which a completed pregnancy, at the population level, results in a transient increase in breast cancer risk followed by a delayed lifetime decrease in breast cancer risk [29,30]. The timing at which risk level "crosses-over" from increased to decreased – relative to the age-matched risk for never-pregnant women – is dependent on age of first pregnancy (Figure 1-1) [31]. Specifically, younger age (<25 years) at first birth results in a shortened window of elevated risk compared to older women and is associated with crossover into the protective effect of pregnancy 8 years after birth. In contrast, older age at first birth (>30 years) is associated with more than 25 years of increased breast cancer risk after birth (Figure 1-1).

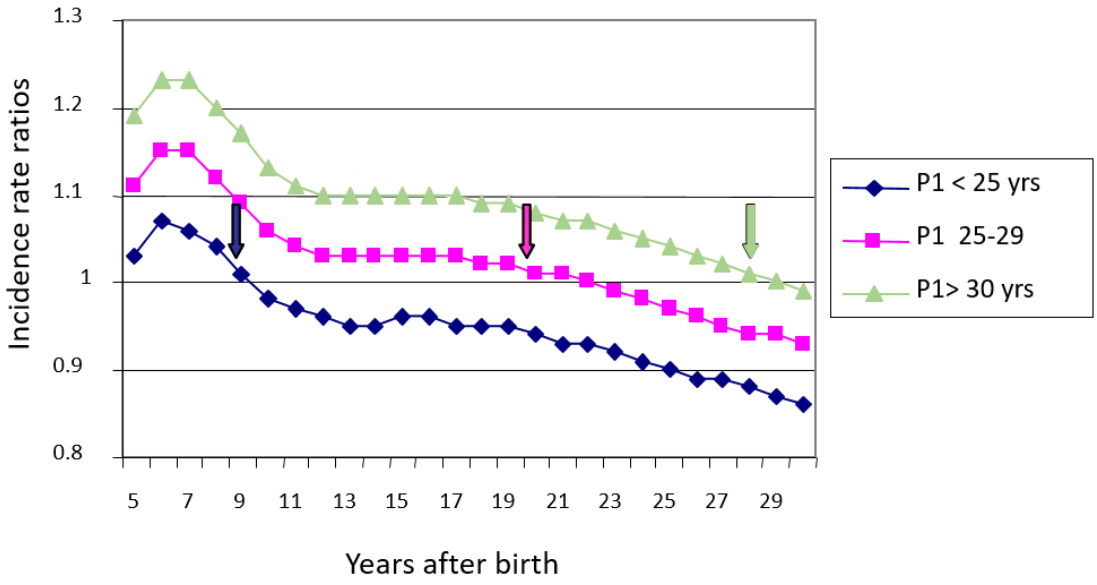

Figure 1-1 "Dual effect" of pregnancy

Predicted incidence-rate ratio of breast cancer for women of parity according to time since first birth (P1), in subgroups of 'age at first birth' (for nulliparous women, the relative-rate ratio = 1.0). Modified from Schedin 2006[32].

Next, researchers sought to investigate overall survival in young women's breast cancer by parity status. Age-matched never pregnant women were compared to women who had recently given birth. In several studies, recent birth was associated with worse prognosis [33–36]. Further, it has been found that poorer prognosis of pregnancy-associated breast cancer extends for 5-10 years after birth [37,38]. Importantly, breast cancer diagnosis during pregnancy does not associate with worse survival compared to diagnosis in never pregnant women [39,40]. These data are consistent with the premise that it is not pregnancy *per se* that associates with worse survival, but rather the postpartum period. In line with this, thought leaders have called for all new reports to use the term *postpartum breast cancer (PPBC)* rather than pregnancy-associated breast cancer [41].

One explanation for the increased rate of metastasis in PPBC is that PPBC cases may be enriched for poor prognostic features, such as larger tumor size, higher proliferation score, later stage at diagnosis, or hormone receptor negative subtypes [42]. A recent large, multi-institutional study evaluated these variables and found no difference between tumor size, tumor cell proliferation, stage, or subtype between nulliparous and postpartum women with breast cancer [38]. These data demonstrate that known tumor intrinsic factors do not account for increased metastasis in postpartum patients. Instead, these data are consistent with host-intrinsic, microenvironmental factors specific to postpartum women as contributing to tumor growth and metastasis.

Weaning-induced mammary gland involution and the "involution hypothesis"

Rodent models have defined the unique biology of the postpartum timeframe. In the context of the mammary tissue, a pregnancy cycle includes the pregnancy itself,

lactation, and weaning. Following weaning, there is a return of the lactation-competent mammary gland to pre-pregnant, pre-lactational state via tissue remodeling. This tissue remodeling is termed weaning-induced involution. Weaning-induced mammary gland involution has been well-described, and is characterized by apoptosis of 90% of the mammary epithelium, immune cell infiltration, extracellular matrix remodeling, and re-emergence of adipocytes [43–46]. These tissue-remodeling events are reminiscent of wound healing [47]. In the human breast after weaning, these same tissue remodeling attributes have been characterized [48,49]. Such data gives credence to the notion that weaning-induced mammary gland involution is a conserved mammalian biology, and suggests that findings in rodent models are relevant to humans.

Because mammary gland involution has attributes of wound healing and wound healing is associated with tumor promotion [50], it was hypothesized that involution would support tumor growth and dissemination [51]. Early studies from the Schedin lab demonstrated that the extracellular matrix of the involuting mammary gland was sufficient to promote metastasis in an experiment where isolated matrix from nulliparous or involution stage glands was mixed with tumor cells then injected back into mammary fat pads [52]. In a subsequent study, mammary tumor cells were injected into the fat pad of mice at either nulliparous or involution stages. Tumor cells injected into the mammary fat pad of dams one day after weaning promoted tumor growth (Figure 1-2) [53,54]. Further, more tumor cells disseminated from glands of involution mice (Figure 1-2). This phenotype was promoted by collagen and inflammatory signaling [53], both of which are dominant in involution. Treatment of involution mice with non-steroidal anti-inflammatory drugs during involution reduced tumor growth to nulliparous levels [53], and

associated with compositional changes to the extracellular matrix and tumor immune milieu [54,55]. Taken together, these studies support the hypothesis that weaning-induced mammary gland involution is tumor promotional and further show that the environment of the involuting mammary gland can be targeted to reduce tumor promotion.

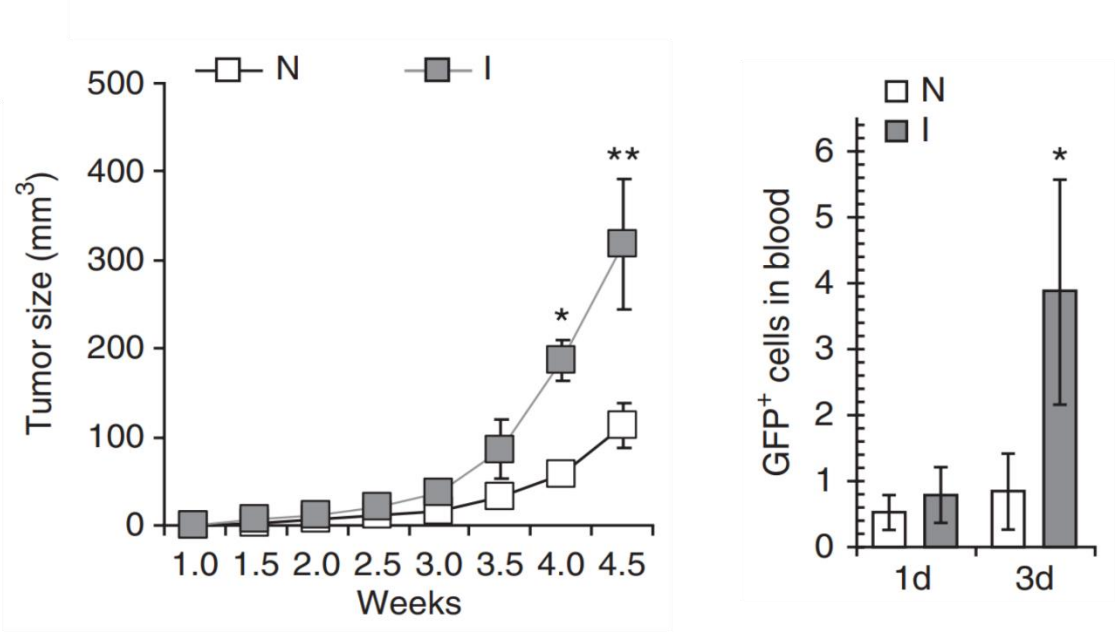

Figure 1-2 Postpartum mammary microenvironment is tumor promotional

Left: Average primary tumor volume in nulliparous (n=7) and involution (I) mice injected with MCF10DCIS mammary tumor cells. **Right**: Quantification of GFP+ tumor cells in peripheral blood following mammary fat pad injection. Reprinted from Lyons 2011[53].

It is possible that the increased tumor dissemination from involuting mammary glands could account for the increased metastasis in postpartum breast cancer patients. In such a scenario, a prediction is that incidence of site-specific metastasis would not differ amongst postpartum patients but rather all sites would be equally elevated compared to nulliparous patients. To investigate this possibility, first site of metastasis was evaluated in a cohort of young women's breast cancer patients that was delineated into nulliparous or postpartum cases. Contrary to the above prediction, liver metastases in particular were elevated in postpartum patients (Figure 1-3) [56]. One caveat of this study was the small cohort size. Yet, recent unpublished data from the Schedin lab collected in collaboration with the Utah Population Database shows similar results, with liver metastases significantly increased in postpartum patients (Figure 1-3). This observation of liver-tropism led to the question of whether the liver in postpartum women was somehow altered in a manner that made it more susceptible to breast cancer metastasis, or in other words—whether the postpartum liver is a pre-metastatic niche.

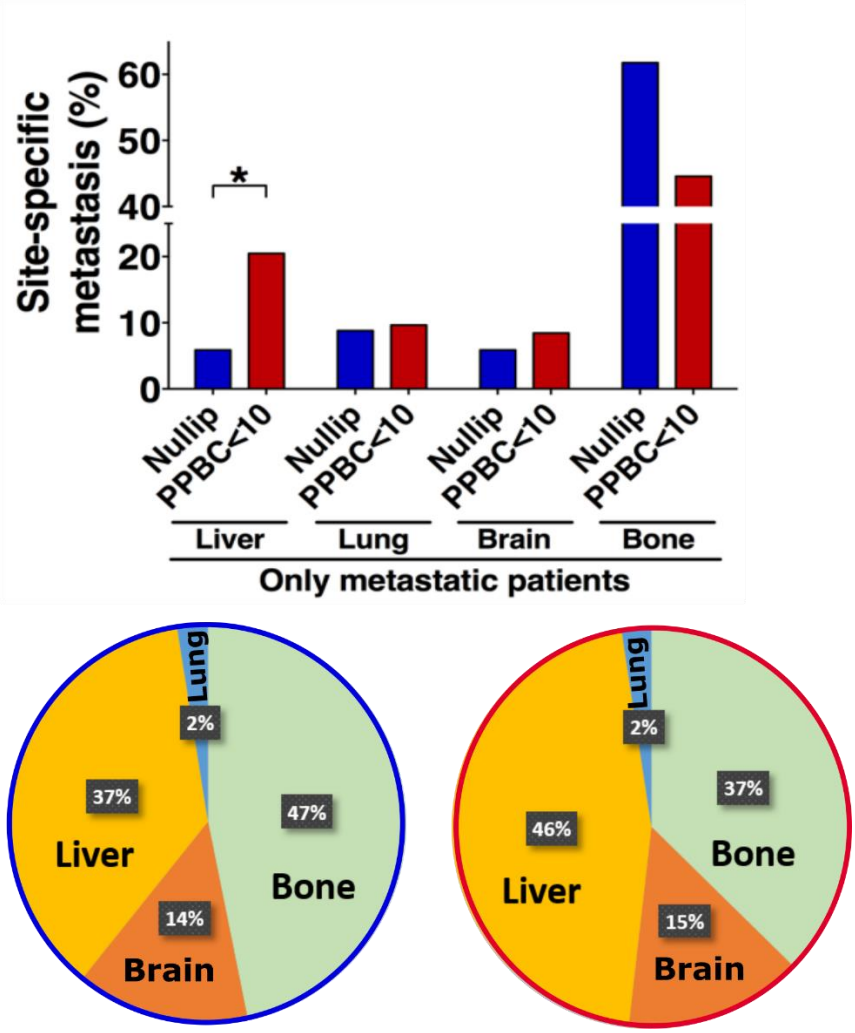

Figure 1-3 Incidence of site-specific metastasis in two studies of young women's breast cancer

Top: Site-specific metastases in women with metastatic disease; Nullip: n = 34; PPBC < 10: n = 83). Frequency of liver metastasis: * P = 0.04, one-sided Fisher exact test; P = 0.058, two-sided Fisher exact test, OR: 4.12 (95% CI, 0.90–18.94); and lung: (P = 1.00), brain (P = 1.00), and bone (P = 0.11) metastasis by Fisher exact test. Reprinted from Goddard 2017[56].

Bottom: Preliminary, unpublished data of site-specific metastasis in women with metastatic disease from the Utah Population Database. Nulliparous young women's breast cancer cases are shown in the left pie chart and postpartum breast cancer cases are shown in the right pie chart.

Weaning-induced liver involution

It is appreciated that the liver changes during pregnancy and lactation, putatively to accommodate increasing metabolic demands. Specifically, the liver and the mammary gland both support lactation by increasing metabolic output to meet the nutritional needs of a nursing infant [57]. As a result, it has been hypothesized that during lactation the mammary gland and the liver work as a functional unit [58].

Early evidence for reproductive state alterations in the liver included the demonstration of increased biosynthetic capability during lactation. For example, in sows, on the day prior to birth, higher circulating urea and creatinine concentrations—both made by the liver—positively correlated with colostrum yield, the first product of lactation [59]. Additionally, fatty acid oxidation and glucose production in the rodent liver significantly increase during lactation, ostensibly to meet the elevated glucose needs of milk production [56,60,61]. Furthermore, prior studies established that the rodent liver expanded in size during pregnancy and lactation [62,63]. Because liver enlargement was associated with the high metabolic demand of pregnancy and lactation, a prediction is that when metabolic demand ceased, the liver would decrease in size. As expected based on this prediction, after weaning—when the metabolic demand of lactation ends—the liver returned to its pre-pregnant size (Figure 1-4A) [56]. However, it was unknown whether this decrease in liver size was associated with the same tissue remodeling hallmarks of mammary-gland involution.

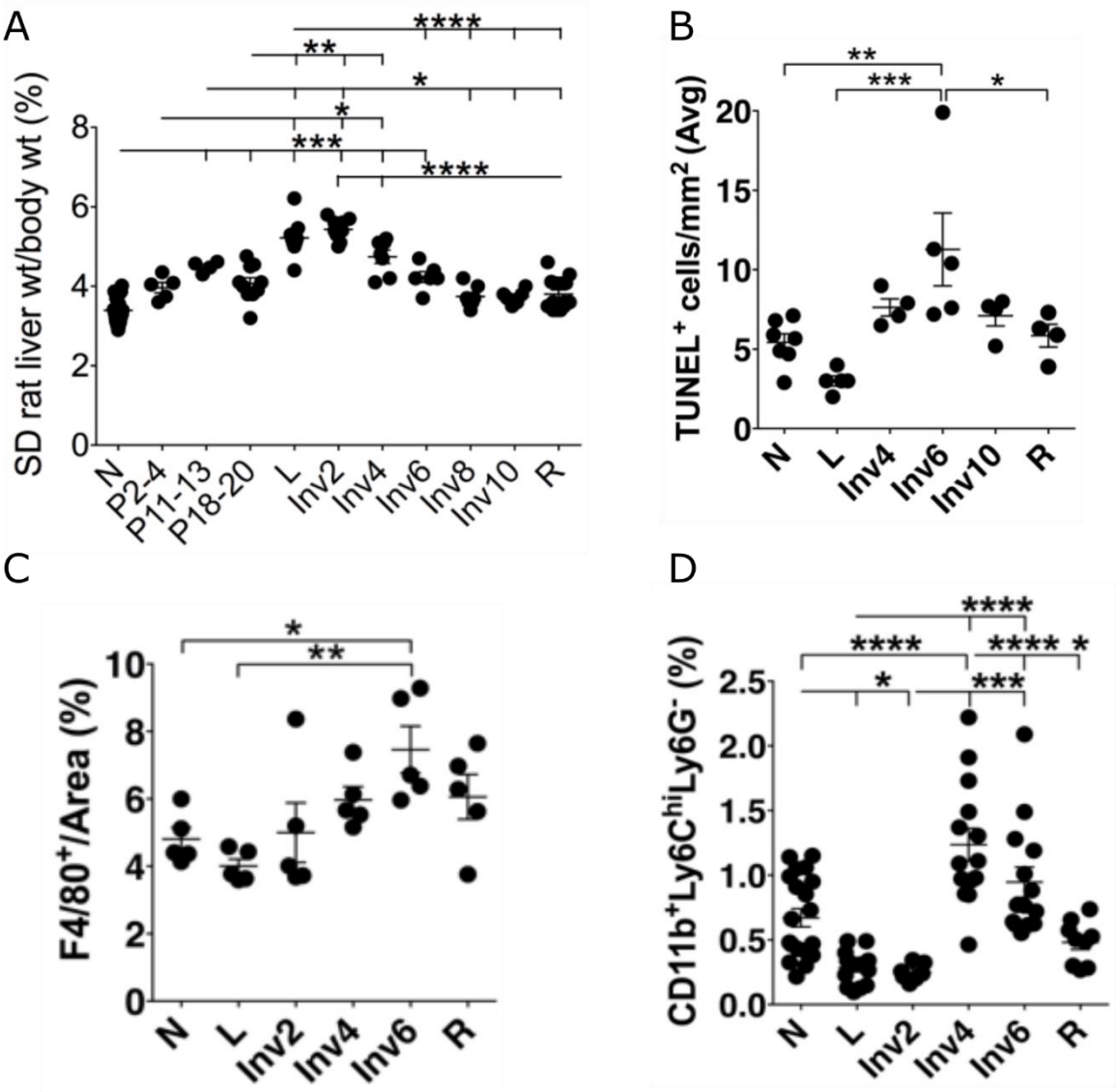

Figure 1-4 Evidence for weaning-induced liver involution

(A) Liver weights from age-matched rats across the reproductive cycle. N: nulliparous, P: pregnancy, L: lactation, Inv: involution, R: regressed. **(B)** TUNEL quantification of apoptotic hepatocytes across the reproductive cycle. **(C)** Macrophage (F4/80+) IHC quantification. **(D)** Flow-cytometric quantification of BALB/c mouse liver CD11bhiF4/80−Ly6C+Ly6G− monocytes. Reprinted from Goddard 2017[56].

Using similar rodent models as were used to study weaning-induced mammary gland involution, the Schedin lab investigated whether the rodent liver also underwent weaning induced involution. Having established that liver size decreased post-wean, Goddard et al showed that hepatocytes underwent cell death during the period that the liver was decreasing in size (Figure 1-4B) [56]. This association of programmed cell death with reduction in liver size was the first evidence that the liver may also undergo weaning-induced involution. To further characterize the post-wean liver, livers were assessed for extracellular matrix (ECM) proteins and various immune cells across the reproductive cycle. Quantitative extracellular matrix proteomics revealed reproductive-state dependencies in the matrisome, with upregulation of collagens and tenascin-C during involution [56]. Further, livers from involution stage hosts had significantly elevated macrophages and immature monocytes as shown via immunohistochemistry (IHC) staining and flow cytometry (Figure 1-4C, D) [56]. Together, these data demonstrated tissue remodeling of the post-wean liver in a manner similar to the post-wean mammary gland and provided compelling evidence that the liver undergoes weaning-induced involution.

Since mammary gland involution is tumor promotional, the Schedin lab predicted that liver involution would be pro-metastatic. To ask about the liver's ability to support metastasis, the Schedin lab developed a model of breast cancer liver metastasis where mammary tumors cells are delivered directly to the liver via portal vein injection (Figure 1-5) [64]. This model isolates the liver as a single variable, as opposed to a spontaneous model of breast cancer liver metastasis where primary tumor growth and dissemination from the primary tumor would be confounding variables. Using this portal vein injection

model, mammary tumors cells were injected into either nulliparous, involution day 2, or fully regressed mice via the portal vein, and incidence of overt metastasis was assessed 5 weeks after tumor cell injection. Involution stage hosts had 3-fold higher incidence of overt liver metastases, while regressed and nulliparous hosts had similar rates (Figure 1-5) [56]. These data demonstrate that weaning-induced liver involution preferentially supports liver metastasis in mice. Furthermore, increased liver metastasis was only observed in mice who received tumor cells during involution – and not after involution had been completed – data consistent with the hypothesis that metastatic promotion requires tumor cells to experience the involution process. In other words, the metastatic promotion of the post-wean liver does not persist after the liver is fully returned to a pre-pregnant, pre-lactational-like state. These data raise the question of what exactly about the involution window promotes metastasis.

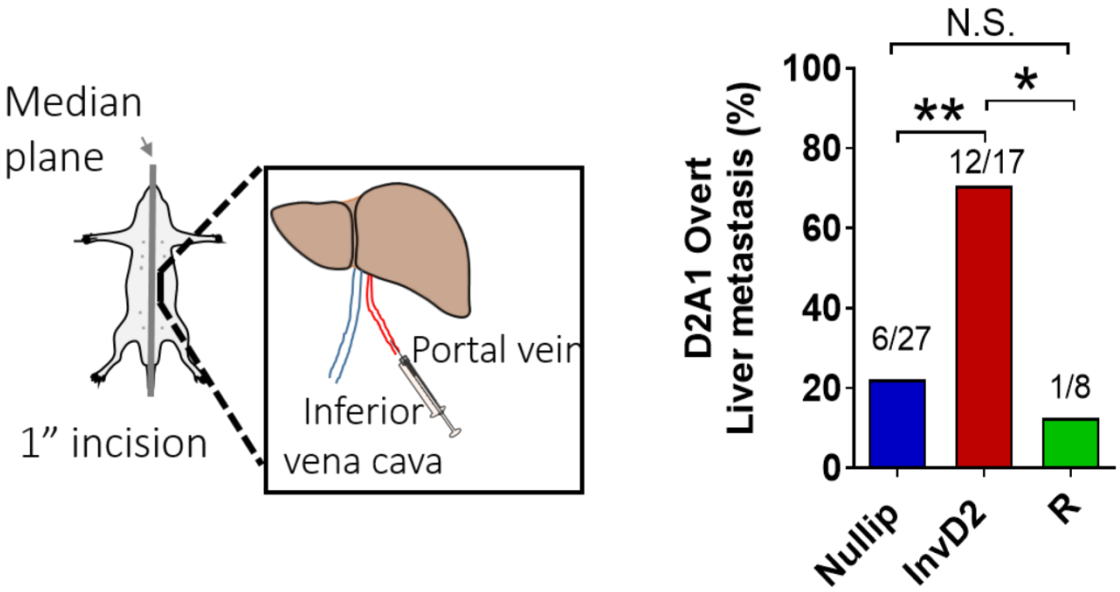

Figure 1-5 Liver metastasis is promoted by the environment of the involuting liver

Left: Schematic of portal vein injection to establish liver metastasis. **Right:** Incidence of overt liver metastasis using the D2A1 mammary tumor cell line in mice of three reproductive stages: nulliparous (nullip), involution (InvD2), and regressed (R). *$p<0.05$; **$p<0.01$, Fisher’s exact test. Reprinted from Goddard 2017[56].

Thesis Aims

This dissertation addresses the overall hypothesis that the microenvironment established by weaning-induced liver involution promotes breast cancer liver metastases. This hypothesis was evaluated using mouse models, an observational clinical study in healthy pregnant women, and clinical data and tissues from women with breast cancer liver metastases. The following chapters of this dissertation will address three aims.

The **first aim** investigated the mechanism of metastatic promotion in the involuting liver using mouse models of PPBC.

The **second aim** addressed the unanswered question of whether the human liver also undergoes weaning-induced involution. Such a finding would connect the results in mice showing that weaning-induced liver involution promotes metastasis with the human epidemiologic data showing increased liver metastasis in PPBC. However, no reports had demonstrated that human liver size increases during pregnancy – which would be required for post-wean involution to occur. To investigate whether the human liver increases in size during pregnancy and shrinks post-wean, we carried out an observational, prospective study in healthy pregnant women.

The **third aim** was an exploratory study of breast cancer liver metastases (BCLM) tissues using histological approaches. This study included "all-comers" with breast cancer liver metastasis regardless of age or parity status. As such, we aimed to answer basic questions on BCLM histology that are yet to be described. What does breast cancer look like in the liver? What breast cancer biomarkers are found in BCLM? How does the adjacent normal liver interface with the liver metastasis? Understanding the heterogeneity (or lack thereof) and histological behavior of BCLMs is anticipated to

improve mouse models of BCLM and direct studies into liver niche components that may foster BCLM growth and survival.

The work presented herein support the overall hypothesis that the microenvironment established by weaning-induced liver involution promotes breast cancer liver metastases. Furthermore, this work suggests new avenues of research to address liver metastases in young women's breast cancer. Future directions are discussed in Chapter 5.

Chapter 2 : Metastatic promotion in the involuting liver

Reprinted from published Manuscript

Bartlett, A.Q.; Pennock, N.D.; Klug, A.; Schedin, P. Immune Milieu Established by Postpartum Liver Involution Promotes Breast Cancer Liver Metastasis. *Cancers* **2021**, *13*, 1698. https://doi.org/10.3390/cancers13071698

Contributions

Conceptualization, A.Q.B. and P.S.; methodology, A.Q.B., N.P., and P.S.; validation, A.Q.B. and P.S.; formal analysis, A.Q.B.; investigation, A.Q.B, A.K, and N.P.; writing—original draft preparation, A.Q.B.; writing—review and editing, A.Q.B. and P.S.; visualization, A.Q.B.; supervision, P.S.; project administration, P.S.; funding acquisition, P.S.

Abstract

In rodents, we identified a physiologic process within the normal liver that creates a pre-metastatic niche. This physiology is weaning-induced liver involution, characterized by hepatocyte cell death, immune influx, and extracellular matrix remodeling. Here, using weaning-induced liver involution as a model of a physiologically regulated pro-metastatic niche, we investigate how liver involution supports breast cancer metastasis. Liver metastases were induced in Balb/c immune competent hosts by portal vein injection of D2OR (low metastatic) or D2A1 (high metastatic) mouse mammary tumor cells. Tumor incidence and multiplicity increased in involution hosts with no evidence of a proliferation advantage. D2OR tumor cell extravasation, seeding, and early survival were not enhanced in the involuting group. Rather, the involution metastatic advantage was observed at 14 days post tumor cell injection. This metastatic advantage associated with

induction of immune tolerance in the involution host liver, reproductive state dependent intra-tumoral immune composition, and CD8-dependent suppression of metastases in nulliparous hosts. Our findings suggest that the normal postpartum liver is in an immune suppressed state, which can provide a pro-metastatic advantage to circulating breast cancer cells. Potential relevance to women is suggested as a postpartum diagnosis of breast cancer is an independent predictor of liver metastasis.

Introduction

Breast cancer deaths are almost exclusively due to spread of the cancer to distant organs, i.e., metastasis, and young women with breast cancer are at a higher risk of dying from metastasis than older women [6,7]. The dominant paradigm to explain the increased deaths in younger women is that their tumors have intrinsic properties that increase metastatic capability. In support of this hypothesis, young women are at increased risk of being diagnosed with poor prognostic HER2+ and triple negative (ER-PR-HER2-) breast cancers [7,8]. However, research shows that young breast cancer patients have worse outcomes compared to older peers regardless of cancer subtype [9]. This suggests that tumor extrinsic factors, such as the microenvironment at the secondary site, might also contribute to increased metastasis observed in young women. Recently, efforts to investigate secondary environments permissive of metastatic growth have gained momentum as an approach to better understand and target metastasis [65–68].

Sites within secondary organs that support tumor cell survival and proliferation are called “metastatic niches” [66]. Stages of the metastatic process that the niche support include tumor cell adherence to organ-specific endothelium, extravasation, survival, immune avoidance, and outgrowth [69]. These pro-metastatic effects are mediated by niche

components including insoluble extracellular matrix (ECM) proteins, soluble proteins, and stromal cells such as fibroblasts, endothelial cells, and immune cells. The evolution of an organ into a pro-metastatic niche has been attributed to tumor education, whereby a primary tumor exerts systemic effects that remodel the distant site to a more permissive state [67,70–74]. However, a largely unexplored hypothesis that may further our understanding of breast cancer metastasis in young women is the idea that physiologic remodeling of secondary sites can form a pro-metastatic niche. To date, how normal physiology impacts a possible metastatic niche is not well-studied, in part due to lack of suitable model systems.

One example of a normal, physiologic process that creates a pro-metastatic niche is weaning-induced liver involution. In rodents, it has been reported that the liver approximately doubles in size during pregnancy and retains elevated size throughout lactation, putatively to accommodate the increased metabolic demands of pregnancy and lactation [56,62,63,75]. Liver involution returns the pregnancy and lactation-enlarged liver to a pre-pregnant state via a process that includes hepatocyte programmed cell death, catabolic metabolism, ECM remodeling, and immune cell influx [56]. Of note, during liver involution pro-metastatic ECM proteins, i.e., collagen and tenascin C, are deposited and the abundance of immature monocytes and macrophages is elevated [56]. Weaning-induced liver involution promoted breast cancer liver metastasis in a model where tumor cells were delivered to the liver via portal vein injection [56]. This observation of increased liver metastasis in postpartum mice, a so-called “involution advantage”, suggests that physiologic liver involution induces a metastatic niche. Of clinical relevance, liver metastases are common in younger breast cancer patients [28]. Further, one recent study

demonstrated that young postpartum breast cancer patients are more likely to develop liver metastasis than age matched, as well as tumor stage and subtype matched, never-pregnant patients [56]. Here, we use weaning-induced liver involution as a model of a physiologic process that induces a metastatic niche, and investigate potential mechanisms by which the involution liver supports metastasis.

We report new evidence that reproductive stage of the liver differentially impacts tumor multiplicity and morphology, including mesenchymal and desmoplastic phenotypes. Further, we found that the normal process of liver involution establishes an adaptive immune suppressed environment, and that the involution metastatic advantage can be recapitulated with depletion of cytotoxic CD8 T cells. These data are evidence for reproductive stage dependent physiologic remodeling of the liver metastatic niche with implications for niche-targeted interventions.

Materials and Methods

4.1. Animal Husbandry

Oregon Health & Science University (OHSU) Institutional Animal Care and Use Committees approved (TR01_IP00000967, approved on 13 April 2020) all animal procedures. Age-matched (10–12 weeks) female BALB/c mice (Charles River Laboratories, Wilmington, MA, USA) were housed and bred as described [76]. Briefly, for involution group animals pup number was normalized across dams to assure equal lactation and pups were weaned between 9-11 days after birth. At study endpoints, mice were euthanized across groups either by CO2 asphyxiation or while under anesthesia by exsanguination via portal vein perfusion with PBS. Whole livers and/or spleens were removed, washed 3× in 1× PBS, and processed for subsequent assays as described.

4.2. Cell Culture

D2.OR, D2.OR-GFP, and D2A1 mouse mammary tumor cells were kindly provided by Ann Chambers (University of Western Ontario, London, Ontario, Canada) and cultured as previously described [77]. For tumor cell injection preparation, cells were washed and suspended in cold 1× PBS. Cells were tested in January 2018, were confirmed murine pathogen and Mycoplasma free, and the origin of cells was validated (Idexx Bioresearch, Columbia, MO, USA). Cells used in these studies were within 3 passages of tested vials.

4.3. Liver Metastases Studies

Liver metastases were induced by intra-portal vein injection of D2OR, D2OR-GFP, and D2A1 mouse mammary tumor cells, as previously described [64]. Tumor cells were suspended in 10µL 1×PBS with various number of cells: 50,000 D2.OR for 6 week endpoint and CD8 T cell depletion studies; 5,000 D2A1 for 5 week endpoint study; 500,000 D2.OR-GFP for 90 min, 1, 3, and 14 day endpoint studies. Tumor cells were injected into either involution group mice 2 days after weaning, involution day 2 (InvD2), or age-matched nulliparous mice. For D2A1 and D2.OR studies, BALB/c mice were used. For D2.OR-GFP studies, "Glowing Head" BALB/c mice (Gnrhr-luc/EGFP) were used as these mice are tolerant to the GFP protein, which were a gift from Lalage Wakefield (National Cancer Institute, USA) [78]. Whole liver was formalin-fixed and paraffin embedded (FFPE) for histological analyses. Liver metastases were assessed following euthanasia at 5 and 6 week time points by visual assessment of the liver and by hematoxylin and eosin staining of FFPE liver sections. For the D2.OR-GFP 90 min, 1, 3, and 14 day endpoint studies, immunohistochemistry (IHC) for GFP+ tumor cells was used for assessment. To assess for solitary tumor cells and micrometastases, two distinct

depths of liver tissue ≥200 μm apart were sectioned per mouse for subsequent IHC analyses.

4.4. CD8 Depletion Experiment

Antibody concentration (BioXcell; clone 2.43) for CD8+ T cell depletion in the liver and spleen was determined by testing two initial dose concentrations (0.2 mg, 0.4 mg) and two maintenance dose concentrations (0.1 mg, 0.2 mg). Antibody was delivered in 200 μL sterile PBS via intraperitoneal injection, with initial dose given at day 0 and maintenance doses given at day 4 and day 8. 72 h post last maintenance dose mice were euthanized and liver and spleen collected for flow cytometry assessment. For subsequent tumor experiments the lowest concentrations combination that was effective at depleting CD8+ T cells was used: 0.2 mg initial dose and 0.1 mg maintenance dose (Figure S4). Mice were randomized, in a rolling study design, to receive either isotype control (BioXcell; BE0090) or CD8 depleting antibody (BioXcell; clone 2.43). In tumor studies, initial antibody dose was given 2 days prior to tumor cell injection and maintenance doses were given every 4 days for the 6 week course of the experiment. Data are presented as percent of CD45+ cells.

4.5. Histological Analyses

Liver FFPE tissue sections representing all liver lobes were stained with hematoxylin and eosin to evaluate for presence of tumors, tumor size, tumor multiplicity, and tumor morphology. Morphology was characterized as epithelial-dominant, mesenchymal-dominant, or metaplastic, defined as tumors with irregular nuclei and a mix of epithelial and mesenchymal components. Histological growth pattern was characterized as established for scoring liver metastases in colorectal cancer into pushing, replacement,

desmoplastic, mixed pattern, and portal/sinusoidal patterns [79]. Assessments were completed by two evaluators blinded to study design.

4.6. Immunohistochemistry

Single-stain IHC detection was performed as described [53]. Briefly, tissues were deparaffinized, rehydrated, and heat-mediated antigen retrieval was performed with EDTA for 5 min at 125 °C. The following primary antibodies were applied for 1 h at room temperature: Ki67 (1:400, Neo-markers #RM-9106-S), phospho-γH2AX (1:400, Cell Signaling #9718), Cleaved caspase 3 (CC3, 1:150, Cell Signaling #9664). Green fluorescent protein was applied overnight at 4 °C (GFP, 1:400 Abcam #ab13970). Secondary antibodies were applied for 30 min at room temperature: anti-rabbit (RTU, Agilent #K400) for Ki67, phospho-γH2AX, and CC3. For GFP, anti-chicken secondary was applied for 1 h at room temperature (1:1000, LSBio, LS-C61278). DAB chromogen (Agilent, K346889-2) with hematoxylin counter stain (Agilent, S330130-2) was used to visualize positive stain. Stained sections were scanned using the Aperio AT2 slide scanner (Leica Biosystems, Wetzlar, Germany). Signal quantification was performed by Aperio ImageScope v12.1.0.5029 as described previously [49]. For quantitation, all mice and tumors found in the stained tissue section were included for every analysis, unless staining was unsuccessful as defined as loss of tissue from slide and/or failure for positive controls to stain. All analyses were done by investigators blinded to study group. Data are presented as percent area positive unless otherwise noted in the figure legend.

Multiplex IHC staining was performed as previously described with modification [80]. Tissues were deparaffinized, rehydrated, and heat-mediated antigen retrieval was performed with EDTA for 5 min at 125 °C. Hematoxylin staining was performed on all

tissues prior to antibody cycles, and tissues were scanned using the Aperio AT2 slide scanner (Leica Biosystems). Table 1 lists the antibodies and conditions used. Secondary antibodies were applied for 30 min: anti-rabbit (Histofine 414341F) and anti-rat (Histofine, 414311F). After each antibody cycle, tissues were scanned using the Aperio AT2 slide scanner (Leica Biosystems). Following scanning, 3-Amino-9-Ethylcarbazole (AEC) chromogen was removed with 1×70% and 1×100% alcohol wash for 2 min each. Primary and secondary antibodies were removed using 20% SDS-glycine pH 2 at 70 °C for 30–60 min. Secondary only and isotype controls were utilized to confirm antibody stripping after each cycle. This cycle was repeated for each primary antibody listed in table 1. Each tissue slide included a positive control tissue microarray (TMA) to confirm primary antibody staining for each cycle. The TMA was comprised of mouse spleen, lymph node, and liver tissue from mice subjected to inflammatory stimuli.

Table 2-1 Multiplex IHC Antibodies and Conditions

Primary Antibody	**Manufacturer**	**Catalog #**	**Lot#**	**Concentration**	**Incubation**	**Secondary Antibody**
CD4	Cell Signaling	ab25229	Lot:4	1:50	O/N 4 °C	anti-Rb
CD45	BDPharminigen	550539	Lot: 4141820 & 9301732	1:50	60 min	anti-Rt
Ki67	Cell Signaling	12202	Lot: 6 (11/20)	1:800	60 min	anti-Rb
FoxP3	eBioscience	14-5773-82	Lot:E023634 + 2172602	1:100	60 min	anti-Rt
CD3	Abcam	ab16669	Lot: GR291605-1	1:100	60 min	Anti-Rb
Tox1	Abcam	ab237009	Lot: GR3241900-3	1:300	60 min	anti-Rt
PD1	Cell Signaling	84651	Lot: 4 (11/20)	1:200	60 min	anti-Rb
CD11b	Abcam	ab133357	EPR1344	1:30k	60 min	anti-Rb
F480	Cell Signaling	70076S	Lot:	1:500	60 min	anti-Rb
CK18	Abcam	ab181597	Lot: GR321105-11	1:1000	60 min	anti-Rb

4.7. Multiplex IHC, Image Processing and Data Analysis

After staining, scanned images from each cycle were analyzed using an image processing pipeline previously described with minor modification [80]. Image alignment and extraction were performed using the SURF algorithm in the Computer Vision Toolbox of Matlab version R2018b (The MathWorks, Inc, Natick, MA, USA). Single cell segmentation and color deconvolution were performed in FIJI, and mean intensity quantification was performed in Cell Profiler version 3.5.1. Image cytometry was performed using FCS Express 6 Image Cytometry RUO (De Novo Software, Glendale, CA, USA). Data are presented as a percentage of CD45+ cells per tumor, averaged by mouse.

4.8. Flow Cytometry

For flow cytometric quantification of liver CD4+ T cell polarization, left and caudate liver lobes were dissected following CO2 euthanasia and rinsed in 1× PBS to wash exterior blood. Liver lobes were minced and digested in 1 mg/mL collagenase I, 0.5 mg/mL hyaluronidase, and 0.5 mg/mL DNase at 37 °C for 30 min while rotating, and filtered through a 100 μm filter. Red blood cells were lysed using 1× RBC lysis buffer (eBioscience). Cell pellets were washed with 1× PBS, resuspended, and cells counted in trypan blue using a hemocytometer. 1×10^6 cells per sample in 100 μL PBS or FACS buffer were blocked with CD16/32 (eBioscience, 1:100) for 30 min, stained for cell surface markers (Live/Dead, Aqua; CD45, 30-F11, PerCP; CD11b M1/70 BV711; CD4 RM4-5, BV786; PD-1 29F.1A12 PE-Cy7) for 30 min at room temperature, stained for intracellular proteins (Tbet 4B10, BV421; RORγT AFKJS-9, PE; FoxP3 FJK-16s, APC) overnight at 4C, and fixed with 4% paraformaldehyde (BD Biosciences, San Jose, CA, USA) for 20 min. Samples were ran on the LSRFortessa (BD Biosciences; Oregon Health

and Science University) and analyzed as described below. Data in figure 5 are presented as % of CD4+ cells that expressed at least one of the following: Tbet, RORγT, FoxP3, or PD1. Data in supplemental figure 3 are presented as percent of total CD4+ cells.

For adoptive transfer experiment, whole liver and spleen were used for flow cytometric quantification of Do11.10 CD4+ T cells. Here a different digestion protocol with the addition of a Percoll gradient was used in order to enrich for immune cells. Whole livers were cut into small pieces and digested with 0.5 mg/mL collagenase 1 and 0.5 mg/mL DNase in RPMI1640 at 37 °C for 30 min, rotating. Tissue digests were filtered through a 100 μm filter and washed in RPMI1640. Samples were fractionated in a 33% Percoll solution with centrifugation at 800 *g* for 30 min at room temperature with no brake. Supernatant was collected and red blood cells were lysed using 1× RBC lysis buffer (eBioscience). Samples were washed and resuspended in RPMI1640 and counted in trypan blue using a hemocytometer. The entire liver sample was advanced to flow cytometry staining. For spleen digestion, spleens were processed through a 70 μm filter. Red blood cells were lysed using 1× RBC lysis (eBiosciences). Samples were washed and resuspended in PBS, counted in trypan blue, and 1×10^6 cells per sample in 100 μL were stained for flow cytometry. The following antibodies were used: Live Dead (Aqua), CD4 (RM4-5, BV786), CD45 (30-F11, PerCP), Do11.10 TCR (KJ1-26, PE-Cy7), CD8 (53-6.7, APCe780). Samples were ran on the LSRFortessa (BD Biosciences; Oregon Health & Science University) and analyzed as described below. Data are presented as % of CD4+ cells.

For the CD8 depletion experiment, the median lobe was digested as in the adoptive transfer experiment and used to confirm CD8 depletion. However, if there was a tumor

visually apparent in the median lobe at time of euthanasia, the caudate lobe was used to confirm CD8 depletion. The following antibodies were used: CD49b (DX5, BV421), CD3 (17A2, BV785), CD4 (RM4-5, FITC), CD8b (H35-17.2, PE-Cy7), CD45 (30-F11, APC), and Live/Dead (NearIR). Due to restrictions imposed by Covid-19, samples for the CD8 depletion study were ran on the Fortessa X50 (BD Biosciences; Fred Hutch, Seattle, WA, USA). One sample from the INV iso group had insufficient cellularity and was excluded from analysis. Data are presented as % of CD45+ cells.

All samples were analyzed using FlowJo v10 software (Becton, Dickinson & Company Franklin Lakes, NJ, USA). Unstained, single color, and fluorescent-minus-one staining controls were utilized for every experiment.

4.9. Adoptive Transfer In Vivo T cell Activation Assay

T cell activation was assessed with an *in vivo* activation assay as described with minor modification [81]. Briefly, CD4+ splenocytes were isolated from Do11.10 transgenic female mice (Jackson Laboratories Stock #003303) and enriched to >95% CD4+ T cells (Figure S4) using a CD4+ negative selection kit (MACS miltenyi) under non-stimulating conditions (putative naïve T cells). Subsequently, 1×10^6 isolated T cells in 100 µL 1× PBS were adoptively transferred via tail vein with insulin syringe into syngeneic BALB/c involution Day 0 or nulliparous age-matched hosts. Two days later either ovalbumin protein antigen (10 µg in 10 µL, Worthington) or 10 µL 1× PBS was injected into the left lobe of the liver via intrahepatic injection. Five days post antigen or PBS injection, whole liver and spleens were harvested, digested and stained for flow cytometry to detect Do11.10 T cells, as described above. A known quantity of absolute counting beads were added to samples (C36950 Invitrogen) and flow cytometry performed. Do11.10 TCR+

CD4+ T cell counts in liver and spleens were calculated by normalizing to the known abundance of counting beads. Data are presented as % of CD4+ cells.

4.10. Statistical Analysis and Hierarchical Clustering

Statistical analyses were performed using GraphPad Prism v.8 or v.9 software (GraphPad Software, San Diego, CA, USA). All data are expressed as mean ± standard error of the mean (SEM) unless otherwise noted. Statistical significance was determined using the following statistical tests with specific test fully described in the figure legends: Two-sided Fisher's exact test, Two-tailed *T* test, One-way ANOVA with multiple comparisons, and Two-tailed Mann-Whitney test. Hierarchical clustering of multiplex IHC data was performed with the Morpheus web-based tool (https://software.broadinstitute.org/morpheus, accessed date: 27 January 2021), as described previously [54].

Results

To model the clinical observation that young women with good prognostic breast cancers can progress to metastatic liver disease [38], we used a syngeneic BALB/c mouse model where mammary tumor cells of low metastatic ability, D2.OR cells [77,82], are delivered directly to the liver via the portal vein [64]. This allowed us to interrogate how liver involution may impact multiple steps of the metastatic process, including tumor cell extravasation into the liver, initial survival in the liver parenchyma, formation of micrometastases, and expansion into overt liver metastases. We first evaluated the formation of overt tumors at 6 weeks post-injection, and found a >2-fold increased incidence of liver metastases in mice injected at involution (InvD2) compared to mice

injected at nulliparous (Figure 2-1A). Tumor multiplicity was also increased in the involution group (Figure 2-1B). We next asked if involution provides a growth advantage to these metastatic lesions. We found no differences between nulliparous and involution groups in tumor size (Figure 2-1C), tumor proliferation as measured by Ki67 (Figure 2-1D,E), nor death as measured by gH2AX or cleaved caspase 3 (Figure 2-1F–I). These data are consistent with the involution metastatic niche promoting tumor establishment rather than growth. Similar results of increased multiplicity in the absence of tumor size or proliferation advantage were observed in the involution group with D2A1 cells, a line with known high metastatic potential [77], suggesting similar mechanisms of promotion in two distinct cancer cell lines with different intrinsic metastatic capabilities (Figure S1 [2-7]).

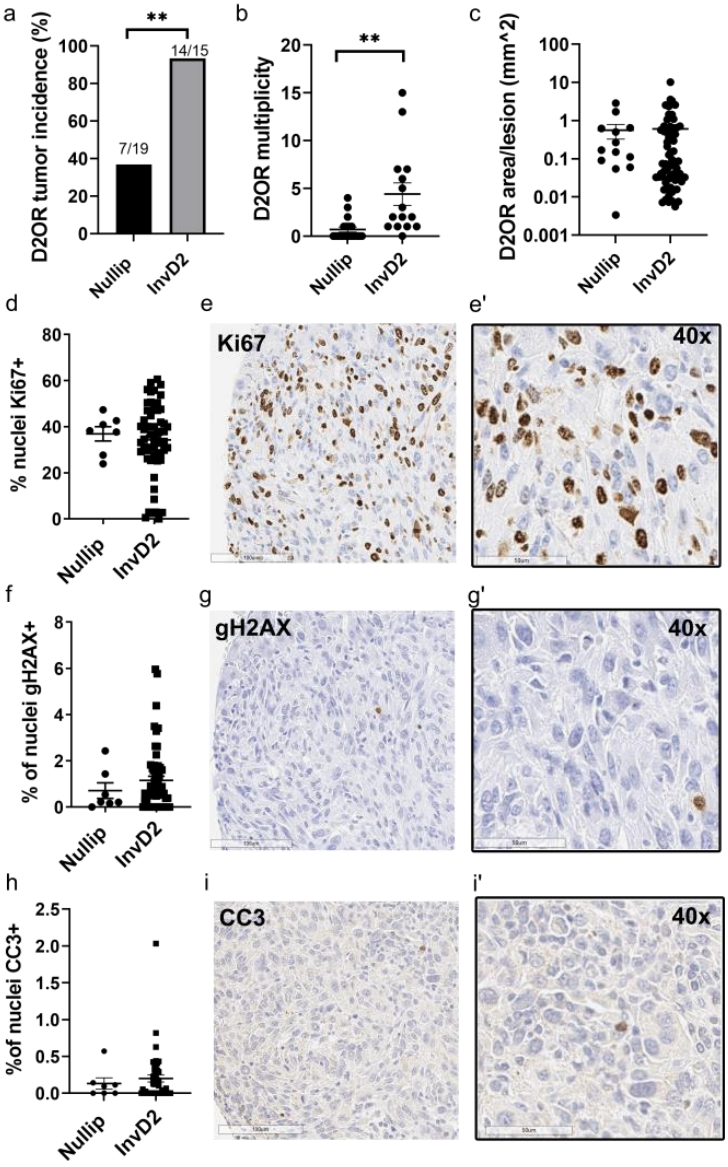

Figure 2-1 Increased metastasis in involution hosts does not associate with enhanced tumor growth.

(a) Incidence of D2OR liver metastases in nulliparous (nullip, n = 19) and involution day 2 (InvD2, n = 15) mice, n = 3 independent studies; Two-sided Fisher's exact test; (b) Number of metastases (i.e., multiplicity) per mouse in nullip (n = 19) and InvD2 (n = 15) groups; Two-tailed T test; (c) Area per tumor in nullip (n = 13 tumors) and InvD2 (n = 66 tumors) hosts; IHC quantification of per-cent of tumor nuclei positive for (d) Ki67 in nullip (n = 7 tumors) and InvD2 (n = 57 tumors); (f) γH2AX in nullip (n = 7 tumors) and InvD2 (n = 58 tumors), and (h) cleaved caspase 3 (CC3) in nullip (n = 7) and InvD2 (n = 48); Representative IHC images at low and high magnification of Ki67 (e, e'), γH2AX (g, g'), and CC3 (i, i') stains. ** $p < 0.01$.

Clinically, metastases to the liver are categorized into distinct histologies, which have implications for disease outcome [79]. Utilizing histological criteria previously reported in humans, we evaluated tumor cell phenotypes as epithelial, mesenchymal, or metaplastic (i.e., heterogeneous tumors composed of both epithelial and mesenchymal regions with irregular nuclear morphology). We also characterized five previously defined human liver metastasis growth patterns: pushing, replacement, desmoplastic, portal/sinusoidal, and mixed patterns [79]. Representative images of the D2OR mammary tumor cells growing within mouse livers are shown (Figure 2-2A1–5). These murine liver metastases were heterogeneous and highly reminiscent of the tumor heterogeneity observed in human liver metastases. We found that reproductive state influenced both tumor cell morphology and growth pattern (Figure 2-2B, C). Specifically, tumors that evolved in the nulliparous host liver were more likely to be epithelial in morphology and have a pushing growth pattern. In contrast, tumors from the involution host liver showed greater diversity with increased mesenchymal cell morphology and heterogeneity in growth patterns including desmoplastic and portal/sinusoidal patterns. This observed conservation in liver metastases histology between mice and humans suggests increased human relevance of our breast cancer liver metastasis model. Further, these data represent the novel finding that tumor histology within the liver is shaped by reproductive state of the host, and are consistent with the hypothesis that the liver microenvironment can dictate tumor histology independent of intrinsic tumor cell biology.

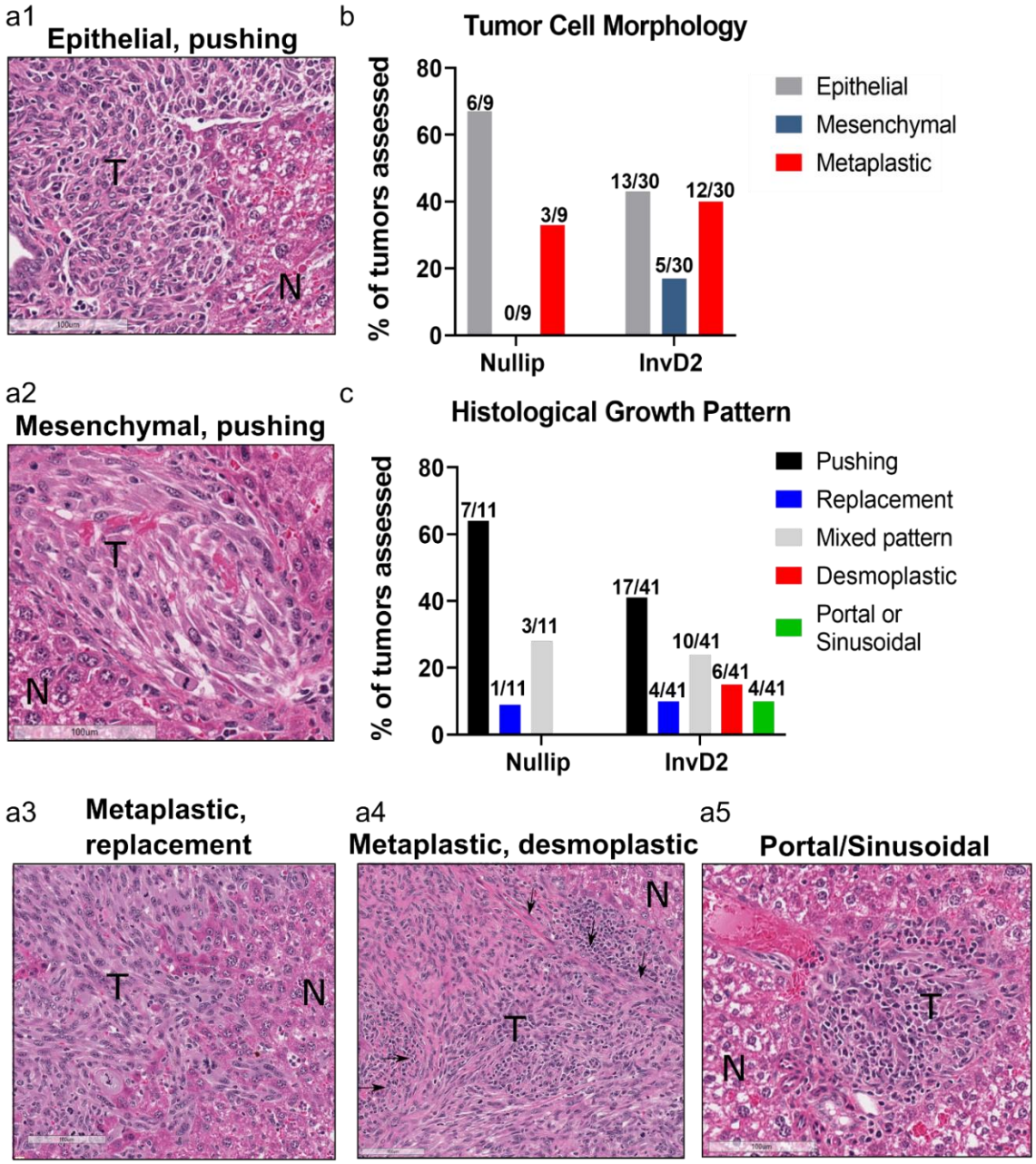

Figure 2-2 Histology of murine mammary liver metastases resembles human disease and shows increased histological heterogeneity in involution hosts.

Representative hematoxylin and eosin stained images from D2.OR tumors classified as (a1) epithelial, pushing, (a2) mesenchymal, pushing, (a3) metaplastic, replacement, (a4) metaplastic, desmoplastic with desmoplastic areas noted by black arrows, and (a5) portal/sinusoidal pattern. Tumors are denoted by "T" and adjacent normal liver by "N"; (b) Quantitation of D2.OR tumor cell morphology and (c) histological growth pattern by host reproductive stage.

Because our data supports tumor cell establishment rather than growth as the metastatic advantage in the involuting liver, we predicted that there would be an increased abundance of tumor cells at early time points post-injection in involution hosts. Such data could be indicative of increased tumor cell extravasation and/or initial survival/proliferation advantage in the involuting liver environment. As a tool to visualized tumor cells before they grow into microscopically detectable lesions, we used GFP-tagged D2OR tumor cells. Because GFP is a foreign protein, we utilized GFP-tolerant mice for these experiments, which were a gift from Lalage Wakefield (National Cancer Institute) [78]. Independent of reproductive state, by 90 min after tumor cell injection, we observed an even distribution of tumor cells throughout the liver, demonstrating uniform tumor cell dispersion (Figure 2-3A, arrows indicate tumor cells). We found no reproductive stage differences in tumor cell abundance at 90 min or one-day post-injection (Figure 2-3B), suggesting that the metastatic advantage in involution hosts is not due to differential tumor cell extravasation or initial survival. Unexpectedly, at three-days post-injection there was greater tumor cell abundance in the nulliparous host liver (Figure 2-3B), indicative that the liver microenvironments are indeed different between nulliparous and involution hosts. In sum, these data do not support the hypothesis that the metastatic advantage in the involution liver is due to increased tumor cell seeding and/or survival at early time points.

We observed two distinct tumor cell patterns at these early time points: single tumor cells (Figure 2-3C) and tumor cell clusters (Figure 2-3D). When we delineated these patterns by reproductive group, there was an increase in single cells found in the involution host, as early as one-day post-injection (Figure 2-3E). An increase in tumor

cell clusters in the nulliparous group was also evident as early as one-day post-injection (Figure 2-3F); however, there was no evidence of a growth advantage in either reproductive group, as measured by tumor area per cluster (Figure 2-3G). Since tumor cell clusters are consistent with a more epithelial-like state and single tumor cells with a more mesenchymal-like state [83], these early time point data may shed light on our six-week endpoint findings, where mesenchymal-dominant tumors were only observed in the involution group (Figure 2-2B). In sum, tumor cell morphology may be established early after tumor cell injection.

Although overt metastases are increased in the involution host liver at five to six weeks post-injection (Figure 2-1, Figure S1 [2-7]), we found no evidence for increased tumor signal in the involution group within three-days of tumor cell injection (Figure 2-3B). Therefore, we extended the study timeline to 14 days and found increased tumor cell signal as measured by area per lesion, multiplicity, and tumor burden in the livers of involution hosts (Figure 2-3H–J). Given that immune recognition and adaptive immune activation is known to take 7–10 days to develop after antigen exposure in viral systems [84], this 14 day timeframe of the involution metastatic advantage is consistent with an altered immune environment that impacts adaptive immune recognition of tumor cells.

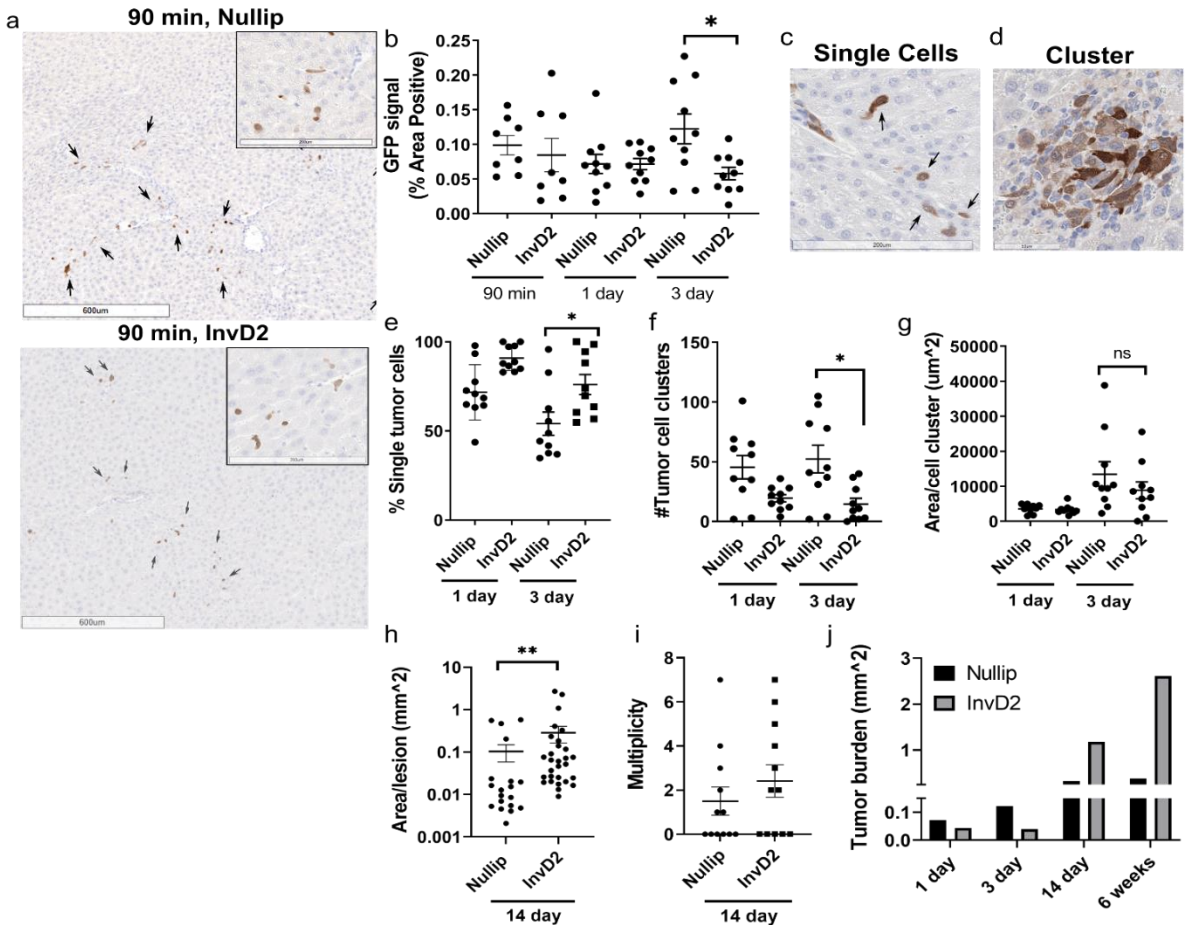

Figure 2-3 Involution metastatic advantage is observed by 2 weeks post-injection but not at earlier time points.

(**a**) Representative low and high magnification IHC images of liver FFPE sections stained to identify GFP-tagged D2.OR cells, arrows indicate tumor cells; (**b**) IHC quantification of GFP+ tumor cells in liver FFPE sections from mice euthanized 90 min (n = 4 mice/group), 1 day (n = 5 mice/group), and 3 days (n = 5 mice/group) after intraportal injection of 500,000 D2.OR-GFP tumor cells per liver. Two sections >200µm apart were assessed per mouse to quantify independent tumor cells; One-way ANOVA; Representative high magnification images showing GFP+ tumor cells as (**c**) single cells (1 day time point) or, (**d**) clusters, defined as >3 tumor cells, i.e., micro-metastases, (3 day time point); Quantification of GFP+ (**e**) single tumor cells as a percent of total tumor cell signal, (**f**) number of tumor cell clusters, and (**g**) size of tumor cell clusters at 1 and 3 days post-injection; One-way ANOVA; IHC quantification of GFP+ (**h**) tumor area and (**i**) multiplicity from mice euthanized 14 days after intraportal injection of 500,000 D2.OR-GFP tumor cells; Two-tailed Mann-Whitney test; (**j**) Timeline of tumor burden in nullip (black) and InvD2 (grey) mouse groups, showing "switch" from early (3 day) advantage in nullip to later (≥14 days) advantage in involution. * $p < 0.05$, ** $p < 0.01$.

Given our prediction that immune cells are involved in the involution metastatic advantage, we sought to profile the intra-tumor immune milieu. We interrogated tumor-bearing livers from nulliparous and involution stage mice 14 days after intra-portal injection of D2OR-GFP tumor cells, the earliest time point where the involution advantage was observed. CD45 staining revealed high levels of tumor infiltrating immune cells, but no differences between groups (Nullip: 12%, InvD2: 14%). Since immune cell abundance did not differ, we next asked whether the activation state of intra-tumoral CD4 or CD8 T cells differed by reproductive group, which could account for differential anti-tumor immune function. We stained for nine common leukocyte lineage and functional state markers (CD45, CD3, CD4, FoxP3, Ki67, PD1, Tox1, CD11b, and F480) using multiplex immunohistochemical (mIHC) methods. Representative pseudo-colored images of select biomarkers, including CK18 marking hepatocytes and some tumor cells, are shown (Figure 2-4A). Using image cytometry, we quantified various T cell and myeloid subsets as percentage of total CD45+ immune cells (Figure 2-4B) and performed hierarchical clustering by case (Figure 2-4C). We found that the profile of tumor immune infiltrate separated cases by reproductive stage of the host, with only one case each clustering outside of its reproductive group (Figure 2-4C). Of note, we found no relationship between tumor size and immune cell infiltrates (Figure S2 [2-8]), suggestive that tumor size alone does not dictate immune cell infiltrate in this model. In sum, these data support the idea that reproductive stage of the host shapes the composition of the intra-tumoral immune milieu with implications for anti-tumor immunity.

The mIHC analyses further revealed that overall, all of the metastatic tumors are "hot" as defined by high CD3+ cell infiltration (Figure 2-4A). The majority of CD3+ cells did not show signs of activation, such as the expression of Ki67 or PD1. There were two out of seven involution cases with CD3+ cells that expressed Ki67, PD1, and Tox1, potentially indicating immune activation with exhausted features [85,86]. We next investigated the intra-tumoral ratio of CD4+ to CD8+ T cells, since higher CD4:CD8 ratios associate with increased functional CD8+ T cell responses and better disease outcomes [87–89]. For these studies we define CD4 T cells as CD45+CD3+CD4+, and identify putative CD8 T cells as CD45+CD3+CD4−, herein referred to as CD8. We found higher CD4:CD8 ratios in tumors from nulliparous mice compared to tumors in involution mice (37:1 vs. 8:1). Finally, while CD3+ and CD3+CD4+ T cells were enriched in tumors from nulliparous hosts, CD45+CD3− (putative myeloid lineage cells) and F480+ cells (mature macrophages) were greater in tumors from involution hosts. Taken together, these data raise the possibility that the immune milieu of involution group tumors is characterized by low CD4 and high myeloid populations, which could result in impaired anti-tumor cytotoxic immunity.

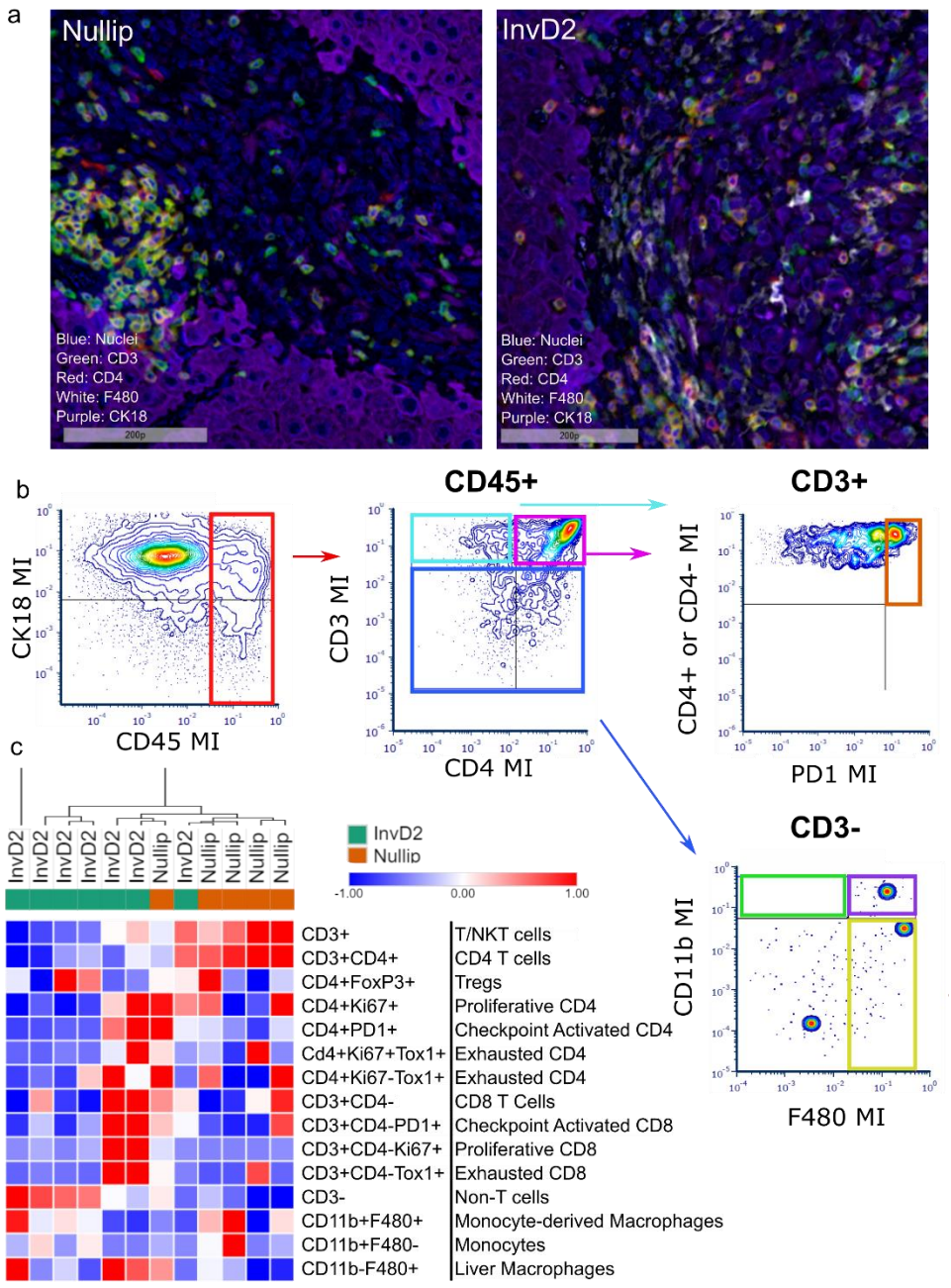

Figure 2-4 Immune milieu of liver metastases differs by host reproductive state.

(**a**) Representative pseudo-colored multiplex IHC images of liver metastases in nullip and InvD2 mice euthanized 14 days after intraportal tumor cell injection showing select biomarkers: nuclei (blue), CD3 (green), CD4 (red), F480 (white), and CK18 (purple); (**b**) Representative image cytometry gating schema, showing the identification of CD45+, CD3+/−, CD4+/−, and PD1+ populations; (**c**) Hierarchical-clustered heat-map of intra-tumoral immune cell populations (%CD45+) identified by image cytometry of multiplex IHC staining for 9 biomarkers (CD45, CD3, CD4, FoxP3, Ki67, PD1, Tox1, CD11b, and F480). Tumor data are reported as average per mouse.

A defining attribute of tumors in the involution group is that they evolved under unique micro-environmental conditions. Liver involution involves programmed cell death of hepatocytes and wound-healing like processes [56], which in other contexts are known to elicit suppression of cytotoxic adaptive immune response [90,91]. This is because phagocytosis of dying cells induces tolerogenic antigen presenting cell functions, which limit autoimmune reactions to the dying cell [90,91]. Based on these prior studies, we hypothesized that the liver metastatic niche during involution may be characterized by immune tolerance, which inadvertently permits tumor cell evasion. To address this hypothesis, we phenotypically assessed CD4+ T cells by flow cytometry at nulliparous, involution day 2, and involution day 6 with the prediction that T cell polarization would be de-pendent on reproductive state. We quantitated CD4+ T cells for expression of Th1, Th17, or regulatory (Treg) transcription factors, as well as PD1 (Figure 2-5A, Figure S3 [2-9]). Each reproductive stage showed a large population of RORgT+ T cells, which we classify as Th17-skewed; however, by involution day 6 (InvD6) this Th17 population had reduced prominence. At InvD6 we also found increased Tbet, PD1, and FoxP3+ CD4 T cells (Figure 2-5A), data consistent with inflammation (Tbet, Th1), T cell activation (PD1) and induction of a regulatory state (FoxP3+, Treg) in the normal, involuting liver.

One feature of immune tolerance is the inability of adaptive immune cells to proliferate in response to their cognate antigen, which can be robustly assessed in functional assays. To this end, we used an *in vivo* CD4+ T cell activation assay where we adoptively transferred ovalbumin antigen-specific CD4+ T cells (Do11.10, Figure S4 [2-10]) systemically and subsequently injected their cognate antigen (OVA) into the liver via intrahepatic injection (Figure 2-5B). Five days after ova or phosphate buffer saline

(PBS) control injection, ova-specific T cells were assessed by flow cytometry in both the liver and spleen as a measure of T cell activation. Representative flow cytometry plots are shown (Figure 2-5C,D, Figure S5 [2-11]). Firstly, we found that the nulliparous host liver responds to ova antigen with a 2-fold increase in ova-specific T cells compared to PBS controls (Figure 2-5E). Conversely, in the involution group there was no increase in ova-specific T cells after exposure to ova antigen compared to PBS, providing functional evidence for immune tolerance. Similar results were observed in the spleen (Figure 2-5F). These data raise the possibility that deficient adaptive immunity contributes to increased liver metastasis in the involution host, while intact adaptive immunity is partially responsible for limiting liver metastasis in nulliparous hosts.

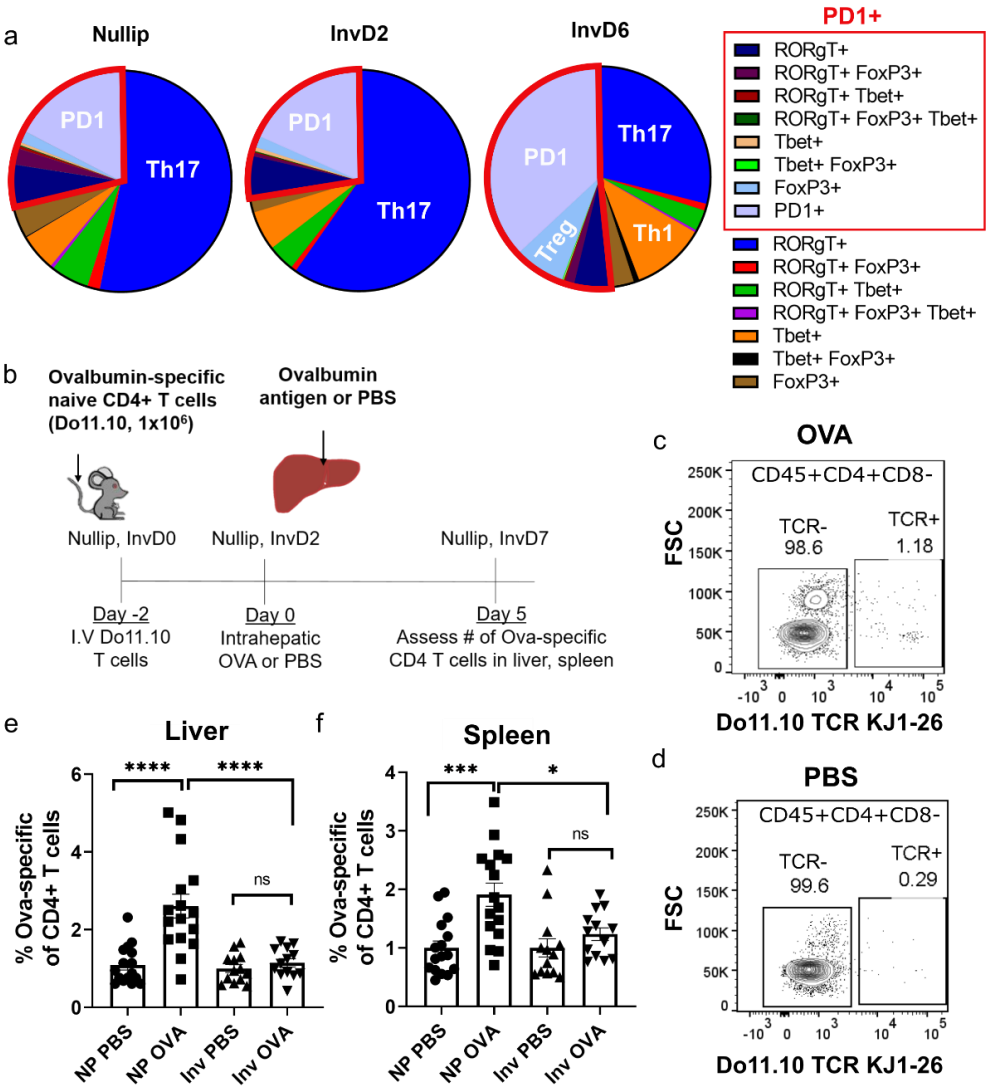

Figure 2-5 CD4+ T cell polarization is reproductive stage dependent with implications for antigen-specific activation.

(**a**) Flow cytometry phenotyping of CD45+ CD4+ T cells from livers of mice at nullip, InvD2, and InvD6 reproductive stages (nullip n = 8, InvD2 n = 5, InvD6 n = 6). Only CD45+ CD4+ T cells that expressed at least one of the four phenotyping markers RORgT, Tbet, PD1, or FoxP3 are shown (see Figure S3 for total CD45+CD4+ T cell polarization); (**b**) Experimental schema for the *in vivo* T cell activation assay (Figure S4 shows transferred CD4+ Do11.10 cells); Representative flow cytometry plots showing expression of ova-specific Do11.10 T cell receptor (TCR) in CD45+ CD4+ CD8- cells from mice intra-hepatically injected with (**c**) ovalbumin (OVA) antigen or (**d**) PBS; Flow cytometry quantification of ova-specific CD4+ T cells (Do11.10 TCR+) as %CD4+ in (**e**) whole liver or (**f**) spleen across 2 independent experiments (nullip PBS n = 16, nullip OVA n=15, InvD2 PBS n = 13, InvD2 OVA n = 13). Data normalized to PBS average for reproductive group, One-way ANOVA. * $p < 0.05$, *** $p < 0.001$, **** $p < 0.0001$.

If an adaptive immune response to tumor cells in nulliparous hosts contributes to reduced liver metastasis, then we expect depletion of CD8+ T cells to increase metastasis and possibly recapitulate the metastatic advantage observed in the involution group. In our portal vein liver metastasis model, nulliparous mice were either CD8+ T cell-depleted via intraperitoneal injection of anti-CD8 antibody (BioXcell clone 2.43, Lebanon, NH, USA) or treated with isotype control. Antibody dosing began two days prior to tumor cell injection (0.2 mg initial dose) and continued every four days for the course of the experiment (0.1 mg maintenance dose). This antibody dosing scheme was designed to minimize antibody concentration and effectively deplete CD8+ T cells in the liver, in order to mitigate possible off-target antibody effects (Figure S6 [2-12]). Depletion of CD8+ T cells (CD45+CD3+CD8+CD4−) in the liver was confirmed at study endpoint by flow cytometry with no discernable effect on CD4+ T cells (CD45+CD3+CD4+CD8−) (Figure 2-6A,B). Incidence and multiplicity of liver metastasis six weeks after injection increased in anti-CD8 treated nulliparous animals compared to isotype control (Figure 2-6C,D). Of note, multiplicity in the anti-CD8 treated nulliparous group was commensurate with multiplicity in the isotype treated involution group. These data are consistent with differential CD8+ T cell activation during involution contributing to the increase in metastatic outgrowth and multiplicity observed in the involution group.

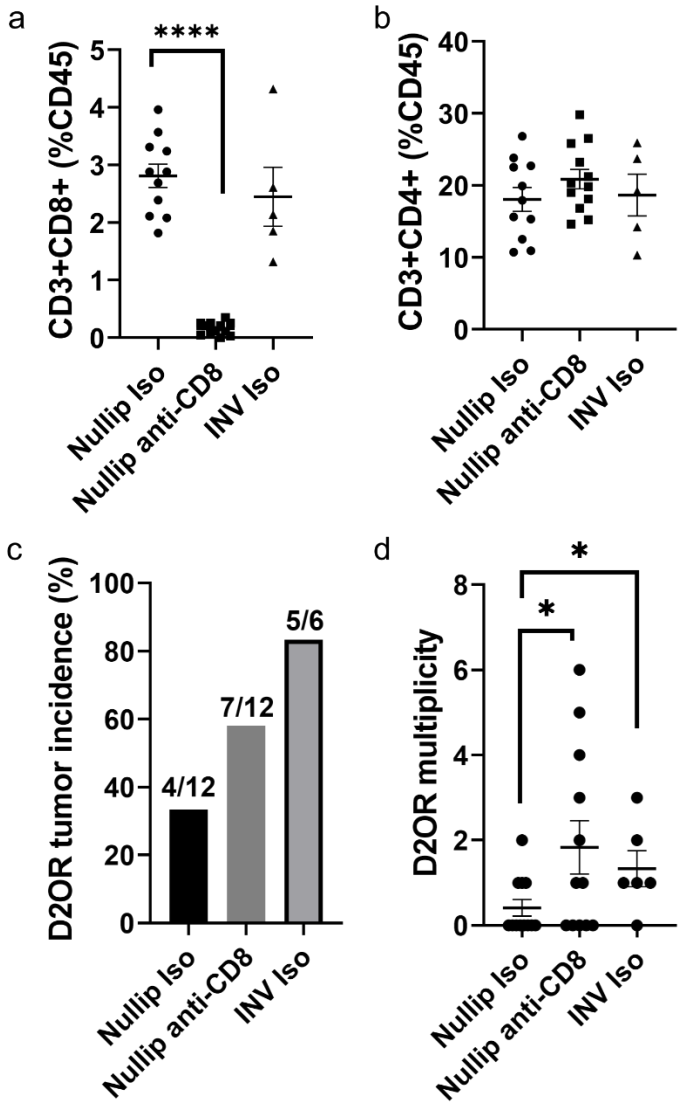

Figure 2-6 Depletion of CD8+ T cells in the nulliparous host recapitulates the involution metastatic advantage.

Flow cytometry quantification of (**a**) CD8 and (**b**) CD4 T cells from livers of mice at endpoint of 6 week metastases study where mice were treated with CD8-depleting or isotype control antibody demonstrating effective CD3+CD8+ T cell depletion; (**c**) Incidence and (**d**) multiplicity of D2.OR liver metastases 6 weeks after intraportal injection of 50,000 D2.OR tumor cells with and without CD8 depletion in nulliparous hosts. Nullip iso $n = 12$, Nullip anti-CD8 $n = 12$, INV iso $n = 6$. One-way ANOVA. * $p < 0.05$, **** $p < 0.0001$.

Discussion

Metastasis has historically been considered an intrinsic property of the cancer cell [92–95], which is in part enabled by a cancer cell's ability to reshape distant sites into favorable environments [66,67,70,74]. In line with this thinking, tumor-induced remodeling of the liver microenvironment has been well described [96,97]. Such tumor-education of the liver pre-metastatic niche includes macrophage and fibroblast activation that results in pro-metastatic inflammatory signaling and ECM protein deposition [71–73]. However, recently it has been posited that pro-metastatic liver niche remodeling could occur independent of a primary tumor, including processes such as liver repair and regeneration following injury [56,98]. Here, we provide further evidence of a physiologic process, weaning-induced liver involution, which induces a liver pre-metastatic niche.

Previously, it was demonstrated that liver metastases were promoted in postpartum mice using the fast-growing, metastatic-competent D2A1 mouse mammary tumor cell line [56]. In the present study, we find that the postpartum liver also supports metastasis of D2OR mammary tumor cells, a cell line with lower growth rate and demonstrated low metastatic potential [77,82]. An advantage of using a cell line with slow growth is that it may permit evolution of tumor cell-microenvironment interactions that are more reminiscent of what occurs in human disease.

Liver metastases can be categorized by growth pattern in relation to adjacent normal hepatocytes using a method developed for colorectal cancer liver metastases [79]. Three main growth patterns have been identified: desmoplastic, pushing, and replacement. Patients whose metastases had a dominant desmoplastic pattern were found to have longer overall and recurrence free survival compared to those with a dominant

replacement growth pattern [79,99]. In our study, we classified mouse mammary cancer liver metastases according to these guidelines. We found potential relevance to human disease, as the heterogeneous histological growth patterns reported in human liver metastases were observed. Use of this histological growth classification for liver metastases is not common in breast cancer. However, a recent study of 58 breast cancer patients found that the replacement pattern was dominant, and as in colorectal cancer liver metastasis, the desmoplastic pattern associated with longer overall survival [100]. Although we found approximately 14% of tumors with desmoplastic growth pattern in murine involution hosts and none in nulliparous hosts, our study was not designed to evaluate survival so we cannot deter-mine survival differences between tumor histologic patterns. While a key strength of our breast cancer liver metastasis model is the observation of a range of tumor histological patterns in the liver, how reproductive state influences these patterns and outcomes will require further investigation.

Tumor cell morphological properties such as cytoplasmic volume, roundness, and elongation have been implicated in metastatic potential [101,102]. These studies viewed tumor cell morphology as a cell-autonomous property, yet the microenvironment may also shape morphology [103,104]. Here, we observed distinct tumor cell morphological patterns based on host reproductive stage. Single, solitary tumor cells were more prevalent in the involution group. The high percent of single tumor cells in the involution host could be indicative of a more mesenchymal phenotype since they lack cell-cell adhesion with other tumor cells and show elongated morphology. In contrast, tumor cell clusters, indicative of tumor epithelial cell interactions, were increased in nulliparous host livers. Further, we have reason to believe the involution liver could preferentially support

tumor cell epithelial-to-mesenchymal transition (EMT). The involution liver has significantly elevated TGFβ and ECM proteins tenascin-C and fibronectin, which are all known to mediate EMT [56,105–107]. Promotion of tumor cell EMT by the involution microenvironment is intriguing, given the connection between mesenchymal state and metastatic promotion [107], including evasion of the immune system [108–111]. Our work does not directly test the potential of tumor clusters versus single cells in the liver environment to form overt metastases. However, our data are consistent with an advantage to the solitary tumor cells since there are more metastatic events in the involution group at study endpoint. Additional studies are needed to explore the relationship between the presence of early single tumor cells and metastatic success in this model.

We show in both D2OR and D2A1 models that liver metastatic advantage involves increased metastasis incidence and multiplicity in involution hosts, which appears to occur without a tumor cell proliferation advantage. Seeing no proliferation advantage, we predicted that the involution microenvironment increases a tumor cell's chance of successfully forming a metastasis, and used the metastatic cascade as framework to investigate this possibility [69,70]. The metastatic cascade describes how a tumor cell escapes the primary site and arrives at a secondary organ, then must lodge, extravasate, survive, form micrometastasis, and grow in order to become a metastatic tumor [69,70]. Prior work has shown that late stages (i.e., after arrival at the secondary organ) are rate-limiting for meta-static success [112,113].

We initially hypothesized that the involution advantage would be evident early, at the tumor cell extravasation, survival, and/or proliferation steps, due to the known, pro-metastatic ECM remodeling that occurs in the liver post wean [56]. The rodent involuting

liver is enriched for collagen I, fibronectin, and tenascin-C [56,114], ECM proteins demonstrated to promote establishment of tumor cells in the niche [115–119]. However, we found no evidence for involution-specific ECM proteins contributing to these early, metastatic events. Specifically, no differences in tumor cell abundance were observed between groups at days one and three post portal vein injection, time points when tumor cells become established in the niche. Rather, the involution metastatic advantage was observed at 14 days after tumor cell injection. This timeframe is consistent with the involuting liver promoting a later step in the metastatic cascade, at the transition from a micro- to an overt metastatic lesion.

Suppression of anti-tumor immunity is one potential mechanism by which the involuting liver promotes tumor growth from micro- to overt metastasis. Others have shown that the liver pre-metastatic niche is characterized by alteration to innate immune composition, including elevated neutrophils, bone marrow-derived myeloid cells, and M2-polarized macrophages [97,120]. Adaptive immune cells, including CD4+ Th17 polarized and T regulatory (Treg) cells, have also been shown to play a functional role in promoting liver metastasis [121,122]. These innate and adaptive immune cell populations sup-port metastasis in part by limiting anti-tumor immunity via active suppression of the cytotoxic T cell response [123]. In previous work from our lab, we showed that the involution liver has increased abundance of neutrophils, immature monocytes, and macrophages compared to the nulliparous liver [56]. Here we build on that dataset to show that CD4+ Th17 polarized T cells are abundant in the murine liver regardless of reproductive state. Furthermore, CD4+ T cell polarization is modulated by reproductive state with the nor-mal, involuting liver being characterized by Th1-skewed inflammation,

upregulation of the checkpoint molecule PD1, and increased abundance of Tregs. This immune composition data demonstrate that the involution liver has most of the immune characteristics attributed to a tumor-educated pre-metastatic niche [120]. Further, utilizing a functional in vivo T cell activation assay, we identify immune tolerance as a new attribute of weaning-induced liver involution, similar to what was recently described in the mammary gland during weaning-induced involution [81].

We propose that the stimulus for tolerance mechanisms is the hepatocyte programmed cell death that occurs post wean to return the pregnancy and lactation-enlarged liver to its pre-pregnant size [56]. Such programmed cell death is considered "immuno-logically silent" [90,91]. This immune tolerization is achieved in part via signaling from the apoptotic cell to the antigen presenting cell (APC), which results in reduction of the co-stimulatory signals on the APC typically required for T cell activation[81,124]. An additional, unexplored possibility is that the unique ECM composition of the involuting liver contributes to regulation of the immune milieu. It is known that collagen, fibronectin, and tenascin-C can regulate immune cell trafficking and function[125], including recruitment of immature monocytes[73] and suppression of T cell activation [126]. These published reports provide further rationale for the matrisome of the involuting liver contributing to impaired anti-tumor immunity, although such a possibility requires future study. In sum, these studies of normal involuting liver provide evidence for both T cell inflammation and tolerance, with implications for tumors emerging in this environment.

Clinically, tumors that are classified as "hot" (i.e., those with robust T cell infiltration) are associated with better prognosis, most likely due to anti-tumor effects of CD3+ T cells [127,128]. In our murine model of breast cancer liver metastasis, we find that

the majority of tumors were CD3+ “hot”, indicating that T cells were able to enter tumors in both nulliparous and involution hosts. While robust intratumoral CD3+ infiltration is typically a positive biomarker for disease prognosis, in our mouse model the majority of tumors in involution hosts and ~1/3 of tumors in nulliparous hosts grew into large metastatic lesions. This paradox could indicate that the effector status of CD3+ cells is differentially compromised by reproductive state, a premise supported by the observation that nulliparous and involution tumors delineated by immune profiling. Specifically, tumors that evolved in involution host livers had lower CD4:CD8 ratios, increased myeloid infiltration, and increased exhaustion markers including PD1 and Tox1 [85,86]. Our finding that depletion of CD8+ T cells in the nulliparous host recapitulates the involution metastatic advantage provides further rationale for the hypothesis that ineffective anti-tumor immunity contributes to the involution metastatic advantage. Whether liver metastases in young women’s breast cancer show similar pro-tumor patterns of tumor immune infiltrates remains to be determined.

The results presented here may have significance for a recently appreciated type of aggressive, young women’s breast cancer called postpartum breast cancer (PPBC) [36,37,129]. A diagnosis of breast cancer within five years of a recent pregnancy is an independent predictor of liver metastasis, which suggests that the postpartum liver may be uniquely susceptible to metastasis as we demonstrate in the rodent models[56]. In support of this hypothesis, we recently found that the size of the human liver is regulated by reproductive state and provided the first data suggesting that weaning-induced liver involution may occur in women[130]. Since we report in the rodent model a relationship between immune composition in the normal involution liver and resulting tumor immune

infiltrate, such a paradigm may also exist in human breast cancer liver metastasis. If so, the rodent studies provide evidence that PPBC liver metastasis may involve immune modulation and be responsive to immune checkpoint therapies. While checkpoint blockade immunotherapy must be tested in preclinical models, our findings could help direct much-needed new treatments for breast cancer liver metastases in young women.

Conclusions

Here we provide the first evidence for reproductive state dependent CD4+ T cell activation in the normal murine liver, including induction of tolerance during weaning-induced liver involution. Further, we show that the immune milieu of mammary tumors evolving within the involuting liver microenvironment are durably altered in a manner consistent with tumor promotion. Our data supports the hypothesis that ineffective anti-tumor immunity within the involuting liver contributes to increased breast cancer liver metastasis. Taken together, our data provide a compelling argument for host reproductive factors being determinative for liver metastasis in the postpartum period with specific implications for young women's breast cancer. Further, weaning-induced liver involution may serve as a robust model to investigate initiation and treatment of liver metastasis with potential utility for liver metastases overall.

Supplementary Figures

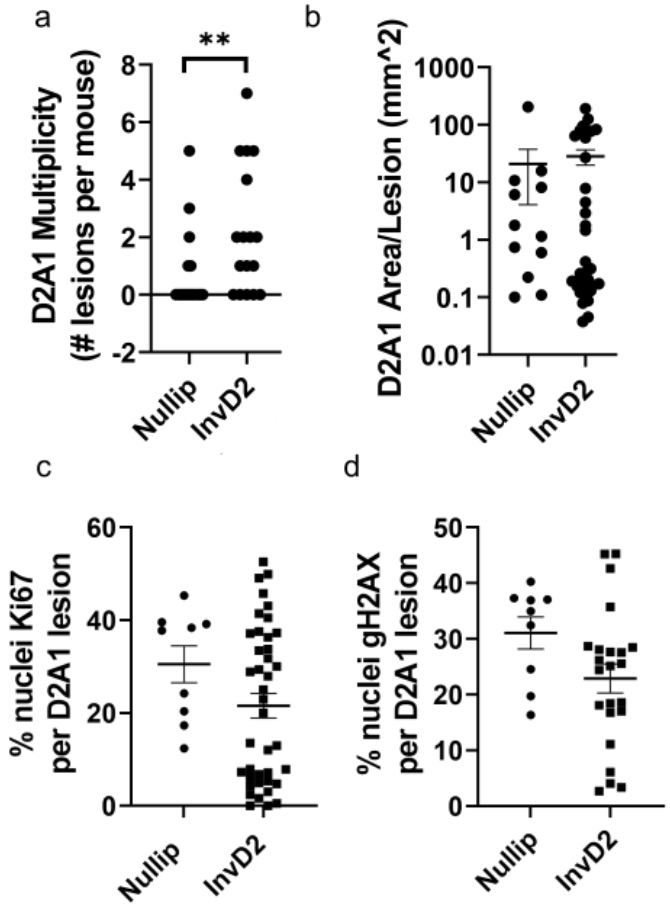

Figure 2-7 Increased D2A1 metastasis in involution hosts does not associate with enhanced tumor growth.

(a) Number and (b) area of D2A1 metastases per mouse in nullip (n=27) and InvD2 (n=17) groups; Two-tailed T test; IHC quantification of percent of tumor nuclei positive for (c) Ki67 and (d) γH2AX. **p<0.01. Figure a and b modified from Cancer Discovery DOI: 10.1158/2159-8290.CD-16-0822.

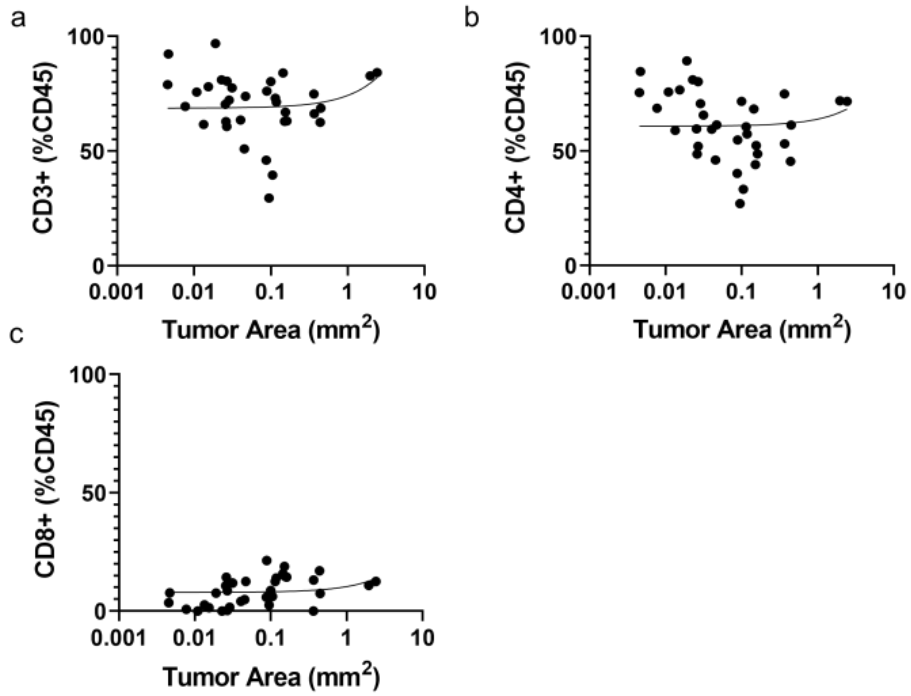

Figure 2-8 Tumor immune infiltrate does not correlate with tumor size.

Pearson's correlation of tumor area (mm2) with (a) CD45+CD3+, (b) CD45+CD3+CD4+, and (c) CD45+CD3+CD4- (putative CD8+) cells captured by multiplex IHC image cytometry.

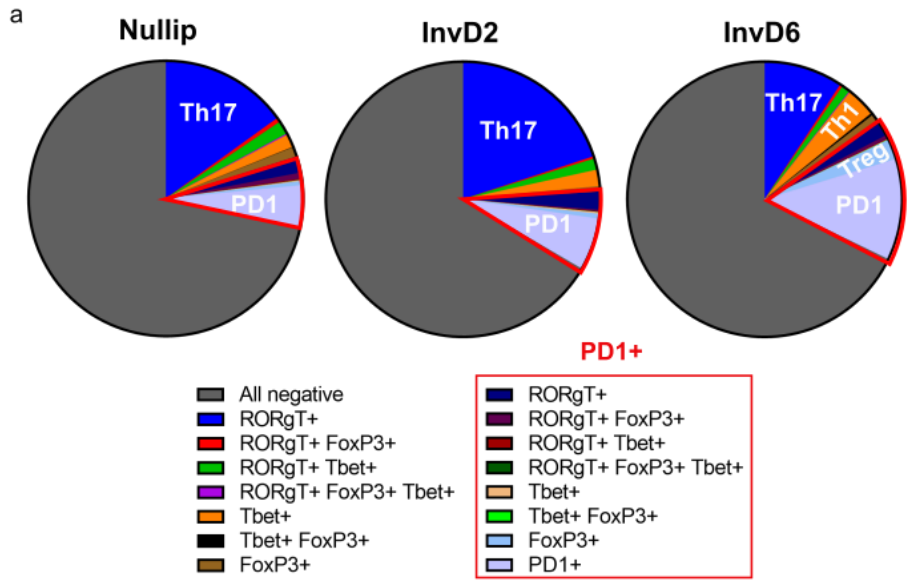

Figure 2-9 CD4+ T cell polarization is reproductive stage dependent.

Flow cytometry phenotyping of CD45+ CD4+ T cells from livers of mice at nullip, InvD2, and InvD6 reproductive stages (nullip n=8, InvD2 n=5, InvD6 n=6). Data represent percent of total CD45+CD4+ T cells.

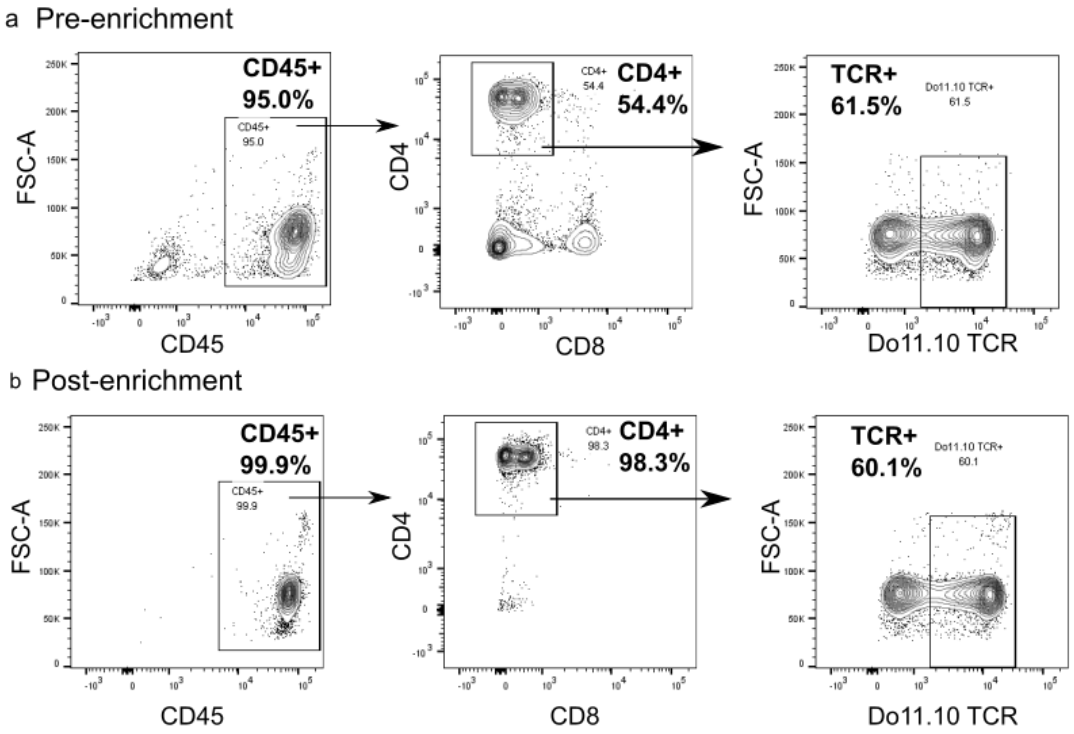

Figure 2-10 Representative flow cytometry plots demonstrate enrichment of CD4+ cells from whole spleen for adoptive transfer in vivo T cell activation experiment.

Flow cytometry plots for CD45+, CD4+, and Do11.10 TCR+ in isolated splenocytes from Do11.10 transgenic mice (a) pre- and (b) post-enrichment with CD4+ negative selection kit.

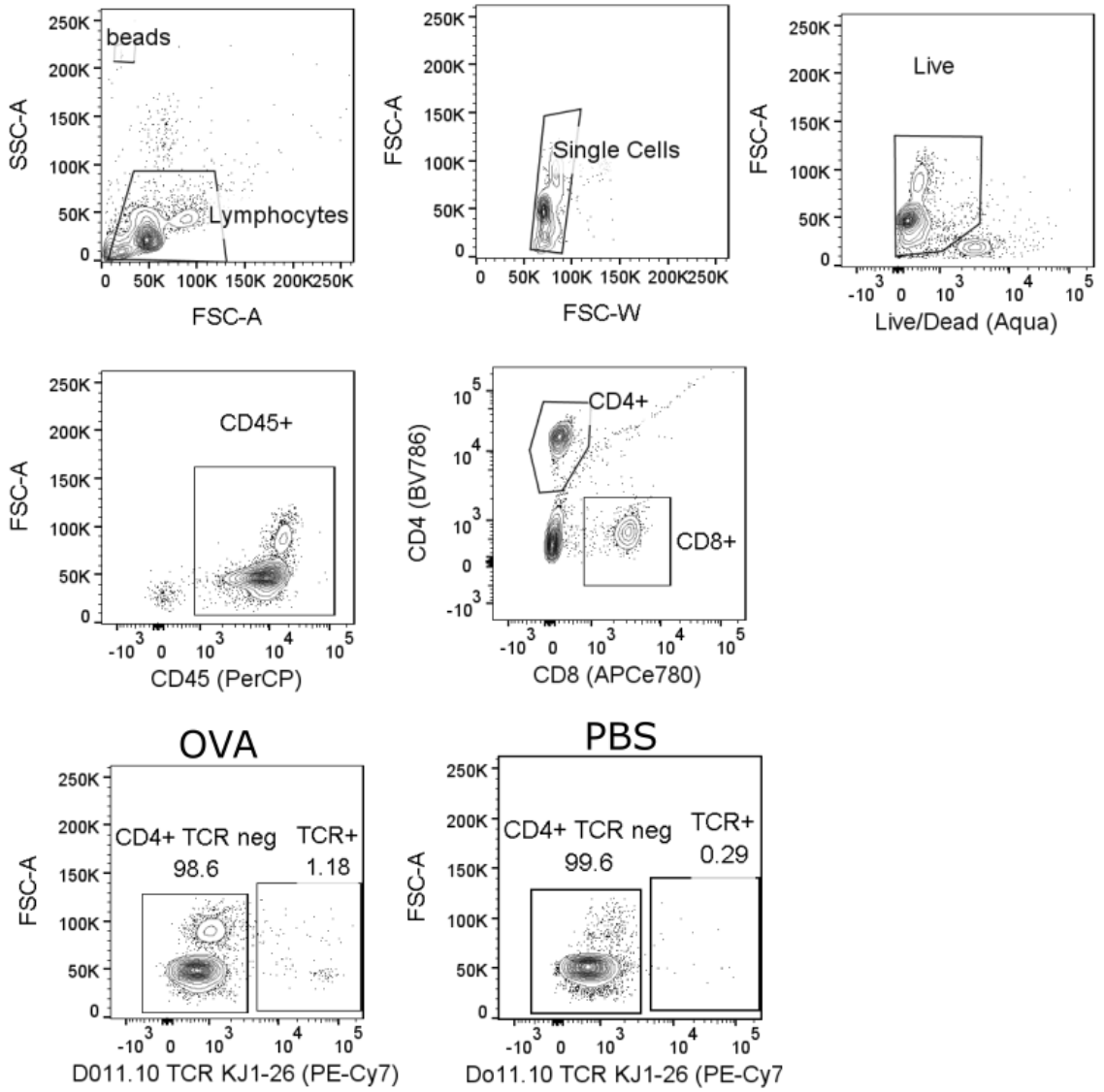

Figure 2-11 Representative flow cytometry gating for adoptive transfer in vivo T cell activation experiment.

Flow cytometry gating scheme for lymphocytes, single cells, live cells, CD45+, CD4+, and CD8+ (upper five panels), and CD4+TCR+/- in the presence of OVA antigen or PBS control (bottom two panels).

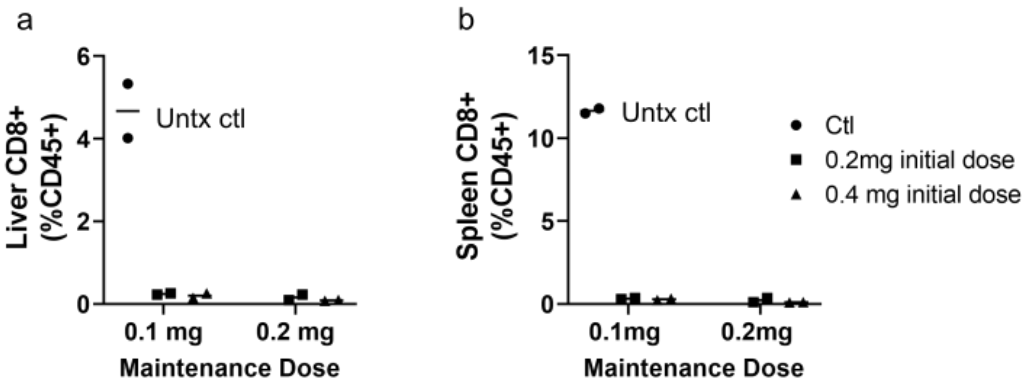

Figure 2-12 Evidence that lowest initial and maintenance dose concentrations of CD8-depleting antibody effectively depletes CD8+ T cells in the liver and spleen.

Flow cytometry quantification of CD45+CD3+CD4-CD8b+ T cells in the (a) liver and (b) spleen with different combinations of CD8-depleting antibody concentrations: initial dose: 0.0mg, 0.2mg, 0.4mg and maintenance dose: 0.0mg, 0.1mg, 0.2mg. Circle symbol represents untreated controls (0.0mg), square symbol represents 0.2mg initial dose, and triangle symbol represents 0.4mg initial dose. The lower initial (0.2mg) and lower maintenance (0.1mg) dose concentrations resulted in same level of CD8+ depletion as higher dose combinations.

Funding

This research was funded by the following grants to PS: Department of Defense grant #BC170206, Department of Defense grant #BC191620, Eccles Foundation, and funds from the Knight Cancer Institute (KCI). This work was also supported by the KCI Cancer Center Support Grant P30CA69533. AQB was partially supported by the following: Ruth L Kirschstein T32 “PERT” Training Grant, Achievement Rewards for College Scientists (ARCS) Foundation, and the OHSU Cancer Biology Graduate Program Student Stipend Award.

Acknowledgments

The authors want to thank Andrea Calhoun for superior histologic support in the multiplex IHC studies, Nina Fletcher for IHC staining of D2A1 metastases, and Erica Goddard for going above and beyond reasonable expectation to run flow cytometry samples for the CD8 depletion study during the Covid-19 lab shutdowns. The authors are grateful to Weston Anderson for outstanding assistance with manuscript writing, editing, and preparation.

Chapter 3 : Evidence for liver remodeling during pregnancy and postwean in women

Preamble: Overarching question and approach

A nontrivial assumption in the overall hypothesis that postwean involution promotes liver metastases in postpartum breast cancer patients is that weaning-induced liver involution occurs in women. While we have established that the rodent liver undergoes weaning-induced involution in rats and mice, it is yet unknown if the same is true in women. At its most fundamental, involution returns the pregnancy and lactation enlarged liver to its pre-pregnant size. Thus, it is expected that if the human liver undergoes involution it must also increase in size during pregnancy; however, this too is unknown. There is reason to think that the liver changes in size with pregnancy in women, as products made by the liver are increased during pregnancy [131,132]. Here, we sought to determine if human liver size increased with pregnancy and decreased post-wean. While such data would support our overall hypothesis, it would also be novel and potentially highly impactful for the field of obstetrics and maternal health.

The study design required healthy pregnant women to be followed over the course of their pregnancy and postpartum. Women were enrolled prospectively at the time of becoming pregnant, attended multiple study visits at early (~12-16 weeks) and late pregnancy (~32-36 weeks) time points, and had the option to return for a study visit ~3 months after weaning. This study design involved coordination with a transdisciplinary team made up of a physician specializing in obstetrics and gynecology, a physician-scientist in cardiology and endocrinology, a radiologist, clinical coordinators, a scientist with expertise in bile acid analyses, statisticians, and basic biology researchers.

The study team worked across two different institutions and required two Institutional Review Board (IRB) protocols – one at each institution. I was responsible for maintaining the IRB at OHSU, including submitting modifications and writing the annual renewal. Additionally, I developed a "lactation survey", which was designed to capture lactation output and duration. These data were important, because we expected liver size to be maintained during lactation due to high metabolic demand of milk production. If there were problems with lactation, there could be an impact on post-wean liver size. Before rolling out the lactation survey to study participants, I performed beta-testing with study team members who themselves previously nursed to ensure questions were clear and written to yield the data we needed. The lactation survey was IRB-approved and subsequently used in this study. The resulting data gave context to our results, but ultimately was not included in the submitted manuscript.

Reprinted from Submitted Manuscript – under review at PNAS

"Pregnancy and weaning regulate human maternal liver size and function"

Alexandra Q Bartlett, Kimberly K Vesco, Jonathan Q Purnell, Melanie Francisco, Erica Goddard, Andrea DeBarber, Michael C Leo, Eric Baetscher, William Rooney, Willscott Naugler, Alex Guimaraes, Patrick Catalano, Pepper Schedin

Contributions

AQB and PS wrote the paper. AQB, KKV, JQP, EG, AG, and PS designed research. AQB, KKV, JQP, EG, AD, EB, WR, and WN performed research. AD contributed new analytical tools. AQB, KKV, JQP, MF, EG, MCL, EB, PC, and PS analyzed data.

Abstract

During pregnancy, the rodent liver undergoes hepatocyte proliferation and increases in size, followed by weaning-induced involution via hepatocyte cell death and stromal remodeling, creating a pro-metastatic niche. These data suggest a mechanism for increased liver metastasis in breast cancer patients with recent childbirth. It is unknown if the human liver changes in size and function during pregnancy and weaning. In this study, abdominal imaging was obtained in healthy women at early and late pregnancy, and post-wean. During pregnancy time points, glucose production and utilization, and circulating bile acids were measured. Independent of weight gain, most women's livers increased in size with pregnancy, then returned to baseline post-wean. Putative roles for bile acids in liver growth and regression were observed. Together, the data support the hypothesis that the human liver is regulated by reproductive state with growth during pregnancy and volume loss post-wean. These findings have implications for sex-specific liver diseases and for breast cancer outcomes.

Introduction

Sex-specific differences in liver disease have been attributed to sexual dimorphisms in steroid production, metabolic enzymes, and behavior patterns [133]. Whether a pregnancy cycle contributes to sex-specific liver disease remains largely unexplored; however, a previously unrecognized liver biology linked to reproductive status has been reported in rodents [56]. This study found that during pregnancy and lactation, hepatocytes proliferated and entered a higher anabolic state accompanied by an overall increase in liver size. Upon weaning, hepatocytes rapidly underwent programmed cell death, liver metabolism shifted towards catabolism, and the liver regressed to its pre-pregnant size in a process

referred to as weaning-induced liver involution [56]. In mice, liver involution promoted breast cancer metastasis to the liver, suggesting a pathophysiological consequence of liver involution [56,134].

Notably, young women diagnosed with breast cancer in the postpartum period were found to be at increased risk for liver metastasis [56]. Taken together, these findings suggest that weaning-induced involution, which we predict would return the enlarged liver to its pre-pregnant, pre-lactational state, may create a pro-metastatic liver niche in women. However, it is unknown whether the human liver changes in size and function across a reproductive cycle, as expected if the liver is tuned to meet the unique metabolic demands of pregnancy, lactation, and weaning. Such evidence would corroborate findings in rodents and would be foundationally important for future studies of liver health in women.

To investigate the impact of reproductive state on liver size and function in women, we conducted a prospective study of healthy pregnant women using magnetic resonance and spectroscopy imaging of the liver and compared findings to a validated rodent model. Here, we show that the human female liver is regulated in both size and function by reproductive state, and provide the first evidence of weaning-induced liver involution in humans. Further, our data provide a hypothesis to explain the increased liver metastasis observed in postpartum breast cancer patients, as well as having potentially broader implications for the understanding of sex-specific liver diseases.

Materials and Methods

Recruitment

We conducted a prospective cohort study of pregnant women receiving care at Kaiser Permanente Northwest (KPNW), or Oregon Health & Science University (OHSU). All study activites were approved by Institutional Review Boards at KPNW (#3993) and OHSU (#10438 and #15264). Recruitment started in December 2014 and was completed in August 2017. KPNW members who met the study inclusion criteria were identified weekly using the electronic health record (EHR). Eligible participants were mailed a recruitment letter and received a follow-up phone call a week later. During this telephone call, study personnel conducted additional eligibility screening and scheduled an explanatory visit. If patients consented at the explanatory visit, this was followed by two visits between 12-16 weeks of gestation and two visits between 32-26 weeks of gestation.

Inclusion/Exclusion criteria

Patients were eligible for the study if they were between 18-45 years of age; were less than 14 weeks pregnant with a singleton gestation at time of enrollment; had a BMI between 18.5 kg/m^2 and 38 kg/m^2; and were fluent English speakers. Participants were excluded if they had any of the following conditions or symptoms: contraindications to MRI study (e.g., claustrophobia, metal implants); pregestational diabetes; gestational diabetes; history of bariatric surgery or other medical conditions requiring specialized nutritional care; anemia; current history of drug, tobacco, or alcohol use; maternal rheumatologic or chronic inflammatory state; or chronic hypertension.

Measures

Data for this paper were collected at two study visits: one at 12-17 weeks of gestation, and one at 32-36 weeks of gestation. Height was measured at the first visit to allow for calculation of BMI; weight was measured using a calibrated scale at each visit.

Demographic variables, including parity and preconception BMI, were extracted from the electronic medical record.

Liver Volume Determination

Magnetic resonance imaging was performed on a Siemens 3T Vereo using an 8 channel phased array torso body coil. The protocol included a volume interpolated 3D gradient echo sequence for 3D volume estimates of the liver (256x192 encoding matrix, asymmetric field of view 30 x 24, TE/TR 2.4/5ms, and voxel size 1.17 x 1.17 x 2.5mm).

Image analysis was performed using OsiriX (OsiriX Imaging Software, Geneva, Switzerland) software and Image J software (National Institutes of Health). For volume estimation, 3D-VIBE (a T1 weighted FLASH technique with fat selective prepulse) sequences were used. The liver was identified on each image, and the outline of the liver tissue annotated by freehand region of interest estimation by operators trained by a body radiologist with over 10 years of experience in MRI of the liver. This allowed for the generation of a liver area on each slice. Liver volume was calculated by multiplying the estimated area of each slice by the interval between slices, summing all volumes containing liver for the total liver volume [135].

Liver volume determinations were performed by 2 blinded operators. Operators independently measured liver volumes for 5 cases with 2 MRI scans per case (early and late pregnancy). The observed inter-operator variability (Table 3-1) was used to benchmark values that are within the range of measurement error, in this case +7 to -7 percent.

Table 3-1 Inter-operator variability in liver volume measurement

Case	Output	Operator #1	Operator #2	Difference between operator #1 and #2
100283	Early Pregnancy (cm^3)	1142	1143	1
	Late Pregnancy (cm^3)	1376	1341	-35
	Late-Early (cm^3)	234	198	-36
	% Change	20.5	17.3	**-3.2**
100445	Early Pregnancy (cm^3)	948	986	38
	Late Pregnancy (cm^3)	982	999	17
	Late-Early (cm^3)	34	13	-21
	% Change	3.6	1.3	**-2.2**
100515	Early Pregnancy (cm^3)	1203	1268	65
	Late Pregnancy (cm^3)	1727	1709	-18
	Late-Early (cm^3)	524	441	-83
	% Change	43.6	34.8	**-8.7**
100662	Early Pregnancy (cm^3)	1015	1026	11
	Late Pregnancy (cm^3)	971	966	-5
	Late-Early (cm^3)	-44	-60	-16
	% Change	-4.33	-5.89	**-1.55**
101089	Early Pregnancy (cm^3)	1300	1322	22
	Late Pregnancy (cm^3)	1835	1816	-19
	Late-Early (cm^3)	535	494	-41
	% Change	41.2	37.3	**-3.8**
		Average Difference in % Change		**-3.9**
		Standard Deviation in % Change		**2.8**

Air Displacement Plethysmography (ADP)

Air displacement plethysmography (BOD POD, COSMED USA, Inc., Concord, CA) was used to determine participants' fat mass, fat free mass, and percent body fat at each visit. Participants first changed into a bathing suit or spandex clothing and a swimming cap. They then sat inside the BOD POD while the air displaced by the body was measured. Results included total mass and body density. Fat mass and fat-free mass were estimated using van Raaj's pregnancy equations to account for changes in the density of fat-free mass during pregnancy [136,137].

Magnetic resonance imaging acquisition

Magnetic resonance imaging and spectroscopy data were collected using a Siemens Prisma Fit 3T whole-body system (Siemens Healthineers, Erlangen, Germany) at the Advanced Imaging Research Center at Oregon Health & Science University. Abdominal MR data were acquired in two stations, the first centered at umbilicus and the second centered over the sternal notch, to acquire MRI and liver MRS. Siemens flexible 18-channel array and spine array receiver coils with body-coil transmission were used. The abdominal MRI protocol included a T1-weighted gradient-echo sequence (TE = 2.5ms, TR = 140ms, flip-angle = 90 degrees, $(1.25mm)^2$ in-plane resolution, 30-slices with 6mm thickness) acquired in 2-breath holds of ~18 sec each. The liver T1-weighted MRI protocol was acquired with identical parameters to the abdominal T1 volume, but with a variable number of slices to cover the entire extent of the liver.

Magnetic resonance imaging processing

The T1-weighted MRI data sets of abdomen and liver were manually spliced together with affine-transformations and overlapping slice elimination. The top of the liver and the

L-4/5 intervertebral disk were identified as the upper and lower bounds, respectively, for the segmentation analysis for abdominal visceral and subcutaneous fat volumes.

Abdominal T1-w MRI volumes were segmented into five classes: unlabeled, subcutaneous adipose tissue (SAT), visceral adipose tissue (VAT), muscle, and organ (including all other abdominal volume). A custom Python pipeline was used to create an initial automated segmentation using inputs from the umbilicus T1-weighted volumes, the liver T1-weighted volumes, and an 11-slice manual segmentation label map, the merged T1-weighted MRI data set, and the affine transforms that map individual volume acquisitions to the merged image space. Manually generated uterus/placenta and liver masks were created as these two regions have high rates of false-positives for classification as adipose tissue.

Processing within the pipeline made use of the following Python libraries: Nipype [138], the Advanced Normalization Tools (ANTs) [139], the Insight Toolkit (ITK)[140], Scikit-image [141], Scikit-learn [142], and SciPy [143]. Following N4 bias field correction, steps in the segmentation pipeline relied upon intensity thresholding and morphological operations. The muscle mask was generated with a compact watershed algorithm seeded with the muscle mask from the 11-slice segmentation. Subcutaneous adipose tissue masking made use of the geodesic active contours (GAC) algorithm [144], coupled with dilation and erosion steps to distinguish the SAT from internal VAT. Visceral adipose tissue was taken as the difference between the total adipose mask and the SAT mask. Segmentation masks output from the automated pipeline subsequently underwent slice-by-slice manual review followed by manual refinement by a single analyst (JQP) using the 3D Slicer software package to ensure accuracy of VAT and SAT masks placements.

Liver segmentation was manually conducted separately using the Osirix and Image J software programs.

Magnetic resonance spectroscopy

Intrahepatic lipid (IHL) was measured using 1H single-voxel magnetic resonance spectroscopy (MRS), following MR imaging. Liver MRS voxels were positioned within the right lobe with voxel sizes ranging from 18 to 24 cm^3.

Liver spectra were collected using a PRESS single voxel spectroscopy (SVS) sequence (TR = 5 s, TE = 30 ms, 1,024 points, 2,000 kHz spectral width). The long repetition time ensured fully relaxed water signal (99.2%), because it serves as an internal standard for quantification. Three separately-acquired MRS series were run, each during a 10-second breath hold.

MRS analysis was conducted using the AMARES time-domain fitting module within the jMRUI software program. All spectral fits were inspected and rerun with additional constraints if fitting contained errors. IHL is expressed as a proportion of primary lipid peak to water peak areas.

Hyperinsulinemic-euglycemic clamp

Hyperinsulinemic-euglycemic clamp with co-infusion of [6,6-2H2] glucose was used to determine whole body and skeletal muscle insulin sensitivity (Rd) and endogenous glucose production (EDP) [145,146]. Subjects were advised regarding a standard diet consisting of 30% of total calories from fat sources, 15% from protein, and 55% from carbohydrates for the three days before study. Following an 11-hour overnight fast, subjects were admitted to the OHSU CTRC where a hyperinsulinemic-euglycemic clamp will be performed. At 0600 hr, an intravenous catheter was placed in one arm for

infusions and in the contralateral hand for blood withdrawal and warmed to 70°C using a warming mitt for sampling of arterialized venous blood. A primed constant infusion of [6,6-2H2] glucose (Cambridge Isotope Laboratories, Andover, MA) was infused at 0.133 ml/min and an enrichment intended to achieve ~1.0 mol percent excess for all subjects. The basal infusion of [6,6-2H2] glucose was continued for 2hr, and plasma samples were obtained from 90 to 120 minutes to estimate basal endogenous glucose production and fasting insulin concentration. Basal endogenous glucose production (EGP) was calculated according to the steady-state equations of Steele [147]. At the completion of the 2-hr infusion glucose isotope, a primed, constant infusion of regular insulin at 40 mU/m2/min was started. Plasma glucose was maintained at 90 mg/dl for the remaining 2 hours. During the final 30 minutes of the clamp, blood samples were obtained every 5 minutes for isotope analysis. Suppression of endogenous glucose production by insulin infusion during the 2-hr clamp was estimated using the method developed by Black [148]. EGP, Rd, and M-value were adjusted for insulin level (mU/L) and fat free mass (kg).

Labs

Venipuncture was used to obtain blood samples with participants in the fasting state. The following measures were assessed and run in the Laboratory Core of the Oregon Clinical and Translation Research Institute (OCTRI): comprehensive metabolic panel, lipid panel, free fatty acids, liver function tests, glucose, and insulin. Insulin was assessed by radioimmunoassay (Mercodia AB, Uppsala Sweden and glucose by a Hexokinase based colorimetric assay (Stanbio laboratory, Boerne Tx 78006).

Bile Acid Profiling

Bile acid profiling was performed in the OHSU Bioanalytical Shared Resource/Pharmacokinetics Core. Plasma samples from early and late pregnancy were utilized to quantify plasma bile acids and 7alpha-hydroxy-4-cholesten-3-one using liquid chromatography-tandem mass spectrometry (LC-MS/MS) performed with a 4000 QTRAP hybrid triple quadrupole-linear ion trap mass spectrometer (SCIEX) operating with electrospray ionization (ESI) in the negative mode. The mass spectrometer was interfaced to a Shimadzu HPLC system consisting of SIL-20AC XR auto-sampler and LC-20AD XR LC pumps. Analyte separation was achieved using a gradient HPLC method and Luna 2.5u C18(2)-HST 50x2 mm column (Phenomenex) kept at 50°C with a Shimadzu CTO-20AC column oven.

The stable isotope dilution LC-MS/MS method to quantify plasma bile acids was previously described [149]. In brief plasma was spiked with internal standards and bile acids were measured following protein precipitation and extraction with methanol, centrifugation and filtration of the supernatant. Calibrants were prepared in charcoal stripped matrix (SP1070 from Golden West Biological) using authentic bile acid and conjygate standards (obtained from Toronto Research Chemicals and Cerilliant).

Data were acquired using SCIEX Analyst 1.6.2 and analyzed using SCIEX MultiQuant 3.0.3 software. Sample values were calculated from calibration curves generated from the peak area ratio of the analyte to internal standard versus analyte concentration that was fit to a linear equation with 1/x weighting. The following bile acids were measured: Taurocholic acid (TCA), Glycocholic acid (GCA), Taurochenodeoxycholic acid (TCDCA), Glycochenodeoxycholic acid (GCDCA),

Ursodeoxycholic acid (UDCA), Cholic acid (CA), Chenodeoxycholic acid (CDCA), Deoxycholic acid (DCA), and Lithocholic acid (LCA).

Plasma 7alpha-hydroxy-4-cholesten-3-one was determined by liquid chromatography-tandem mass spectrometry (LC-MS/MS) following protein precipitation and extraction with acetonitrile. To each 100 µl sample of EDTA plasma was added 1 ng of internal standard 7alpha-hydroxy-4-cholesten-3-one-d7 (prepared at 0.2 ng/µl in methanol) and 300 µl of acetonitrile. The samples was vortex mixed and centrifuged at 12,000 xg for 10 min. The supernatant was removed and filtered prior to injection for analysis with LC-MS/MS.

Calibration standards were prepared across the range 1 to 100 ng/ml in charcoal stripped plasma SP1070 (Golden West Biological) using authentic 7alpha-hydroxy-4-cholesten-3-one (obtained from Toronto Research Chemicals).

LC-MS/MS was performed using a 5500 Q-TRAP hybrid triple quadrupole-linear ion trap mass spectrometer (SCIEX) with electrospray ionization (ESI) in the positive mode. Shimadzu HPLC system consisting of SIL-20AC XR auto-sampler and LC-20AD XR LC pumps. The 5500 QTRAP was operated with the following settings: source voltage 4500 kV, GS1 40, GS2 30, CUR 40, TEM 650 and CAD gas high.

Compounds were quantified with multiple reaction monitoring (MRM) and transitions optimized by infusion of pure compounds and as outlined in Table 2. The bold transitions were used for quantification.

Analyte separation was achieved using a Gemini 3u C6-Phenyl 110A 100x2 mm column (Phenomenex) kept at 35 °C using a Shimadzu CTO-20AC column oven. The gradient mobile phase was delivered at a flow rate of 0.4 ml/min, and consisted of two

solvents, A: 0.1% formic acid in water, B: 0.1% formic acid in acetonitrile. The initial concentration of solvent B was 40% followed by a linear increase to 95% B in 10 min, this was held for 2 min, then decreased back to 40% B over 0.1 min, then held for 3 min. The retention time for 7alpha-hydroxy-4-cholesten-3-one was 8.2 min.

Data were acquired using SCIEX Analyst 1.6.2 and analyzed using SCIEX Multiquant 3.0.3 software. Sample values were calculated from calibration curves generated from the peak area ratio of the analyte to internal standard versus analyte concentration that was fit to a linear equation with 1/x weighting.

FGF19 ELISA

Serum concentration of FGF-19 was determined using the Human FGF-19 Quantikine ELISA (R&D Systems, DF1900). Assay was completed according to manufacturer's instructions with samples ran in duplicate.

Rodent Studies

Postpartum rodent model

The University of Colorado-Anschutz Medical Campus approved animal procedures. Age-matched Sprague-Dawley female rats (Harlan, Indianapolis, IN) were housed and bred as described [52]. For tissue collection, rats were euthanized across groups via CO_2 asphyxiation and cardiac puncture. Whole livers were removed, washed 3x in 1x PBS, and tissues weighed. Left lobes were fixed in 10% neutral buffered formalin (Anatech ltd) and processed for FFPE and caudate lobes were flash frozen on liquid nitrogen for protein and RNA extraction.

Immunohistochemistry

Immunohistochemical (IHC) detection was performed as described [150]. Briefly, tissues were deparaffinized, rehydrated, and heat-mediated antigen retrieval was performed with EDTA for 5 minutes at 125ºC. Primary antibodies used were: Ki67 (Neomarkers RM-9106-s, 1:50) for 2 hours at RT and Adipophilin (LS-B2168/34250 Lifespan Biosciences, 1:400) for 1 hour at RT. Secondary antibody was anti-rabbit (Agilent Envision+ K4003, RTU), used for Ki67 at 1 hour at RT and for Adipophilin at 30 minutes at RT. DAB chromogen (Agilent, K346889-2) with hematoxylin counter stain (Agilent, S330130-2) was used to visualize positive stain. Stained sections were scanned using the Aperio AT2 slide scanner (Leica Biosystems). Number of Ki67+ hepatocytes were counted in 5-1x1mm areas. Adipophilin signal quantification was performed by Aperio ImageScope v12.1.0.5029 as described previously [53]. All analyses were done by investigators blinded to group.

Quantitative real-time RT-PCR (qPCR)

RNA was isolated from flash frozen rat liver for cDNA synthesis and qPCR. One microgram total RNA was used for reverse transcriptase (RT)-mediated synthesis of cDNA using Superscript II RT (Invitrogen) and random hexamer primers for Cyp7a and Superscript IV (Invitrogen) for FXR. Quantitative PCR for rat Cyp7a and reference gene GAPDH was performed using FastStart Essential DNA Green Master (Roche) in an Applied Biosystems theromocycler with 45 cycles of 95ºC for 20 seconds, 60ºC for 40 seconds, 72ºC for 20 seconds. Rat primer sequences were: Cyp7a, forward CTGTCATACCACAAAGTCTTATGTCA and reverse ATGCTTCTGTGTCCAAATGCC; GAPDH forward CGCTGGTGCTGAGTATGTCG and reverse CTGTGGTCATGAGCCCTTCC.

Quantitative PCR for rat FXR and reference gene GAPDH was performed using SsoAdvanced Unviersal SYBR Green Supermix (BioRad) in the ViiA 7 Real-Team PCR System (Thermo Fisher) with the following times: 95○C for 2 minutes, 40 cycles of 95ºC for 15 seconds and 56ºC for 60 seconds, then 95ºC for 15 seconds, 61ºC for 60 seconds, and 95ºC for 15 seconds. Rat primer sequences were: FXR, forward AGGCCATGTTCCTTCGTTCA and reverse TTCAGCTCCCCGACACTTTT; GAPDH, forward ACCACAGTCCATGCCATCAC and reverse TCCACCACCCTGTTGCTGTA.

Results

Forty seven healthy pregnant women completed early (12-16 weeks gestation) and late pregnancy (32-36 weeks gestation) study visits (Fig 3-1A). Study participants underwent liver magnetic resonance imaging (MRI) (Fig A'), provided blood samples, had insulin sensitivity assessed via hyperinsulinemic-euglycemic clamp, and completed body composition analyses. Participant demographics are shown (supplemental material Table 3-3).

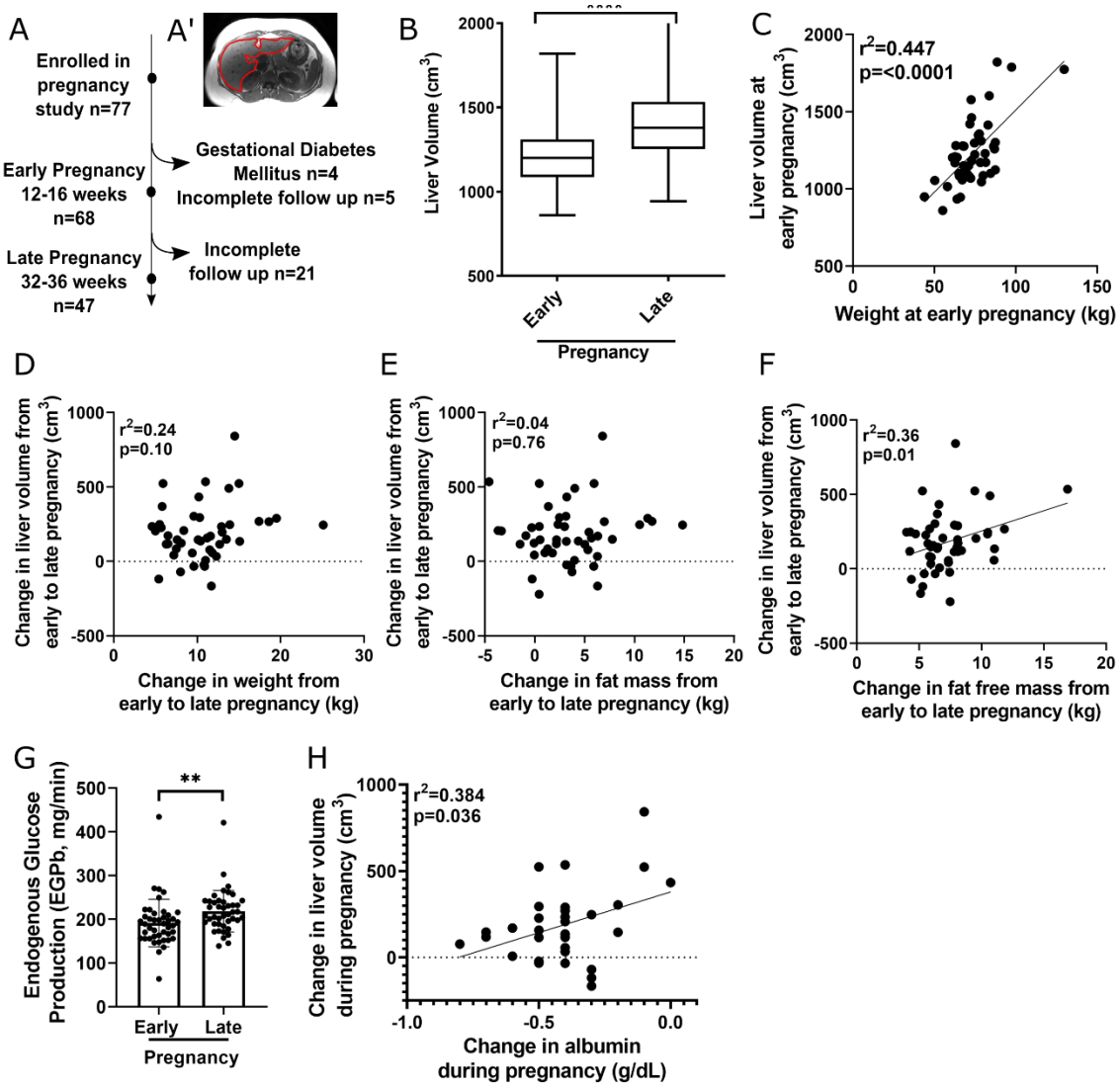

Figure 3-1 Liver changes during pregnancy.

(A) Diagram of the observational study. (A') Liver MRI cross-section. (B) Average liver volume at early and late pregnancy (P: **** < 0.0001 by Two-tailed paired T test). (C) Pearson's correlation of liver volume and BMI at early pregnancy (N = 47). Pearson's correlation of change in liver volume with change in weight (D), fat mass (E), and fat free mass (F). (G) Endogenous glucose production (EGB-b) at early and late pregnancy (P: ** < 0.01 by Two-tailed paired T test). (H) Pearson's correlation of change in liver volume and change in albumin (N = 30).

To assess whether liver size is increased during pregnancy, we measured livers via MRI and found that, on average, liver volumes increased 15% (182 cm3 ± 197 cm3) from early to late pregnancy (P <0.001) (Fig 3-1B). Average liver size at early pregnancy was 1239 cm3 +/- 220.8 cm3 and at late pregnancy was 1421cm3 +/- 298.6 cm3 (Fig 3-1B).

Because liver size is attuned to overall body size via the "hepatostat" [151], we next determined whether the increase in liver size from early to late pregnancy correlated with increased body mass of pregnancy. First, we investigated the existence of the "hepatostat" at baseline, using body weight at the early pregnancy visit as a baseline surrogate, as pregnancy-related weight gain is minimal at this time point [152]. Liver volumes at early pregnancy correlated with body weight (Fig 3-1C), confirming previous studies in non-pregnant individuals [151]. In contrast, the change in liver volume during pregnancy did not correlate with gestational weight gain (Fig 3-1D). Further, we found no relationships between pregnancy liver volume change and change in total fat mass (Fig 3-1E), subcutaneous abdominal, or visceral adipose tissue volumes (Table 3-2). However, we the change in a woman's fat free mass, which includes liver, fetal tissue, placenta, and plasma did correlate with change in liver size (Fig 3-1F). This association between change in fat free mass and liver volume is confounded as fat free mass is not an independent variable from liver mass. These data suggest that liver size increase during pregnancy is unlinked to overall body size, i.e., it is not controlled by the "hepatostat" mechanism. Rather, these data may reflect an unrecognized, reproductive state-controlled program regulating liver size during pregnancy.

Table 3-2 Change in liver volume correlated with measures of body composition and metabolism

Variable	Mechanism of Collection	Sample Size	Pearson Correlation Coefficient	P-value
Body Composition				
Change in Weight	Scale	47	0.260	0.078
Change in BMI	Scale, stadiometer	47	0.213	0.150
Change in Fat Mass	BODPOD	47	0.077	0.605
Change in Fat Free Mass	BODPOD	47	**0.335**	**0.021**
Change in SAT	MR Imaging	47	0.123	0.409
Change in VAT	H-MR Spectroscopy	47	0.245	0.097
Change in Intrahepatic Lipid	H-MR Spectroscopy	47	-0.035*	0.814*
Metabolism				
Change in M Value	Hyperinsulinemic-euglycemic clamp	43	-0.015	0.926
Change in EGP	Hyperinsulinemic-euglycemic clamp	43	-0.047*	0.763*
Change in Rd	Hyperinsulinemic-euglycemic clamp	43	0.053	0.736
Change in Fasting Insulin	Blood draw	45	0.095	0.537
Change in Total Cholesterol	Blood draw	45	0.062	0.684
Change in Triglycerides	Blood draw	45	0.176	0.248
Change in LDL	Blood draw	45	-0.119	0.438
Change in HDL	Blood draw	45	0.103	0.500
Change in VLDL	Blood draw		-0.103	0.500

Abbreviations: BMI – body mass index; SAT: subcutaneous adipose tissue; VAT: visceral adipose tissue; EGP: endogenous glucose production; Rd: glucose disposal rate; LDL: low density lipoprotein; HDL: high density lipoprotein; VLDL: very low density lipoprotein; MR: magnetic resonance; H-MR: proton-magnetic resonance
*Denotes Spearman Correlation analysis

We next asked if metabolic measures were associated with liver volume change and found no relationship with cholesterol concentrations or with measures of insulin sensitivity, i.e. endogenous glucose production (EGP) and glucose disposal rate (Rd) (Table 3-2). We also found no relationship between change in liver volume and change in intrahepatic lipid content (Table 3-2). Assessment of intrahepatic lipid content in rodents also showed no change in intrahepatic lipid during pregnancy [supplemental material: figure 3-4]. In sum, we observed that the increase in human liver volume with late pregnancy occurred independent of weight gain of pregnancy, various other measures of body composition, circulating metabolites, and intrahepatic lipid storage.

In rodents, hepatocyte proliferation contributes to increased liver size and metabolic output during pregnancy and lactation [56,63]. Obtaining timed liver biopsies would be the most direct way to investigate hepatocyte proliferation during pregnancy in women; however, liver biopsies were not performed in our study for participant safety. Thus, we indirectly assessed for increased hepatocyte number by evaluating hepatocyte function. We found evidence for increased liver output as measured by increases in endogenous glucose production (Fig 3-1G) and serum albumin concentration (Fig 1H), two surrogates of liver function [153,154]. Of note, an additional contributor to increased liver volume during pregnancy is increased blood flow, which rises ~50% by late pregnancy [155]. However, increased blood flow during pregnancy is not reported to associate with elevated hepatocyte metabolic output. In sum, these data are consistent with an increase in liver size and synthetic capacity during pregnancy, which may be due to increased hepatocyte proliferation as observed in rodents. Additional studies are required to determine if hepatocyte proliferation is increased during pregnancy in women.

We next looked for evidence of weaning-induced liver involution in women, a biology not previously described in humans. Of the 47 women who participated in our pregnancy study, 36% completed a liver MRI >3 months post-wean (median 5.7 months) (Fig 3-2A). Liver volumes trended toward a decrease in size between late pregnancy and post-wean (Fig 3-2B), and post-wean liver volumes were similar to early pregnancy, indicative of a return to baseline (Fig 3-2C). These data provide the first evidence of postpartum liver involution in women.

While our data showed a statistically significant increase in liver size during pregnancy and a trend toward decrease after weaning, there was heterogeneity in how individual's liver size changed with pregnancy and post-wean. During pregnancy, we found that 72% (34/47) of women had an average increase in liver volume of ~20% (Fig 3-2D, black bars). However, 21% of participants (10/47) had no measurable liver volume change and 6% (3/47) had a reduction in liver volume (Fig 3-2D, black bars, table 2). We saw similar heterogeneity with regard to liver volume change from late pregnancy to post-wean (Fig 3-2D, grey bars).

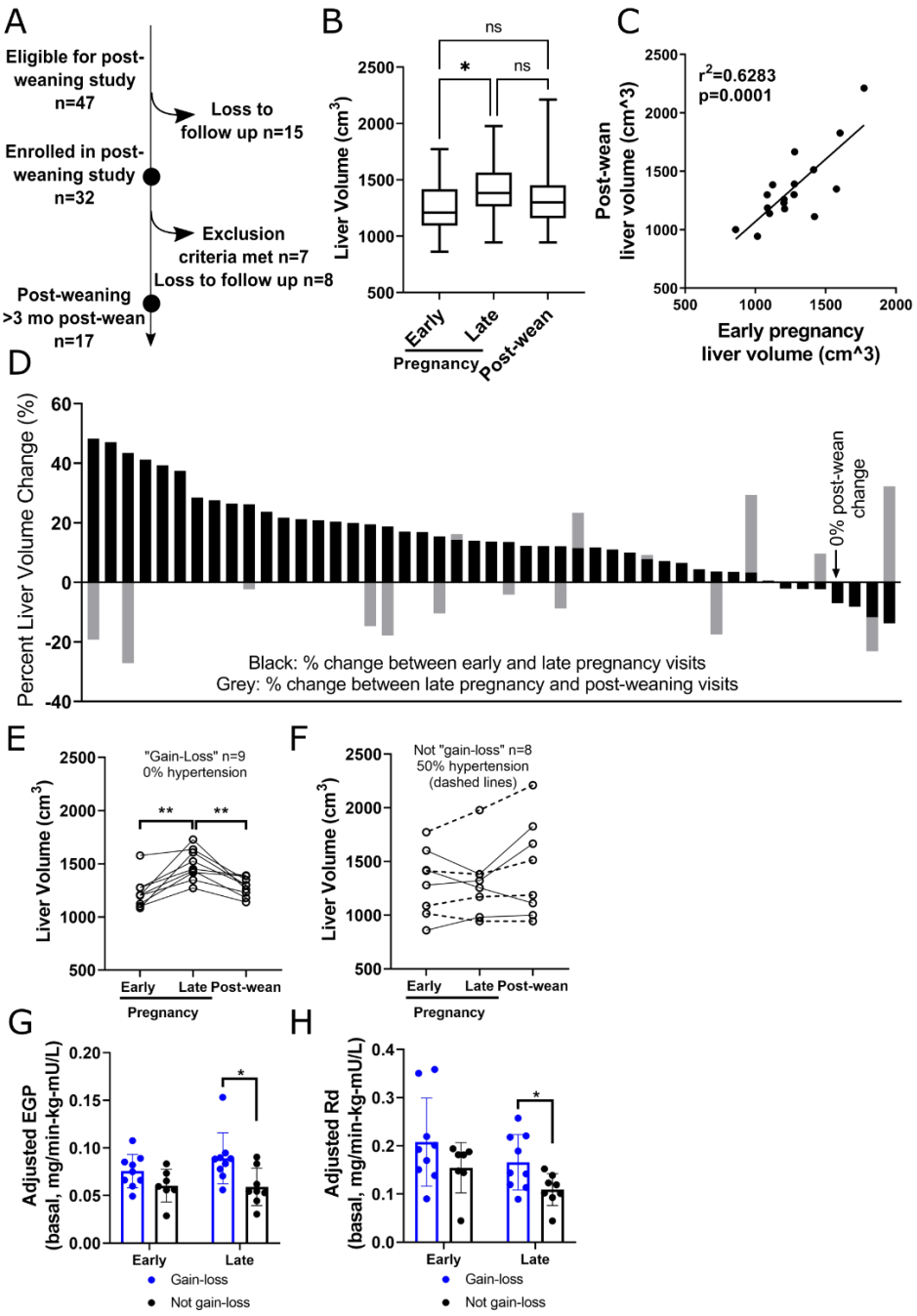

Figure 3-2 Human liver volumes post-wean.

(A) Diagram for post-wean observational study. (B) Liver volume at early, late, and post-wean time points (N = 17). (C) Pearson's correlation of liver volumes at early pregnancy and post-wean (n = 17). (D) Liver volume change between early and late pregnancy (black bars) and between late pregnancy and post-wean (grey bars) per participant. Primary pattern (E) and secondary patterns (F) of liver volume change with pregnancy and post-wean. Dashed lines show participants with hypertension (Paired T-test). Endogenous glucose production (EGP) (G) and glucose disposal rate, Rd, (H) in women in gain-loss group compared to women in not gain-loss group. Pearson's correlation. P value: * < 0.05, ** < 0.01.

Considering the heterogeneity in liver volume change, as well as what is known of normal rodent liver biology (i.e. liver weight gain with pregnancy and loss post-wean) [56], we performed subgroup analyses. We delineated the participants into two groups: "gain-loss", the observed pattern in the normal rodent, or "not gain-loss" for those that did not display the rodent pattern. 53% of women displayed the anticipated liver "gain-loss" pattern (Fig 3-2E). The "not gain-loss" group comprised heterogeneous patterns and included three women who lost liver volume during pregnancy and re-gained post-wean, three women with no significant liver volume changes, and one woman each with either continuous liver size loss or gain across the 3 visits (Fig 3-2F). Of note, liver volume patterns with pregnancy and post-wean did not correlate with a woman's overall weight gain of pregnancy [supplemental material: figure 3-5].

Upon further exploration, we found that none of the women whose liver changes were similar to the normal rodent pattern of "gain-loss" had gestational hypertension, yet 50% of the "not gain-loss" group did (Fig 3-2F, dashed lines). Further, measures of insulin sensitivity differed between these groups. Specifically, we found the "gain-loss" participants had greater endogenous glucose production at late pregnancy (Fig 3-2G), consistent with published data showing elevated endogenous glucose production in healthy pregnancy [131]. We also found greater glucose disposal rates at late pregnancy in the "gain-loss" group (Fig 3-2H), consistent with greater insulin sensitivity in the muscle. These data suggest that the "not gain-loss" pattern may be associated with suboptimal gestational metabolic health and gestational hypertension. One question is whether these metabolic parameters impact fetal outcomes. In this cohort, maternal liver size patterns

did not correlate with newborn weight, length, or Ponderal index, three common neonatal health measures.

To investigate the mechanistic relationship between reproductive state and liver size, we utilized a rat model, as previously described [56]. We found liver weight increases during pregnancy were greater than expected due to gestational weight gain alone (Fig 3-3A). These data suggest rat liver weight during pregnancy is unlinked from the "hepatostat", corroborating our human data (Fig 3-1D). Next, we confirmed maximum hepatocyte proliferation in the rat livers to occur during pregnancy (Fig 3-3B), consistent with previous reports [56,63]. Together, these data suggest a physiological model in which increased liver volume of pregnancy is due to increased hepatocyte proliferation that is activated via an unrecognized, pregnancy-mediated developmental program.

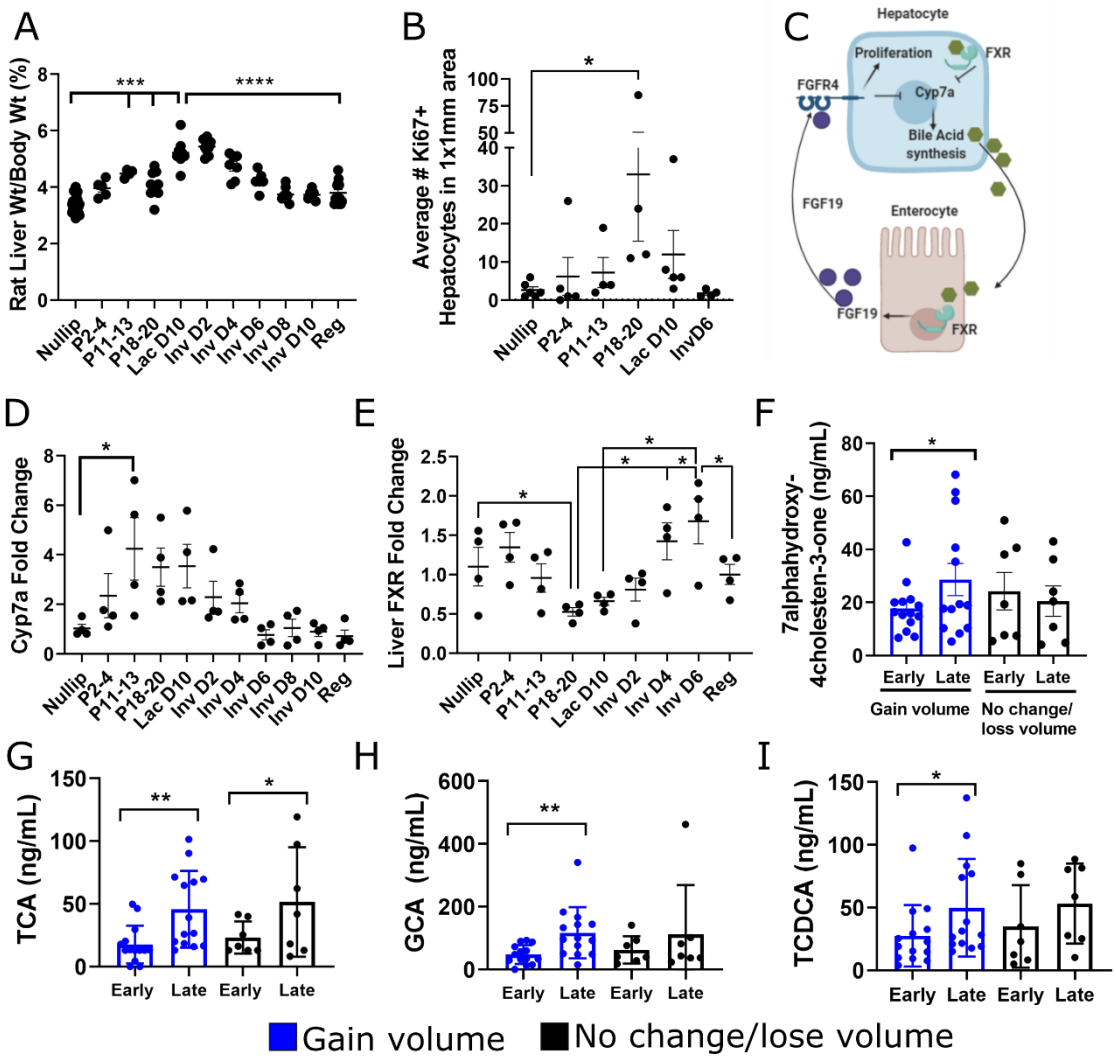

Figure 3-3 Hepatic bile acid signaling and liver size.

(A) Rat liver weight normalized to body weight: Nulliparous (nullip) n=24; early (P2-4) n=5; mid (P11-13) n=4; and late (P18-20) pregnancy n=10; lactation day 10 (Lac D10) n=9; involution (Inv) day 2 n=9; InvD4 n=7; InvD6 n=6; InvD8 n=7; Invd10 n=6; Regressed (Reg) n=14; One-way ANOVA. (B) Ki67+ hepatocytes in rat livers, n=3-5/group. (C) Bile acid signaling model. Cyp7a (D) and FXR (E) mRNA fold change in liver, n=4 per group; One-way ANOVA. (F) Human 7alphahydroxy-4cholesten-3-one plasma concentrations at early and late pregnancy, separated by liver gain (n=14) and no gain (n=7). Plasma concentrations of bile acids TCA (G), GCA (H), and TCDCA (I) Paired T test, P value: * < 0.05, ** <0.01, *** < 0.001, **** < 0.0001.

As a possible mechanism underlying a pregnancy-associated liver growth program, we investigated bile acid metabolism in our rat model. Bile acid signaling contributes to liver regeneration following partial hepatectomy and can control liver size independent of body size [156,157]. Further, bile acids have been shown to regulate hepatocyte proliferation in a pathway dependent on intestinal fibroblast growth factor 15/19 and FXR (Fig 3-3C) [156,158,159]. To investigate if the bile acid pool is modulated by reproductive state, we measured liver Cyp7a, a rate limiting enzyme in bile acid synthesis. We found a 3-4 fold increased expression of Cyp7a with pregnancy, which remained elevated during lactation, followed by a rapid decline with weaning (Fig 3-3D). Since hepatic FXR signaling acts as a negative regulator of Cyp7a (Fig 3-3C), we measured hepatic FXR. We found FXR was downregulated during late pregnancy, when Cyp7a was high, and increased with weaning, when Cyp7a was low (Fig 3-3E). These data associate increased bile acids with the physiologic expansion of the liver during pregnancy—consistent with a previous report [157]—and extend these observations to suggest a role for bile acids in maintaining liver size during pregnancy, lactation and weaning.

We then examined associations between liver growth and the bile acid pool in pregnant women by measuring a biomarker of bile acid production, and serum bile acid concentrations at early and late pregnancy. Serum concentrations of 7α-hydroxy-4-cholestene-3-one (7αC4), a readout for cholesterol 7α-hydroxylase (Cyp7a1) enzyme activity [160], were significantly increased at late compared to early pregnancy only in the women who had an increase in liver volume during pregnancy (Fig 3-3F). This finding supports the hypothesis that increased bile acid production during pregnancy may be

required for liver size increase. Further, among the women whose liver increased in size during pregnancy, we found increases in several primary bile acids and their conjugates (Fig 3-3G-I). Of note, changes in secondary bile acids, which are metabolic products of gut bacteria, only weakly correlated with liver volume change [supplemental material: table 3-4] . In this human cohort, we did not find associations between concentration of plasma FGF19, an enterocyte product shown to induce hepatocyte proliferation and liver growth in rodents [supplemental material: figure 3-6] . One potential caveat to our FGF19 analysis is that plasma concentrations of FGF19 may not reflect concentration in the portal vein that links the gut and liver. In sum, these human data are consistent with an increased bile acid pool during pregnancy, which may contribute to the increased liver size observed in pregnancy.

Discussion

In this study, we find evidence for a previously unreported liver biology in women, namely that during the course of a normal pregnancy cycle liver volume increases during gestation and decreases post-wean. Multiple observations and reports demonstrate tight control of liver size in proportion to body size, a phenomenon that has been referred to as the "hepatostat" [151]. Yet, in our study, increased liver volume during pregnancy is not accounted for by change in body size. Since liver size is presumed to be directly linked to a physiologic function of the liver [161], our data suggest that a metabolic demand above and beyond body size accounts for increased liver size during pregnancy. Consistent with this hypothesis, in rodents we find that liver size remains elevated through lactation even though body size is reduced compared to late pregnancy.

One potential mechanism controlling liver size during a pregnancy cycle is the circulation of bile acids, which have been shown to modulate liver size independent of the body size hepatostat [162,163]. Such a paradigm where liver size is controlled by bile acid flux would allow for a situation in which body size could become "unlinked" from liver size. The data presented here obtained from rodent models and human correlates support the idea that increased production of primary bile acids during pregnancy and lactation via the Cyp7a synthetic pathway leads to hepatocyte proliferation and thus a larger liver. Since the primary function of bile acids is to facilitate fat absorption in the intestine, an increase in liver parenchyma capable of bile acid synthesis would make sense given increased caloric demand during pregnancy and lactation. In sum, our human data are consistent with dynamic size regulation of the liver to accommodate the unique metabolic demands of pregnancy and lactation. Further, our combined human and rodent data suggest a mechanism whereby physiologically regulated bile acid synthesis underlies liver size changes across a pregnancy cycle. Future studies directly testing this mechanism are needed.

While the pattern of liver size gain with pregnancy and loss upon weaning was observed in the majority of women in this pregnancy study, we also identified a subset of women for whom liver size did not follow a "gain-loss" pattern. Gestational hypertension and reduced liver insulin sensitivity were elevated in this subset. Therefore, an intriguing hypothesis is that a new facet of healthy pregnancy is the gain-loss pattern of liver volume. A corollary to this hypothesis is that pre-existing and/or pregnancy specific conditions such as gestational hypertension, could underlie the inability of the liver to appropriately respond to pregnancy [164]. Of note, gestational hypertension affects 5-10%

of pregnancies, and can progress to preeclampsia with known pathogenic liver involvement in ~15-20% of cases [165]. Gestational hypertension is attributed to a vascular disorder that is initiated at the placental interface, specifically due to incomplete maturation of the maternal spiral arteries [166]. If related, the question of whether the same pathophysiology that leads to gestational hypertension can also impair the normal liver response to growth cues of pregnancy, or vice versa, remains unknown. On the other hand, albeit a small study - our data show that liver gain with pregnancy is not a requisite for normal fetal growth, as we observed no differences in newborn size between women who did and did not experience liver gain with pregnancy. Future studies would be required to determine if there are any long-term impacts due to a lack of maternal liver growth during gestation, as has been described for other variations in neonatal nutrition and lifetime risk of disease [167–169].

The data presented here shows that the human liver responds to a pregnancy cycle in a similar manner to rodents; namely: increased size with pregnancy and lactation, followed by a decrease in size post-wean. The process that returns the rodent liver to its pre-pregnant state, weaning-induced liver involution, promotes metastasis to the liver [56,134]. Given that women have an increased risk of liver metastasis if diagnosed with breast cancer within 5 years of pregnancy, we speculate that weaning-induced liver involution creates a pro-metastatic microenvironment in the liver. Although we cannot definitively demonstrate liver involution in humans, it has recently been demonstrated that the breast undergoes weaning-induced involution in women much like has been shown in rodents [49,170]. Therefore, we theorize that there is a conserved mammalian developmental program that links the mammary gland and the liver through a pregnancy

cycle, putatively to meet the elevated metabolic demands of pregnancy and lactation. The potential importance of this biology for supporting reproduction and infant health are apparent; however, weaning-induced breast and liver involution may have unanticipated consequences, including the transient increased risk of breast cancer and liver metastasis [32,38,56,171,172]. Additional impacts on risk for liver disease may be anticipated given known disparities in liver disease by sex, including increased risk for acute liver failure and autoimmune liver conditions in women [133].

A key strength of our study is that each woman serves as her own control, allowing us to see how an individual's liver changes during a pregnancy cycle. However, our human cohort study cannot draw mechanistic conclusions because it was purely observational. Additionally, these data were generated in a small, predominately White, non-Hispanic cohort and require validation in a larger study with a diverse population to generalize these findings.

In summary, this work describes a new observation in normal women, specifically increased liver size with pregnancy and decreased size post-wean, putatively to accommodate the dramatic changes in metabolic demands across a pregnancy-lactation-wean cycle. This finding demonstrates reproductive control of liver size and function in women, and concurs with recent observations in rodents, suggesting a conserved liver biology. The question of whether this newly described liver biology has implications for maternal health during pregnancy or sex-specific risk for liver disease remains to be determined [133,173,174]. However, our evidence suggest weaning-induced liver involution in women, which if validated, may lead to improved understanding of the high rates of liver metastasis observed in young postpartum breast cancer patients.

Supplementary Material

Table 3-3 Participant Demographics

	Full Liver Volume Population (N=47) N (%)	Liver Volume measured at pregnancy visits *only* (N=30) N (%)	Liver volume measured at pregnancy and postpartum visits, (N=17) N (%)
Age (years)			
mean (SD) *[min-max]*	30.2 (4.6) [19.0-39.0]	29.6 (4.7) [19.0-39.0]	31.2 (4.4) [22.0-38.0]
Preconception BMI (kg/mg^2)			
mean (SD) *[min-max]*	25.9 (4.4) [18.4-35.9]	26.4 (4.2) [18.4-35.6]	25.2 (4.7) [20.0-35.9]
Normal or Overweight (<30)	40 (85.1)	26 (86.7)	14 (82.4)
Obese (≥30)	7 (14.9)	4 (13.3)	3 (17.6)
BMI at late pregnancy (kg/m^2			
mean (SD) [min-max]	29.5 (4.1) [22.9-38.9]	30.4 (3.7) [22.9-38.9]	28.0 (4.3) [22.9-37.1]
Normal or Overweight (<30)	27 (57.4)	15 (50.0)	12 (70.6)
Obese (≥30)	20 (42.6)	15 (50.0)	5 (29.4)
Parity			
0	28 (59.6)	21 (70.0)	7 (41.2)
1	10 (21.3)	3 (10.0)	7 (41.2)
>1	9 (19.1)	6 (20.0)	3 (17.6)
Race			
White only	40 (85.1)	25 (83.3)	15 (88.2)
Multiple races	3 (6.4)	1 (3.3)	2 (11.8)
Unknown	4 (8.5)	4 (13.3)	
Ethnicity			
Hispanic	6 (12.8)	5 (16.7)	1 (5.9)
Non-Hispanic	41 (87.2)	25 (83.3)	16 (94.1)
Gestational Age at Early Pregnancy (weeks)			
mean (SD) *[min-max]*	15.6 (0.8) [12.9-17.6]	15.4 (0.8) [12.9-16.6]	16.1 (0.8) [14.7-17.6]
Gestational Age at Late Pregnancy (weeks)			
mean (SD) *[min-max]*	34.3 (1.5) [31.6-37.7]	34.5 (1.5) [32.3-37.7]	33.8 (1.3) [31.6-36.1]
Gestational hypertension/pre-eclampsia			
Yes	6 (12.8)	2 (6.7)	4 (23.5)
No	41 (87.2)	28 (93.3)	13 (76.5)
Intrahepatic cholestasis of pregnancy			
Yes	2 (4.3)	2 (6.7)	0
No	45 (95.7)	28 (93.3)	17 (100.0)
Newborn weight (kg)			
mean (SD) *[min-max]*	3.4 (0.5) [2.0-4.5]	3.4 (0.4) [2.6-4.5]	3.5 (0.7) [2.0-4.5]
Newborn length (cm)			
mean (SD) *[min-max]*	51.1 (2.8) [44.0-56.0]	51.3 (2.4) [47.0-56.0]	50.9 (3.4) [44.0-56.0]
Ponderal index (kg/m^3)			
mean (SD) *[min-max]*	25.5 (2.7) [20.4-32.1]	25.2 (2.9) [20.4-32.1]	26.0 (2.5) [21.9-29.6]

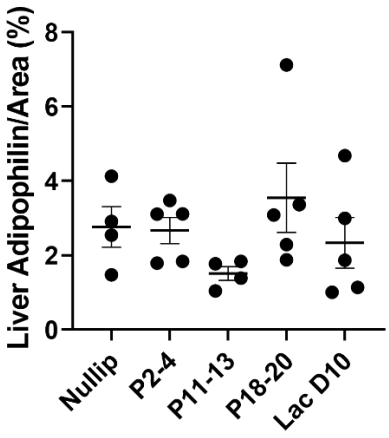

Figure 3-4 Quantification of adipophilin IHC staining in rat livers, n=4-5/group.

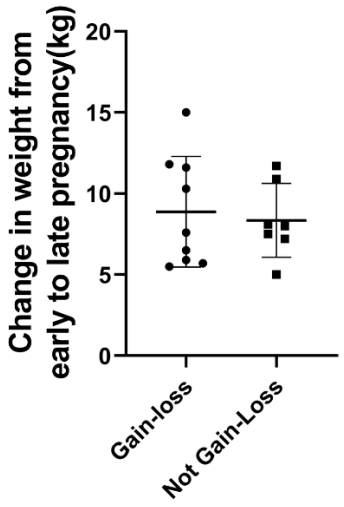

Figure 3-5 Relationship between weight gain of pregnancy and liver size pattern

Change in weight from early to late pregnancy in participants who completed all 3 study visits, separated by whether their liver volume followed the gain-loss or not gain-loss pattern during pregnancy and post-wean.

Table 3-4 P-values for individual bile acid species

	Early vs. Late Pregnancy		
	All Participants Measured (n=21)	**Participants with Increase in Volume (n=14)**	**Participants with No Change or Loss in Volume (n=7)**
TCA	P<0.001	P<0.01	P<0.05
GCA	P<0.01	P<0.01	n.s.
CA	n.s.	n.s.	n.s.
TCDCA	P<0.05	P<0.05	n.s
GCDCA	n.s.	n.s.	n.s.
CDCA	n.s.	n.s.	n.s.
UDCA*	n.s.	n.s.	n.s.
DCA*	n.s.	n.s.	n.s.
LCA*	n.s.	p<0.05	n.s.
Total Serum Bile Acids	n.s.	Trending (p=0.0551)	n.s.
Total Primary Bile Acids	n.s.	Trending (p=0.0574)	n.s.
Total Secondary Bile Acids	n.s.	n.s.	n.s.
*Denotes secondary bile acid			

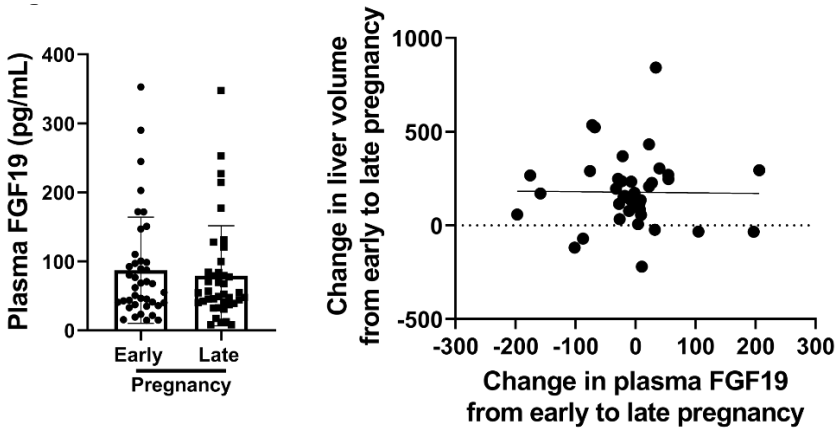

Figure 3-6 FGF19 Quantification

(A) Quantification of plasma FGF19 by ELISA at early and late pregnancy time point. (B) Pearson's correlation of change in FGF19 and change in liver volume.

Funding
OHSU Center for Women's Health Circle of Giving to PS, KV and JP, DoD grant #BC170206 to PS, OHSU School of Medicine Dean's Fund to PS, AC, AQ. National Institute of Diabetes and Digestive and Kidney Diseases (NIDDK), #R01DK098707 to KV.

Acknowledgements
We want to thank Mara Kalter and Claire Dorfman for participant outreach and scheduling, and to our study participants, whose generous gift of time and trust made this study possible. We are grateful to Dr. Gordon Mills for constructive review of the manuscript, and Weston Anderson for outstanding assistance with manuscript writing, editing, and preparation.

Chapter 4 : Characterization of human breast cancer liver metastases

Preamble: Overarching problem and approach

Study of the liver metastatic niche in patients is a nascent field, despite the concept of the metastatic niche itself dating back to 1889 with Stephen Paget's famous "seed and soil" hypothesis [175]. Here, we aimed to characterize how tumor cells interface with the metastatic niche or "soil" in liver metastasis tissue from women with metastatic breast cancer. We studied the tumor histology, biomarker expression, and extracellular matrix composition adjacent to tumor cells. The results presented here are descriptive, as this is the first study of its kind and is further limited in sample size. Additional studies will expand these findings to larger patient cohorts as well as encompass adjacent normal liver.

The study cohort was comprised of all patients with breast cancer metastatic to the liver for whom tissue was available at OHSU. We included "all-comers", rather than focusing only on postpartum or young women's breast cancers, as the number of available cases was limited. The study design, combined with low numbers of samples, meant we were limited in ability to draw conclusions about the histological data in relation to clinical information, such as age or parity status. However, the study remains open so there is the opportunity to expand the cohort and power it to ask questions regarding impact of parity status.

These investigations were funded by a grant from the Department of Defense Breast Cancer Research Program (BC #170206). The scope of the funded project included initial set up of this study on human BCLM, as there was not yet an IRB in place. Thus, my initial efforts toward this study were to write the IRB protocol, consent

form, and other required documents for ethics approvals. Because this study included participants who may have a "research-only" biopsy, the protocol was classified as greater than minimal risk. This greater than minimal risk designation required a greater level of oversight and documentation, which I coordinated. The process of IRB protocol development began in November 2017 and initial study approval was granted February 2019. Since then, the study has accrued 32 participants and 18 cases have advanced through multiplex IHC staining and analysis.

This exploratory work is expected to develop a framework of the histologic organization and stromal composition of breast cancer liver metastases and adjacent normal liver. The observations from human disease can help improve mouse models, as well as suggest specific avenues of investigation in the liver metastatic niche. For example, we may identify particular ECM proteins that underlay tumor nests. Then, we could test whether ablation of that ECM protein or blocking the interaction between tumor cell and ECM protein would result in tumor cell death or increased sensitivity to therapy. The same kind of approach of "bedside-to-bench" could be applied to other observations from this exploration of the liver metastatic niche in breast cancer.

Plan to publish

This work will be adapted and submitted for publication at a journal such as *American Journal of Pathology* or *Breast Cancer Research*.

Introduction

Deaths attributed to breast cancer are due to distant spread of the disease to organs such as bone, brain, lung, and/or liver. Thus, metastatic breast cancer is the critical problem to address to improve breast cancer survival; yet many research studies focused on breast

cancer metastasis rely on cell culture or primary tumors. Such approaches are useful for understanding tumor-drug interactions, tumor growth, invasion into surrounding stroma, and dispersion from the primary site. However, these approaches may not capture the most salient features required to understand and treat metastasis.

Because metastatic success is primarily determined by tissue interactions at the secondary organ [112,113], studies that use cell culture or primary tumors are limited in ability to make conclusions about metastasis. An additional consideration is the observed latency between surgery to remove the primary breast tumor and metastatic recurrence. As there is no longer a primary tumor present, all data indicate that for cases that progress to metastasis over time, the tumor cells must have already disseminated at time of surgery, likely by time of diagnosis [176,177]. This leaves a very narrow – if any – window available to target tumor cells before they disseminate into the periphery. Mouse models have borne this theory out, showing that very early dissemination from a primary tumor (followed by surgical resection of the early stage tumor) is sufficient to seed metastasis [178–180]. These data indicate that studying tumor cell dissemination from the primary site may not be impactful in the clinical setting of metastasis. Therefore, heightened focus on studying disseminated disease, via patient derived materials and improved models of metastatic breast cancer is necessary.

The vast majority of mouse models for breast cancer metastasis result in lung or lymph node metastases [181–183]. However, this situation does not fully reflect clinical realities. Where breast cancer spreads for a given patient is not random, as site of metastasis is influenced by factors such as breast cancer subtype [27,184,185], patient age [21,26], and parity status[56]. For example - excluding bone metastasis - HER2+ breast cancers

have the highest rates of liver metastases [27,185,186], and younger parous women are at higher risk for spread to the liver compared to brain or lung [56]. Moreover, a recent study examined all breast cancers cases diagnosed from 2010-2016 in the SEER database, and specifically looked for cases that had liver recurrence. The authors demonstrated that recurrence with liver metastasis associated with young age, high pathological grade of the primary tumor, and HER2+ (regardless of hormone receptor status) and triple negative subtypes [187]. Young women (<40 years of age) comprised 6.8% of the total number of breast cancer cases, yet were 12.1% of cases with liver metastasis. In comparison, women aged 41-60 made up 44.1% of total cases and 46.3% of liver metastases [187]. These data illustrate two key points: 1) women <60 years of age are the majority of patients with BCLM; and, 2) young women have disproportionately high rates of liver metastases. One limitation of these studies is that parity information were not included, so it is unknown whether a postpartum diagnosis further increases the risk of liver metastasis in young women.

Reported mechanisms underlying breast cancer liver metastases describe intrinsic properties of breast tumor cells that promote liver spread [188,189]. Additional, tumor extrinsic mechanisms that involve the liver microenvironment have been suggested, but lack experimental validation with mouse models of breast cancer liver metastasis [190]. Given the relative paucity of data on how the liver niche contributes to breast cancer metastatic promotion, an intermediate approach is to examine results from models of colorectal and pancreatic cancer where liver metastases are extensively studied. Such studies demonstrated that tumor cells induce changes in the liver that result in promotion of metastasis. These effects on the liver metastatic niche include upregulation of adhesion

molecules on liver sinusoidal endothelial cells [191,192], increased production of pro-metastatic extracellular matrix proteins (e.g. fibronectin [71,73], periostin [72]) by hepatic stellate cells), and induction of inflammatory signaling [73,193–195]. In turn, these effects facilitate tumor cell adherence to endothelium, entry into the liver parenchyma, survival, and immune evasion [120]. These findings provide rationale for investigation of adhesion molecules, extracellular matrix proteins, and immune cells in breast cancer liver metastases.

ECM composition has been demonstrated to be altered at the metastatic niche [115–119]. Although many ECM proteins are endogenously expressed in the secondary organ under homeostatic conditions, cancer cell-derived signals can induce remodeling by increasing ECM deposition and altering the ECM structure [116,118]. The ECM provides a structural support for epithelium and also induces intracellular signaling events. Cells receive signals from the ECM via transmembrane receptors, such as integrins on the cell surface [196]. In non-transformed epithelial cells, attachment to tissue-specific ECM prevents anoikis, and thus ECM acts as a survival signal [197]. A key characteristic of tumor cells is anchorage-independence, in which anoikis avoided despite no attachment or attachment to "wrong" (i.e. not tissue of origin) ECMs [197,198]. Despite this feature of anchorage-independence, ECMs have still been found to promote survival in tumor cells by activating pro-proliferative and anti-apoptotic pathways [199].

ECM proteins exert pro-metastatic effects at almost every step of the metastatic cascade [119]. Collagen IV is a major component of basement membrane, which separates epithelium from endothelium and stroma, and underlies all of the liver sinusoids. Tumor cells interact with collagen IV via β1 integrins, which promotes tumor cell invasion [196]

and thus is predicted to support dissemination from the primary cancer and entrance through secondary organs. Fibronectin (FN) and tenascin-C (TNC) are also found under normal conditions in the liver. Fibronectin has been associated with tumor cell proliferation and migration via β1 integrin binding [196]. Further, when breast cancer cells are cultured on fibronectin, the cancer cells upregulated matrix metalloproteinase -9, which associated with invasive potential [200]. In the liver, fibronectin found on the luminal surface of sinusoidal endothelium promoted tumor cell extravasation into the tissue via talin [201] . Host-derived TNC was found to promote lung metastasis in a breast cancer model by increasing blood vasculature invasion and reducing tumor cell apoptosis [202]. Of note, breast tumor cells can produce their own TNC, which facilitated survival and metastatic outgrowth a lung metastasis model [117].

While these advances suggest mechanisms that may contribute to BCLM, the fundamental tumor histology of breast cancer liver metastasis remains largely unexplored. To address this gap in knowledge and better inform our mouse models of breast cancer liver metastasis, we set out to histologically characterize breast cancer metastasis in the liver. We first asked about tumor organization/histology using a panel of multiplex IHC stains chosen based on clinical usage for primary breast cancer (e.g. cytokeratin proteins, Gata3, ER, Ki67), as well as ability to differentiate adjacent normal liver from metastatic tissue. Specifically, we included Heppar to mark hepatocytes [203] and Aquaporin 1 (Aqp1) to mark bile ducts and endothelium [204]. Furthermore, we examined extracellular matrix proteins using multiplex IHC with a staining panel designed to capture ECM proteins identified as either important in liver metastases or as being regulated by reproductive stage.

GATA3 is a transcription factor expressed in normal mammary epithelial cells that promotes differentiation to a luminal cell type [205,206]. Since the majority of breast cancers are luminal in origin, GATA3 is often expressed by breast cancer cells, and is used to as a diagnostic biomarker for metastatic breast cancer [207,208]. As may be predicted considering the basic biology of GATA3 as directing luminal differentiation, the majority of luminal breast cancers (i.e. hormone receptor positive) are GATA3+. Tumors that are HER2+ or triple negative are less likely to expresses GATA3, but the range of percentages expressing GATA3 is highly variable between studies [206,209,210].

Cytokeratins are intermediate filament proteins that are commonly assessed biomarkers in breast cancer, and are used to help delineate between luminal and basal origin. Specifically, cytokeratins 7, 8, 18, and 19 identify luminal cells, whereas cytokeratins 5, 14, 17 identify basal and myoepithelial cells [211]. A study using a tissue microarray of primary breast cancer tissues found that the majority of cases expressed luminal cytokeratins, a minority express a combination of luminal and basal cytokeratins, and very rare cases express only basal cytokeratins [212]. This study also associated cases with any basal cytokeratin expression with worse survival [212].

A limitation to the above studies on GATA3 and cytokeratin proteins is that these studies have only assessed expression in primary tumors. However, a recent study investigated clinico-pathologic features of breast cancer metastases to gynecological organs, and compared results to matched primary breast cancer tissues [213]. Primary breast cancers from the study cohorts almost all expressed GATA3, but in some cases GATA3 expression was reduced in metastases. Specifically, tumor cells from 46% (6/13) of cases showed decreased GATA3 positivity in metastases, with four of those six cases going

from 100% GATA3 positivity in the primary to 0% in the metastasis [213]. Another study representing at least eight metastatic sites, including 44 cases of liver metastases, evaluated GATA3. The authors report that 41/44 cases of liver metastases were GATA3+ [214]. Yet, it was unclear if the GATA3 negative metastases were associated with GATA3 negative primary breast cancers.

Additional literature on breast cancer liver metastases describes how hormone receptor status shifts between the primary and metastatic site. A recent meta-analysis of 39 studies found that incidence of estrogen receptor conversion in liver metastasis – that is, going from positive to negative or vice versa between the primary tumor and metastasis – was on average 14%. This was significantly less than receptor conversion in bone (29%) or CNS (21%) [215]. Such data can inform treatment decisions, and may also provide clues about mechanisms of site-specific metastasis. Further, additional context from biomarker expression or tumor histology may yield new insights.

Here we assessed tumor differentiation, growth pattern relative to the adjacent normal liver interface, cytokeratin expression, proliferation, and ER expression to help build basic, foundational understanding of breast cancer liver metastasis tissues. Further, we have analyzed the composition of ECM substratum that tumor cells interact with and assessed for correlations between abundance of intra-tumoral ECM proteins. While these studies are ongoing, preliminary findings suggest BCLMs are luminal-like, grow in the non-angiogenic manner, and have extensive interaction with ECM proteins.

Materials and Methods

Ethics Approval

The research was conducted on archived and prospective formalin fixed, paraffin embedded (FFPE) tissue samples collected under IRB approved protocols at Oregon Health & Science University (OHSU). Tissues were de-identified for use in IHC studies.

Study Description

The aim of this study was to histologically describe breast cancers that have metastasized to the liver. All cases of BCLM with FFPE tissue available at OHSU were solicited as part of our research protocol, including retrospective cases stored in the OHSU Biolibrary, patients currently being treated by OHSU physicians, and patients participating in clinical trials at OHSU. Breast cancers in the liver and adjacent normal liver obtained through liver biopsies or surgical excision, and FFPE processed were evaluated for tumor and tumor microenvironment biomarkers using multiplex immunohistochemistry (IHC) staining.

Eligibility Criteria

To be included, participants had to be greater of equal to age 18, diagnosed with breast cancer that metastasized to the liver, and consented to provide a tissue sample of breast cancer liver metastasis for research purposes. Exclusion criteria were:

1. Known autoimmune condition, chronic systemic steroid use, underlying immune disease, use of immunomodulatory prescription drugs for any medical condition.

2. Known bleeding diathesis or use of anticoagulation medications.

3. The presence of other comorbid conditions known to impact immune function, (such as: type I diabetes, uncontrolled adult onset diabetes, uncontrolled infection or known HIV infection.)

4. History of malignancy other than breast cancer.

5. The presence of liver disease other than breast cancer metastasis to the liver (such as: cirrhosis, non-alcoholic fatty liver disease, hepatitis).

6. For prospective research-only biopsy collection: current pregnancy. If liver tissue is not being collected as part of clinical care, then pregnant women are excluded.

Histological assessment

FFPE sections of breast cancer liver metastases were evaluated by hematoxylin and eosin staining for differentiation grade and histological growth pattern. Differentiation grade was called as poorly, moderately, or well-differentiated based on the tumor's morphological organization into duct like structures, and nuclear characteristics, as previously described [216]. Histological growth pattern of the tumor in relation to the adjacent normal liver was evaluated, and classified as either replacement, pushing, or desmoplastic based on established scoring for liver metastases in colorectal cancer [79]. Tissue sections that did not contain a liver-tumor interface were not evaluated for histologic growth pattern. All assessments were completed by two evaluators blinded to study groups.

Multiplex immunohistochemistry

Multiplex IHC staining was performed as previously described with modification [80]. Tissues were deparaffinized, rehydrated, and heat-mediated antigen retrieval was performed with EDTA for 5 min at 125 °C. Hematoxylin staining was performed on all tissues prior to antibody cycles, and tissues were scanned using the Aperio AT2 slide scanner (Leica Biosystems). Table 4-1 and 4-2 list the antibodies and conditions used for the "Basic" and "ECM" multiplex staining panels, respectively. All primary antibodies were incubated for 60 minutes at room temperature, and all secondary antibodies incubated for 30 minutes at room temperature.

Table 4-1 "Basic" mIHC Staining Panel

Primary Antibody	**Manufacturer**	**Catalog #**	**Lot#**	**Concentration**	**Secondary Antibody**	**SDS-glycine Elution**
CK18	Abcam	Ab181597	GR321105-11	1:10,000	anti-Rb	60 min @ 50C
GATA3	Biocare	CM405A	92016	1:50	anti-Ms	30 min @ 50C
Aqp1	Millipore Sigma	AB2219	3015336	1:15,000	anti-Rb	30 min @ 50C
ER	Leica	NCL-er-6f11	6059509	1:100	anti-Ms	30 min @ 50C
CK7	Abcam	Ab181598	GR3214132	1:20,000	anti-Rb	90 min @ 50C
CK5	Leica	NCL-L-CK5	60334842	1:500	anti-Ms	30 min @ 50C
Ki67	Thermo	RM9106-S	910681607E2	1:350	anti-Rb	60 min @ 50C
ColIV	Dako	M0785		1:50	anti-Ms	120 min @ 50C
Heppar	Dako	M7158	81384	1:50	anti-Ms	120 min @ 50c

Table 4-2 "ECM" mIHC Staining Panel

Primary Antibody	Manufacturer	Catalog #	Lot#	Concentration	Secondary Antibody	SDS-glycine Elution
CD45	Dako	M0707	20026786	1:300	anti-Ms	30 min @ 75C
TGM2	Abcam	Ab2386	GR2385641-3	1:500	anti-Ms	n/a
TNC	EMD Millipore	AB19011	2483158	1:200	anti-Rb	30 min @ 80C
FN	Bio-Rad	4470-2750	0909	1:200	anti-Ms	n/a
CK7/CK18	Abcam	Ab181598/ Ab181597	GR3214132/ GR321105-10	1:30,000/ 1:8,000	anti-Rb	30 min @ 80C

After each antibody cycle, tissues were scanned using the Aperio AT2 slide scanner (Leica Biosystems). Following scanning, 3-Amino-9-Ethylcarbazole (AEC) chromogen was removed with 1×70% and 1×100% alcohol wash for 2 min each. Primary and secondary antibodies were removed using 20% SDS-glycine pH 2 as listed in Tables 1 and 2. Secondary only and/or isotype controls were utilized to confirm antibody stripping after each cycle. For the ECM panel, isotype specific control antibodies were necessary, as overlap in staining patterns of distinct ECM proteins was anticipated. This primary/secondary/scan/strip/control cycle was repeated for each primary antibody listed in tables 1 and 2. Each tissue slide included a positive control human tissue microarray (TMA) to confirm primary antibody staining for each cycle. The TMA was comprised of normal human liver, primary breast cancer, and adjacent normal breast.

After staining, scanned images from each cycle were captured using an image processing pipeline previously described with minor modification [80]. Image alignment and extraction were performed using the SURF algorithm in the Computer Vision Toolbox of Matlab version R2018b (The MathWorks, Inc, Natick, MA, USA). Color

deconvolution was performed in FIJI and pseudo-colored multiplex images were created in Aperio ImageScope v12.1.0.5029.

For quantification of IHC signal, tumor borders were annotated by a pathologist and subsequent analyses were performed on tumor only. Signal quantification of stains was performed using modified color deconvolution algorithms in Aperio ImageScope v12.1.0.5029 as described [49]. All analyses were done by investigators blinded to study group. Data are presented as percent area positive.

Results

Demographics

This cohort was comprised of 22 women with metastatic breast cancer to the liver. This single-institution (OHSU) cohort includes n=19 cases with available liver metastases tissues, n=3 cases lacking sufficient tissue for analysis, and n=3 cases with matched primary breast cancer tissues, collected between 1995-2021. Liver metastasis tissues were obtained from either biopsies (n=7/19) or surgical resection (n=12/19). The cohort characteristics are presented in **Table 4-1**. This cohort is enriched for young women who were diagnosed with estrogen receptor positive primary breast cancer. The majority of young women's breast cancer cases in this cohort were from parous women with eight of 17 parous cases considered post partum breast cancer, as defined as a breast cancer diagnosis <45 years of age and within 10 years of last childbirth. Time between breast cancer diagnosis and recurrence with liver metastasis was on average ~3.5 years with a range of synchronous diagnosis (i.e. 0 years) to 11 years. The liver was the first site of metastasis for 13/20 patients for whom first site of metastasis was documented, and another 2/20 had concurrent diagnosis with liver and bone metastasis.

Table 4-3 Demographics and clinical characteristics

	N (%)
Age	
<45	10 (45.5)
45-60	9 (40.9)
>60	1 (4.5)
Unknown	2 (9.1)
Parous	
Yes	17 (77.3)
Dx < 5 years after birth?	*2*
Dx 5-10 years after birth?	*6*
No	2 (9.1)
Unknown	3 (13.6)
Race	
White	20 (90.9)
Black	0 (0.0)
Asian	1 (4.5)
Hispanic	1 (4.5)
Estrogen receptor	
Positive	17 (77.3)
PR+	*9*
PR-	*6*
Unknown	*2*
Negative	3 (13.6)
Unknown	2 (9.1)
HER2	
Positive	6 (27.3)
ER+	*5*
ER-	*1*
Negative	13 (59.1)
Unknown	3 (13.6)
Endocrine therapy	
Yes	11 (50.0)
No	9 (40.9)
Unknown	2 (9.1)
Radiation therapy	
Yes	8 (36.4)
No	12 (54.5)
Unknown	2 (9.1)
Chemotherapy	
Yes	13 (59.1)
No	7 (31.8)
Unknown	2 (9.1)

Histology of liver metastases

To examine how histology of the liver metastasis is altered from the primary tumor, we compared H&E sections from case where matched primary and liver metastases were available (n=3 cases, Fig 4-1). In these three cases, we found that tumor cell morphology and arrangement were largely conserved between the primary breast cancer and liver metastasis, such that the two are not easily differentiated at high magnification (Fig 4-1).

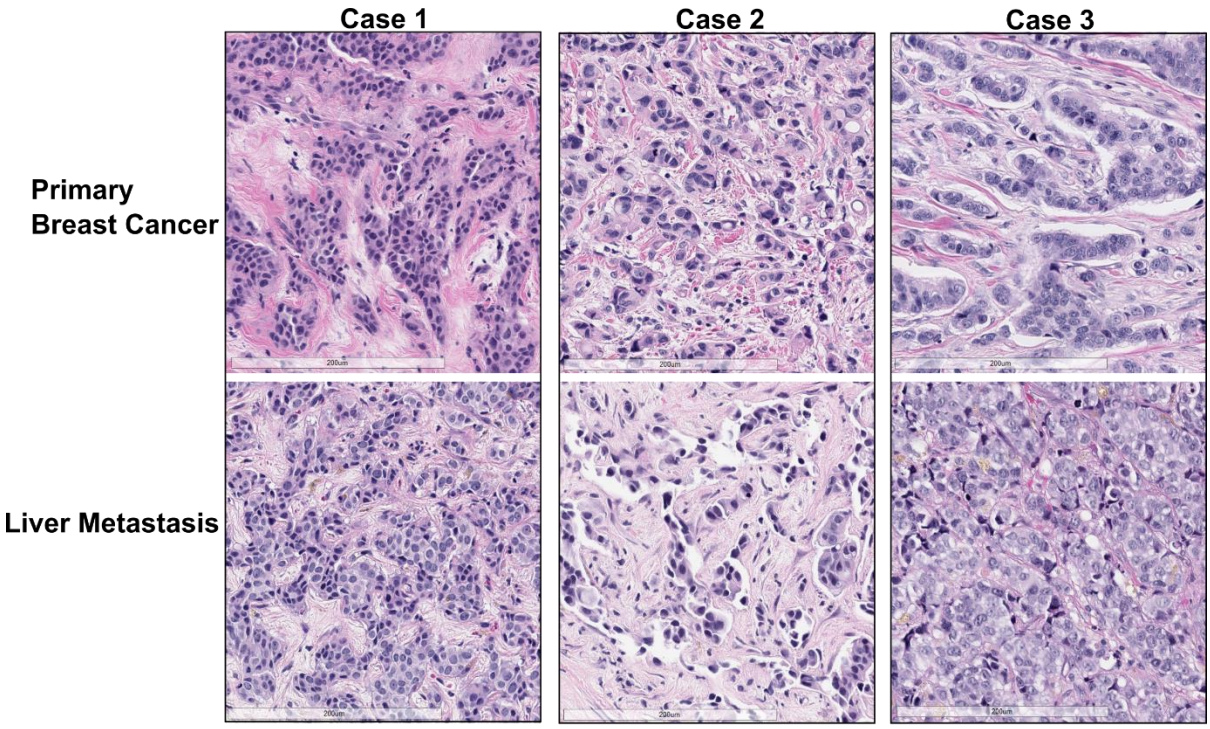

Figure 4-1 Histology of primary breast cancer and matched liver metastases

Paired cancer tissues from the primary breast cancer and subsequent liver metastasis metastases show similar tumor organization and morphology in n=3/3 paired samples. Case 1 is characterized by large tumor cell “nests” in abundant stroma. Case 2 is characterized by smaller tumor cell “nests” surrounded by stroma. Case 3 is comparatively well-differentiated with “tracts” of tumor cells that are arranged in parallel to the stromal components

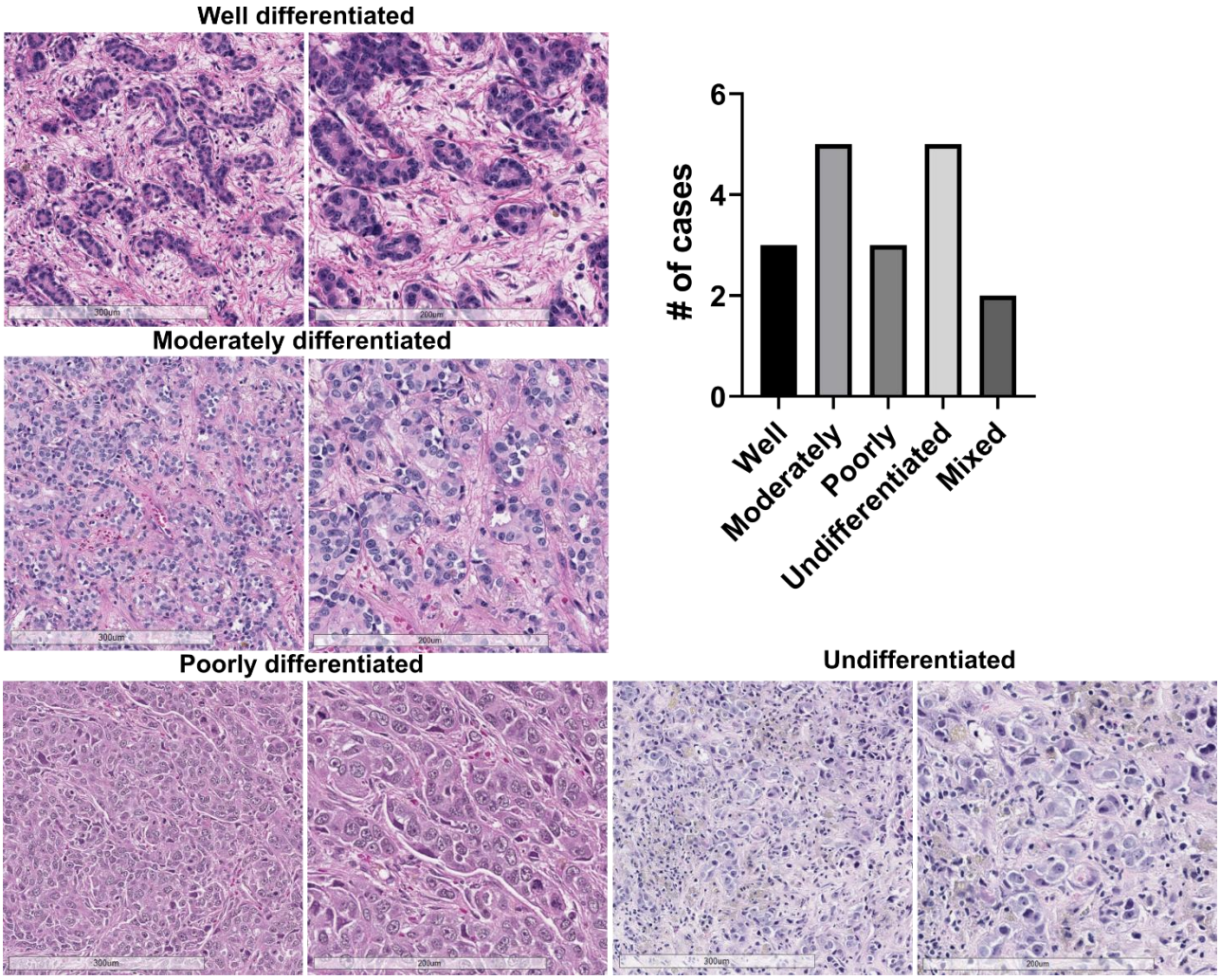

Figure 4-2 Patterns of differentiation of breast cancer liver metastases

Patterns of tumor organization and nuclear morphology in liver metastases range from well- to un-differentiated, with number of cases identified as each pattern.

Table 4-4 Association between tumor differentiation grade in liver metastases and clinical features

Tumor Differentiation	Primary cancer ER status	% tumor Ki67+	Chemotherapy treated?
Well	+	1	No
Well	+	20	Yes
Well	+	20	Yes
Moderately	+	10	No
Moderately	+	20	No
Moderately	+	30	Yes
Moderately	+	4	No
Moderately	unknown	unknown	unknown
Poorly	+	5	No
Poorly	+	80	Yes
Poorly	+	30	Yes
Undifferentiated	+	20	No
Undifferentiated	+	5	Yes
Undifferentiated	-	80	No
Undifferentiated	+	5	Yes
Undifferentiated	-	90	Yes
Mixed	+	1	Yes
Mixed	-	30	Yes

We next examined the differentiation state of the breast cancer liver metastases by H&E. It has been reported that adenocarcinomas metastatic to the liver can retain some of the glandular morphology of the primary tissue [217]. Such a tumor that retains organization similar to that of the normal tissue is considered well-differentiated. For breast cancer, additional features including size and shape of nuclei and mitotic index are considered when determining if a tumor is well- or poorly-differentiated [216]. The liver metastases in this cohort showed examples of well-, moderately-, poorly-, and un-differentiated (Fig 4-2). Women whose primary breast cancer was ER negative had liver metastases that were either undifferentiated or mixed category (Table 4-4). Higher percentage Ki67 positivity in the metastases also associated with less differentiated tumors (Table 4-4). However, such associations are limited in power due to small sample size.

An additional approach to histological evaluation of liver metastases is to score the histological growth pattern, defined as the pattern of tumor growth in relation to adjacent normal liver. Such characterization is often used in colorectal cancer metastatic to the liver [79]. Three primary growth patterns have been described: replacement, desmoplastic, and pushing. In this BCLM cohort, the dominant observed pattern was replacement (n=7/10), which could be further subdivided into type 1 or type 2 depending on whether the metastasis forms continuous plates with the liver cells (Fig 4-3). There were two instances of desmoplastic pattern and one of pushing pattern; the remaining cases could not be evaluated for histological growth pattern because the tissue section lacked a tumor-adjacent normal liver interface (Fig 4-3).

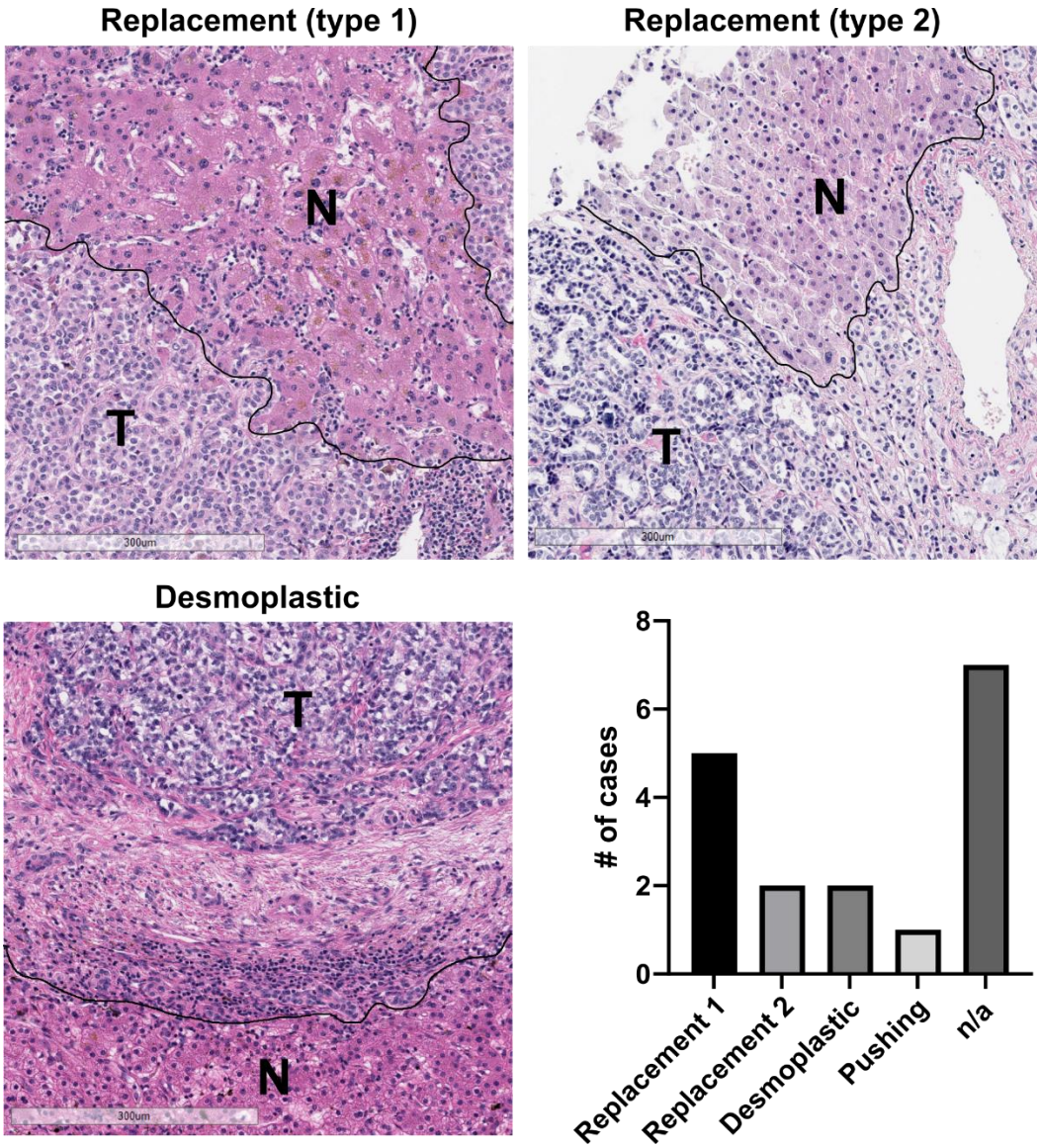

Figure 4-3 Histological growth pattern of breast cancer liver metastases

Representative examples of HGPs and enumeration of number of cases in each pattern in breast cancer liver metastases. Replacement types are delineated according to the arrangement of hepatocytes to the tumor-liver interface, outlined in black. Replacement type 1 is characterized by hepatocytes being perpendicular to the interface, whereas type 2 is characterized by hepatocytes in parallel to the interface.

Biomarker expression

We next evaluated for expression of biomarkers can help delineate basal- vs luminal-like disease. The four biomarkers used for this analysis were cytokeratins 5, 18, 7, and GATA3. Basal-like breast cancer is ER- CK5+ GATA3-, and is considered to be more aggressive, although this designation is typically applied in the context of a primary tumor, not a metastasis [218,219]. Immunohistochemical staining was quantified in tumor areas of the liver metastases. All but 3 of the liver metastases expressed GATA3 (Fig 4-4a, a'). Cytokeratin 5, a clinical biomarker for basal disease, was absent from all liver metastases (Fig 4-4a). In comparison, most metastases had some staining for cytokeratin 18 or 7 (Fig 4-4a). Within a case, cytokeratin 7 was reduced compared to CK18 (Fig 4b). Together, the staining pattern of these biomarkers is consistent with a luminal-like breast cancer in the liver.

To ask about the proliferation state of the liver metastases, we stained for KI67 and a pathologist determined the positivity within the tumor. We observed a wide range of % Ki67 positive nuclei with mean 25%, mode of 20%, minimum 1%, and maximum 90% (Fig 4-4c). One prediction is that Ki67 positivity may be impacted by chemotherapy treatment, with chemotherapy-treated tumors having less proliferating cells. However, there was no association between tumor cell proliferation, as measured by Ki67 positivity, and chemotherapy treatment (Fig 4-4c, black dots).

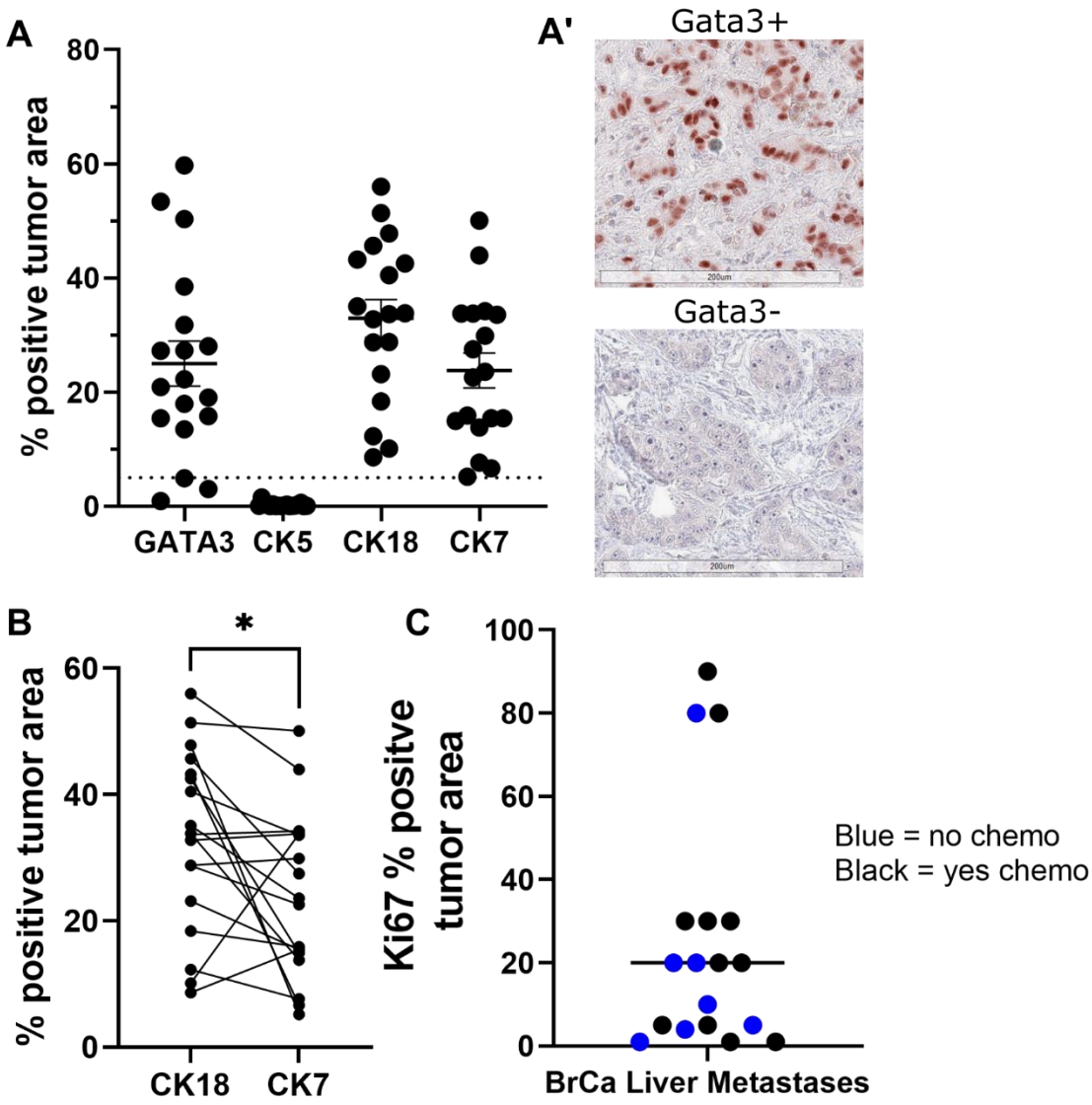

Figure 4-4 Breast cancer liver metastases biomarker expression

A. Signal quantification of IHC stains in intra-tumoral areas of liver metastases; **A'.** Representative images from metastases that were Gata3+ or Gata3-; **B.** Paired analyses of CK18 and CK7 in metastases show significant reduction in CK7; paired two-sided T test $p<0.05$; **C.** Percent of Ki67 positive nuclei in liver metastases as called by pathologist. Cases with chemotherapy prior to liver tissue collection are shown in black and no prior chemotherapy shown in blue.

Extracellular matrix in the tumor & adjacent normal

To begin to understand how breast tumor cells may interact with liver extracellular matrix (ECM), we stained for ECM proteins found in the liver and/or associated with metastasis. The choice of ECM proteins stained for was also informed by previous studies that describe ECM components of the normal rodent mammary gland and liver across reproductive stages [56,114]. In particular, high abundance and/or ECMs altered by reproductive stage were chosen.

Technically, development of the "ECM" multiplex IHC panel presented a challenge, as antibodies proved difficult to elute between cycles. Extensive optimization was thus required to ensure antibody removal between cycles. Antibody elution between cycles is routinely checked with application of the secondary antibody and chromogen after the elution step, which should remove the primary and secondary antibody of the mIHC prior cycle (Fig 4-5A). In a post-elution check, we observed secondary-only controls that appeared clean (i.e. successful elution) (Fig 4-5A). Yet when we checked elution with a non-specific primary antibody isotype-matched to the target primary, significant signal appeared from the previous antibody cycle (Fig 4-5A). Thus, we instituted use of isotype-matched primary antibodies to optimize elution conditions for each staining cycle. Using this approach, we finalized experimental conditions that resulted in successful elution (Fig 4-5 B-E, Table 2).

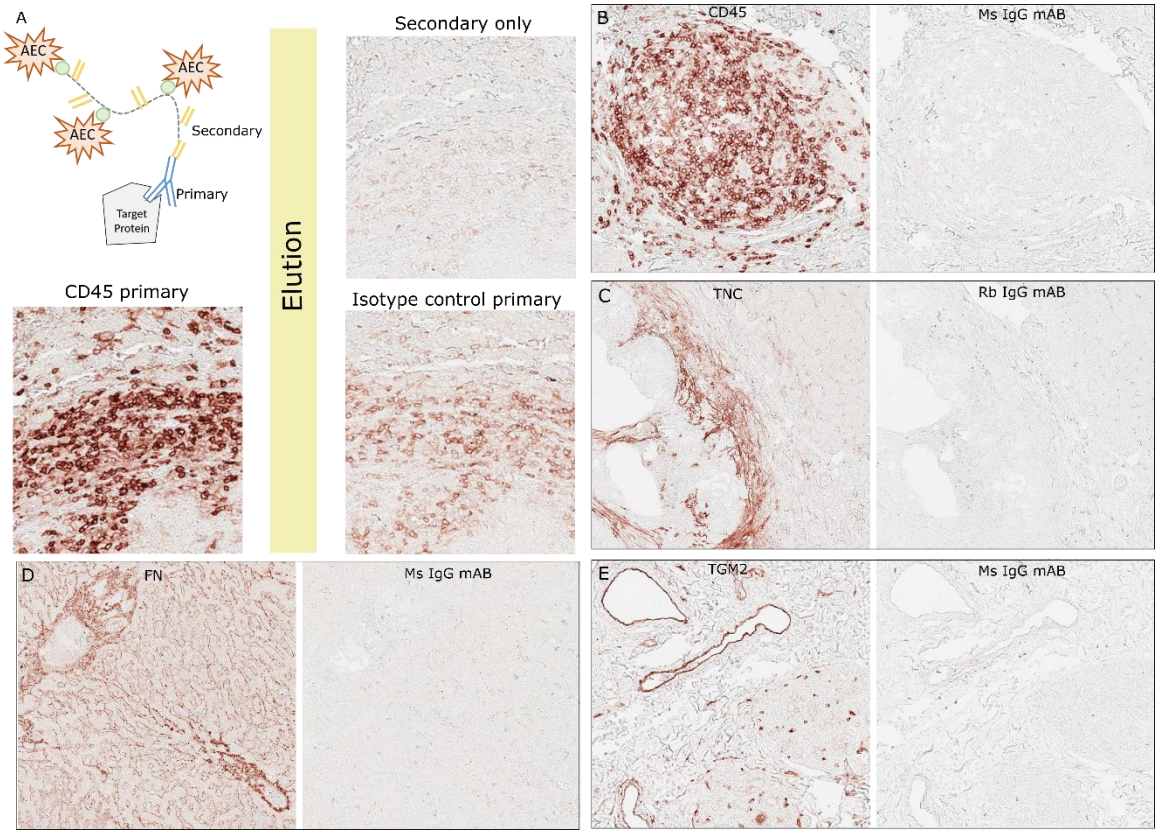

Figure 4-5 Optimization of ECM panel mIHC staining confirmed with isotype antibodies

A. Diagram of primary-secondary-chromogen structure (top left); Signal after cycle with CD45-specific primary antibody (bottom left); Post-elution check with either secondary only (top right) or isotype-matched control primary (bottom right). Representative images from optimized primary antibody staining and subsequent, post-elution isotype antibody staining for cycles to detect **B.** CD45, **C.** tenascin-C(TNC), **D.** fibronectin (FN), and **E.** transglutaminase 2 (TGM2).

Collagen IV was found, as expected, in normal breast and liver, and was reduced in primary breast cancer samples (Fig 4-6). In contrast, collagen IV was abundant in breast cancer liver metastases and was often found surrounding tumor cell "nests" (Figs 4-6, 4-7). Preliminary investigation into the pattern of collagen IV expression revealed possibly increased thickness in liver metastases compared to adjacent normal liver (Fig 4-7).

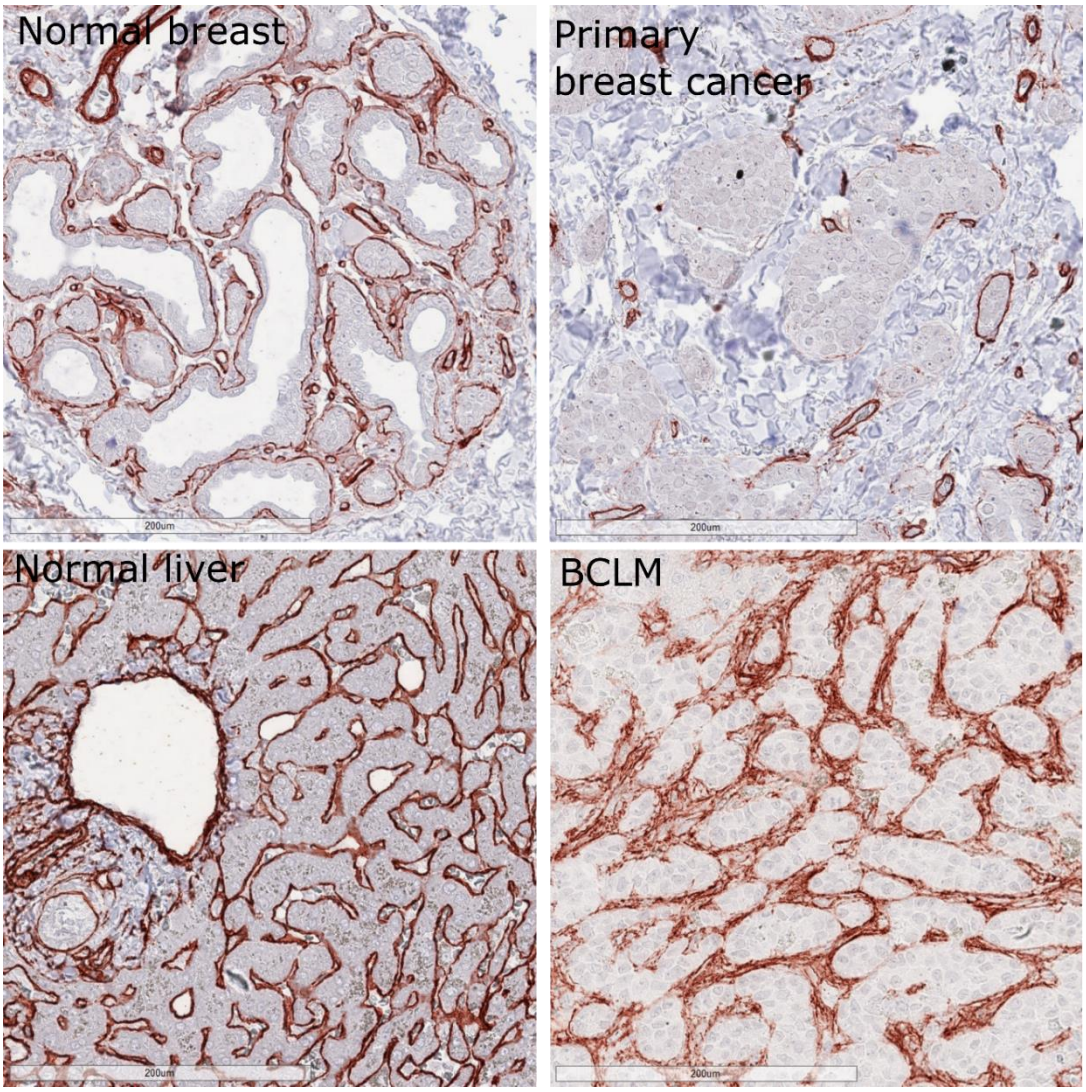

Figure 4-6 Collagen IV staining in normal and cancer tissues

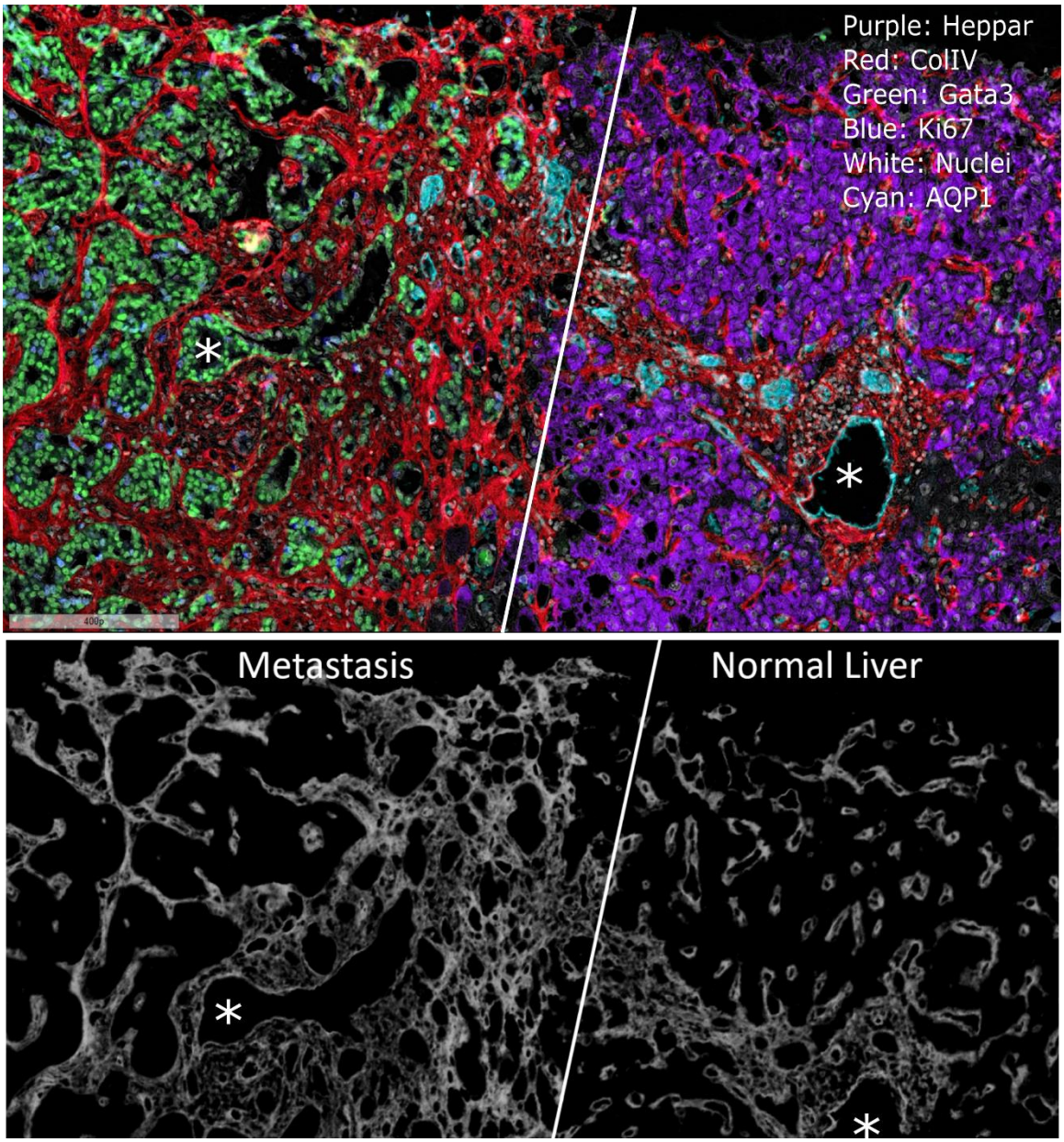

Figure 4-7 Collagen IV structure in metastasis versus adjacent normal liver

Top: Pseudo-colored image showing Heppar (purple), ColIV(red), Gata3 (green), Ki67 (blue), Aquaporin 1 (cyan), and nuclei (white). Gata3 marks tumor cells, while Heppar marks normal hepatocytes.
Bottom: Black and white image showing ColIV in the metastasis versus adjacent normal liver. Asterisks denote the same area on each part of the two images.

Intra-tumor abundance of ECM proteins was quantified, and ECM proteins fibronectin (FN), Col IV, and tenascin-C (TNC) had similar average abundance of ~40% positive tumor area (Fig 4-8). TNC abundance appeared to separate into “high” and “low” groups (Fig 8). Tissue transglutaminase 2 (TGM2) had the lowest overall abundance with an average of 26% positive tumor area. Abundance of Col IV and FN (Fig 4-8b), as well as TNC and TGM2 (Fig 4-8c), correlated within a tumor. No correlations were observed between other ECM proteins analyzed (Fig 4-8D-G).

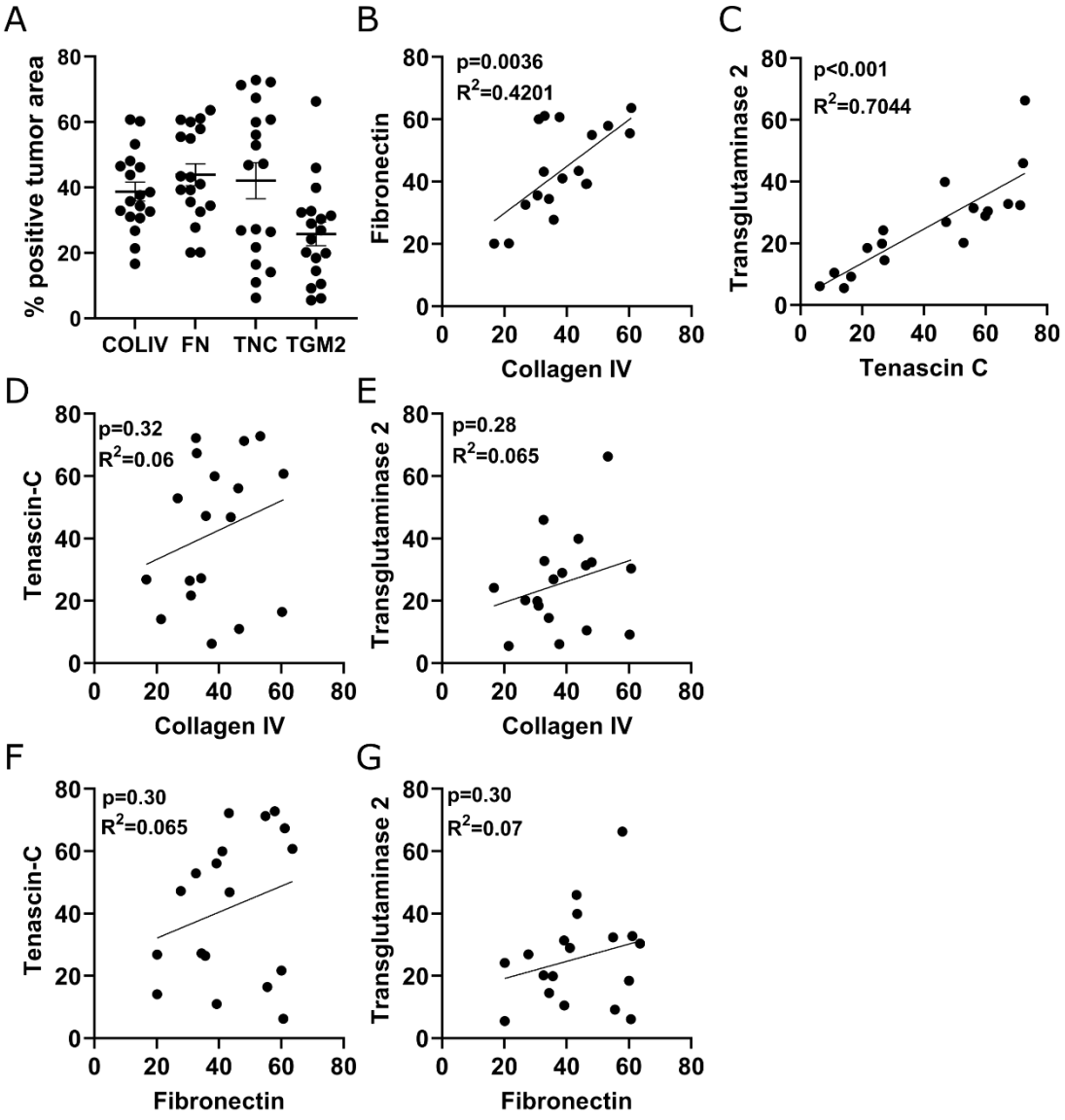

Figure 4-8 Signal quantification of ECM proteins in liver metastases

(A) IHC quantification of four ECM proteins in tumor areas of liver metastases tissues. Linear correlation demonstrating significant association of ECM proteins (**B)** Col IV and FN and (**C**) TNC and TGM2 within the same case. Linear correlation with no association of ECM proteins **(D)** Col IV and TNC, **(E)** Col IV and TGM2, **(F)** FN and TNC, and **(G)** FN and TGM2; simple linear regression.

Discussion

This study yielded insights into the phenotype and composition of metastatic tumors from women with breast cancer liver metastases. This findings are novel, as current literature on BCLM does not describe the metastasis itself but rather focuses on characteristics of primary breast cancers that eventually spread to the liver [22,28,215,220]. These studies can help guide prognosis and may indicate that certain kinds of breast tumor cells survive best in the liver environment. Additional studies on BLCM investigate efficacy of treatment strategies, and have shown that surgical resection provides the best opportunity for long-term survival [221,222]. Yet, eligibility criteria for surgical resection of BCLM preclude most patients from receiving this option [223]. This suggests an unmet need for new targeted therapeutics, which will require understanding of the tumor intrinsic- and extrinsic characteristics of breast cancer growing in the liver. Without knowledge of what the metastatic lesion looks like, what proteins are expressed, and what niche components surround that lesion –development of new treatment modalities lack a defined target. Here, we described breast cancer liver metastases in terms of tumor organization, differentiation grade, histological growth pattern, biomarker expression, and ECM composition.

We found expression of GATA3 – a luminal-differentiation transcription factor – in all but three of the liver metastases. Accordingly, all tumors had expression of luminal cytokeratins CK18 and CK7. In contrast, no tumors showed CK5 staining, indicative that the metastases were likely not basal-like in origin. Consistent with this observation that liver metastases express luminal-like markers, liver metastases also resembled primary (luminal-like) breast cancer in structure and cell morphology. Moreover, there were

examples of tumor areas that looked like *normal* mammary lobules and the majority of cases had structure resembling the breast. The functional significance of this conservation of tissue organization between the breast and breast cancer liver metastasis is unknown, but merits study. Tumor cells that maintain tissue of origin structure could be refractory to treatment or perhaps represent a mechanism of dormancy.

Liver metastases from colorectal cancer are scored for histological growth pattern, which describes how the metastasis grows in relation to adjacent normal hepatocytes [79]. The most often observed patterns are desmoplastic, pushing, and replacement with pushing being most common in colorectal cancer liver metastases [99,224]. This HGP classification provides clinical utility, as the desmoplastic growth pattern is associated with better disease prognosis [79,99]. Additionally, the HGP could indicate mechanism of metastatic growth. The pushing pattern has been associated with angiogenesis, whereas the replacement pattern uses existing vasculature in the liver for blood supply [224,225]. In breast cancer, two independent studies showed that the replacement pattern was most common [100,225], but as with reports in colon, the desmoplastic pattern was associated with better survival [100]. Our data supports the prior finding that the replacement pattern was most common, as 70% of evaluable cases were classified as replacement. This pattern is suggestive that BCLMs do not rely on angiogenesis for blood supply, an idea that is supported by prior work that found downregulation of blood vessel development in liver metastases compared to other breast cancer metastatic sites [226]. Because the replacement pattern does not rely on angiogenesis for blood supply, these data suggest that anti-angiogenic drugs would not be effective for treating BCLM. Indeed, anti-angiogenic drugs failed to produce a good response in cases of colorectal cancer liver metastases

with the replacement pattern [225]. This study went on to show in a mouse model of colorectal cancer liver metastasis that if migration of tumor cells was impaired, then the prevalence of the replacement pattern was diminished and anti-angiogenic therapy had improved efficacy [225]. Whether such a strategy would be effective for BCLM has yet to be tested.

In this study, collagen IV was present in all liver metastases and seemed to surround tumor cell "nests". Furthermore, it appeared that the thickness of collagen IV was increased in tumor areas compared to adjacent normal, potentially indicative of tumor-induced collagen remodeling. It is possible that tumor cell binding to collagen IV via β1 integrin helps facilitate invasion into liver parenchyma [196]. Additionally, collagen IV in the liver niche has been associated with high levels of chemokines CCL5 and CCL7, two factors that were implicated in mouse models as promoting liver metastasis [194]. These murine data, coupled with our finding of high collagen IV in liver metastases, is suggestive that future study of immune cells responsive to CCL5 and CCL7 in the liver may be fruitful. Both FN and TNC were also abundantly present in liver metastases and displayed altered organization in the tumor compared to adjacent normal. For each of these three ECM proteins (Col IV, FN, and TNC), we observed tumor cells in direct contact with the ECM proteins. In chemotherapy-treated cases, there was indication that tumor cells "sitting" on an ECM protein were protected from death, as surrounding areas appeared necrotic and devoid of additional tumor cells.

Future analyses will assess ECM structure and organization in the liver metastasis compared to adjacent normal. Structural arrangement of ECMs are important to understand, as particular orientations and patterns have been implicated in disease

prognosis [227]. Whether the tumor cells themselves produce and remodel the ECM in the liver niche is an open area of investigation. Alternatively, it could be that liver fibroblasts are induced by tumor cells to remodel ECM proteins. The functional significance of ECMs in BCLM remains to be fully elucidated. Future studies investigating integrins and other ECM receptors on breast tumor cells in liver metastases are needed to address these important questions.

This study cohort was generated in an unbiased fashion, by enrolling any patients we could identify at OHSU who had BCLM with available liver metastasis tissue. Assessment of the resulting cohort showed that 45% were young women's breast cancer (YWBC) cases, which is consistent with the idea that liver metastasis is a significant problem for young women diagnosed with breast cancer. Furthermore, of those YWBC cases – 80% were considered PPBC. Another notable observation was that the majority (77%) of cases were associated with a primary breast tumor that was estrogen receptor positive. However, because the sample size is small we were limited in ability to make associations between these clinical features and our biomarker study results.

Next Steps

The work presented here is ongoing. We will extend the data set to a second set of cases that have not yet been stained. Additionally, we plan to assess ER levels in the liver metastases and perform new mIHC staining for immune cells in the niche. The "immune" mIHC panel will focus on T cells and myeloid derived suppressor cells, based on results from our work in PPBC models [54,81,130] and other studies demonstrating roles of certain immune cells in metastasis [120,121,195,228]. Further analyses include quantification of ECM protein organization using a recently developed software tool [229]. We will also perform

subgroup analyses after expanding the data set to investigate if factors such as age of diagnosis or parity status influence tumor histology, biomarker expression, or ECM proteins.

Acknowledgements

Andrea Calhoun and Jayasri Narasimhan provided excellent histology support, including optimization and staining of the two multiplex IHC panels. Sonali Jindal contributed to tissue acquisition and histological evaluation. Andrea Calhoun performed Aperio-based quantification of biomarkers in the “Basic” mIHC panel; Michelle Ozaki performed Aperio-based quantification of ECM proteins in the “ECM” mIHC panel.

Chapter 5 : Future Directions

Immune attributes of the normal, involuting liver

In my thesis work, as reported in Chapter 2, I defined immune suppression as a new attribute of weaning-induced liver involution [134], similar to what has been demonstrated in the mammary gland [81]. Classically, immune suppression is defined as suppression of antigen-specific T cell activation. Specifically, we found that antigen-specific T cells in the involuting liver and mammary gland are impaired in their ability to respond to their cognate antigen. In the mammary gland, reduced costimulatory molecules on mammary dendritic cells associated with immune suppression [81]. Activation of naïve T cells, that is T cells that have not before "seen" their cognate antigen, requires three signals (Fig 5-1). First, the T cell receptor engages with antigen presented in the context of a MHC protein on the surface of an antigen presenting cell. Then, costimulatory molecules on the antigen presenting cell engage receptors on the T cell (e.g. CD28), leading to pro-survival signaling. Finally, cytokines provide the final "push" to T cell activation (Fig 5-1). Deficiencies in any of these three steps could lead to impaired T cell activation, despite presence of cognate antigen.

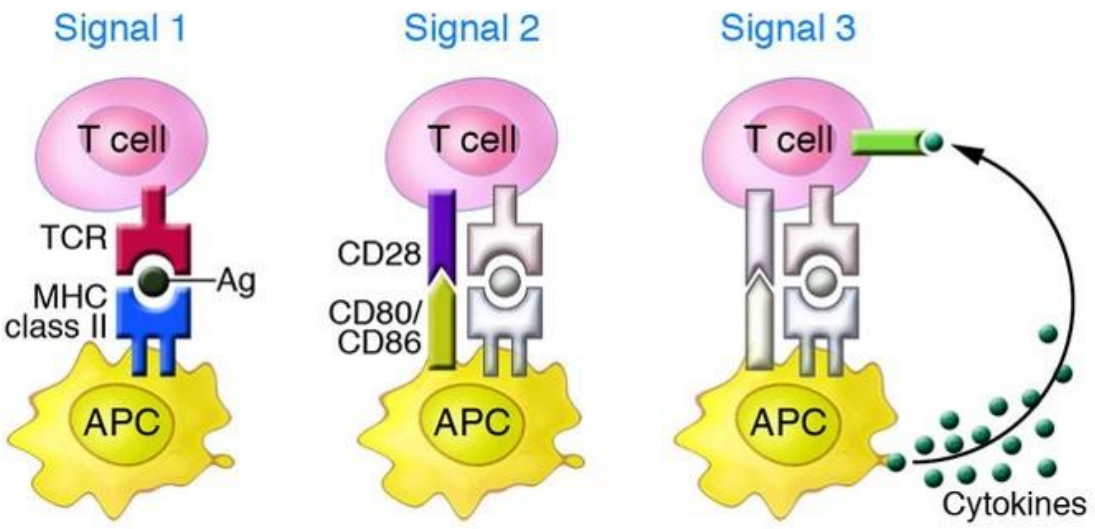

Figure 5-1 Three signals needed for naive T cell activation

Reprinted from J Clin Invest DOI: 10.1172/JCI31720 [230]

To further investigate potential mechanisms of T cell suppression in the involuting liver, an initial approach would assess the phenotype and functionality of antigen presenting cells in the liver from nulliparous and involution stage hosts. In our experimental system, ovalbumin antigen was directly injected into the liver. A few days later, CD4+ cells that expressed only one TCR clonotype, which was specific for the ovalbumin antigen, were injected intravenously. In order for the ovalbumin antigen to be presented to the CD4+ T cell, this protein antigen needed to be phagocytosed by antigen presenting cells, processed, and presenting in the context of MHC class II. As is the case for the involuting mammary gland [81], costimulatory molecules on antigen presenting cells may be reduced during liver involution. Antigen presentation in the absence of adequate stimulation is known to induce T cell apoptosis, anergy, or skewing towards a regulatory phenotype [90]. The possibility that APCs downregulate costimulatory molecules during involution is readily testable using a flow cytometry approach to measure level of of B7 family proteins, which include costimulatory and inhibitory ligands [231]. Antigen uptake

and processing can be tested using a labeled ovalbumin antigen that when processed emits fluorescence [232], followed by flow cytometry that includes phenotyping markers for various APCs. Antigen presentation via MHCII can be similarly tested, although for this analysis, it is necessary to use unlabeled ovalbumin and stain with an antibody that recognized peptide-bound MHC. For each proposed experiment, APCs from involution host livers would be compared with APCs from nulliparous hosts livers.

An additional experimental approach could investigate the functionality of liver APCS. Liver APCs include dendritic cells, macrophages, sinusoidal endothelial cells, and hepatic stellate cells [233]. Isolated APCs from livers of nulliparous or involution hosts would be incubated with antigen and subsequently cultured with CD4 T cells specific for that antigen. Readouts such as T cell proliferation and interferon-γ production would indicate whether APCs from involution hosts had impaired ability to activate T cells.

Additionally, the cytokine milieu of the liver is likely modulated by reproductive stage. Rationale for this is provided by our results showing altered polarization of CD4+ T cells in the involution liver (Figure 2-5). Because T cell polarization is influenced by distinct cytokines [234], these data support the prediction that cytokines are different between nulliparous and involution stages. Additionally, a preliminary (unpublished) study found increased TGFβ and IL-10 signaling in the liver during involution via RNA-sequencing of whole liver. Such cytokines are considered “anti-inflammatory” and would not be expected to support naïve T cell activation [235]. Further evidence for this hypothesis could be generated by measuring liver cytokines via ELISA.

Targeting liver metastasis

In our rodent models, weaning-induced mammary gland and liver tissue involution is tumor promotional and pro-metastatic. Mouse models have used preventative approaches to target the pro-tumor environment of the involuting mammary gland. Ibuprofen, given at the start of weaning at human equivalent dose of 200mg per day, was sufficient to reduce tumor growth and dissemination to the lower, nulliparous levels [53,54]. This approach was preventative, as the treatment was given before a tumor was established and aimed to preclude promotion of tumor growth and dissemination from the mammary gland during involution. One aim is to translate this preventative strategy from mice to humans. Such a strategy would have women take ibuprofen during the window of involution, which the Schedin lab has defined as being less than 3 months in humans [49]. It could be that only a subset of mothers at high risk for breast cancer would adopt this preventative strategy. Retrospective, population based studies on young women are ongoing in the Schedin lab to identify risk factors that put women at high risk of developing postpartum breast cancer.

Despite success at the primary site, similar preventative strategies that used ibuprofen or metformin, have not proven efficacious at preventing the promotion of metastasis in the involuting liver (unpublished data, Erica Goddard and Alex Bartlett). It is possible that a preventative approach could work at the metastatic site, and previous studies just didn't have the "right" target. For example, prostaglandins, which are downstream inflammatory mediators of arachidonic acid metabolism, are much lower in concentration in the involuting liver compared to the involuting mammary gland, providing one plausible explanation for why ibuprofen was ineffective at preventing liver

metastasis. Further, we found that ibuprofen treatment is sufficient to reduce prostaglandins in the involution liver (Figure 8-2), yet no treatment effect is observed, suggesting that COX2 activity may not be important for the pro-metastatic effect of liver involution. Instead, results from future investigations of the mechanism of immune suppression in the liver may shed light on alternative preventative targets in the liver. Yet in the reality of the clinical setting, a preventative approach that targets pro-metastatic attributes of the involuting liver may not be feasible, as breast cancer is thought to be either metastatic or non-metastatic at the time of primary breast cancer surgery and treatment. Instead, developing a therapeutic strategy for established liver metastasis may be more beneficial.

A therapeutic approach, by definition, treats disease once it is established. As such, mouse models to test possible therapeutics require a period where liver metastases grow prior to treatment with a drug. Treatment approaches could target the tumor cells themselves are/or components of the microenvironment that support metastasis.

As an example thought experiment, we initially hypothesized that tumor cells would use involution-specific ECM to facilitate establishment and survival in the liver niche. Our time course study that quantified tumor cell abundance at 1 and 3 days after portal vein injection into the liver was designed to help test that hypothesis. However, contrary to expectations, there was not an early advantage for tumor cells in the involution host with respect to increase tumor cell numbers, and instead nulliparous hosts had greater tumor cell abundance in the liver. This result suggested that ECM proteins do not promote early events related to tumor cell adhesion, intravasation, survival or proliferation after tumor cells encounter the involuting liver. Yet, tumor cell interaction

with ECM proteins could still be functionally significant for metastatic promotion. In support, we find that tumor cells in the involuting liver were more likely to exist as single cells, whereas in the nulliparous liver tumor cells were more likely to form clusters. This tumor cell behavior could be driven by interaction with ECM proteins, with involution-specific ECMs promoting tumor cell survival as single cells. Single tumor cells could be indicative of a mesenchymal phenotype, as solitary cells lack cell-cell adhesion with other tumor cells and show elongated morphology. In turn, these single – possibly mesenchymal-like - cells may have a metastatic advantage, possibly via evasion of the immune system [108,109,236]. Such possibilities could be investigated. First, one could study epithelial and mesenchymal biomarkers on tumor cells in involution or nulliparous hosts. The impact of ECM proteins specific to nulliparous or involution stages could also be modeled in vitro. Tumor cells could be cultured with isolated ECM from nulliparous and involution stage livers in order to assess outcomes such as cell morphology and EMT gene expression. If involution-specific ECMs seem to be inducing a mesenchymal phenotype, a strategy to block the interaction between tumor cell integrins specific for that ECM could be developed and tested.

Additional therapeutic approaches could be leveraged for liver metastases in general and not just targeted to the PPBC setting. One option would investigate ECM proteins that facilitate tumor cell survival in the liver niche irrespective of reproductive state. In our human BCLM histological characterization, we observed abundant intra-tumor ECM proteins. The tumor cells often sat directly on the ECM proteins, and there was evidence in chemotherapy-treated cases that tumor cells directly interacting with the ECM protein were protected from death. Thus, blocking that integrin-ECM interaction

prior to or concurrent with chemotherapy might act as a chemo-sensitizer. Another strategy could be immune-targeted. Preliminary data (presented in chapter 6) is suggestive that natural killer cells might be particularly potent at eliminating liver metastases. We showed that in the absence of T cells – yet presence of NK cells, no liver metastases grew into large (i.e. overt) tumors, whereas orthotropic injection of tumor cells into the mammary fat pad of the same mice formed tumors as expected (Figure 6-1). In that experiment, depletion of NK cells restored growth of liver metastases (Figure 6-2). Prior studies have demonstrated that NK cells and the cytokine IL-15, which supports NK cell survival, limit outgrowth of metastases in lung (tumor cells: melanoma) [237] and liver (tumor cells: gastric) [238]. These promising preclinical results are currently being tested in early stage human trials (NCT04150562, NCT03905135, NCT03759184, and NCT03388632). Here, we could test the efficacy of recombinant IL-15 in our mouse model of PPBC liver metastases.

Post-wean liver involution in women

I describe in chapter 3 of this thesis our finding in healthy normal women that liver size increases during pregnancy and decreases post-wean [130]. The goal of this study was to determine if the human liver underwent weaning-induced liver involution, as is the case for rodents [56]. Although we found that liver size was decreased post-wean compared to late pregnancy, we were unable to conclude that the reduction in liver size occurred after weaning. This is because the study design was limited to pregnancy and post-wean time points, and did not include a study visit while participants were still nursing. Based on our rodent data, we predict that liver size remains elevated in women through lactation – putatively because that increased liver size is required to meet the high metabolic

demands of milk production. Only with cessation of nursing (i.e. weaning), is the liver expected to return to its baseline size. However, as our human study did not have a lactation time point, and conceivably the decrease in liver size could have happened at parturition, we cannot definitely conclude the occurrence of weaning-induced liver involution in women. Therefore, future investigation into weaning-induced liver involution in women must include a lactation time point.

We also identified an association between bile acids and liver size in rodents and women. In rodents and women, during pregnancy, we found evidence of elevated activity in the bile acid synthetic pathway and increased bile acid concentrations. In rodents with weaning, bile acid synthesis is shut down. Since we do not have lactation data form women, we do know if bile acid production is also linked to lactation in women. In total our data are consistent with an increase in bile acids associating with increased liver size, and a decrease in bile acids associating with liver involution. Importantly, in other settings, bile acids are linked to liver regeneration and size regulation [156,162,163]. Together, these data support the hypothesis that during pregnancy an increase in the bile acid pool induces increased liver size. In mouse models, bile acid sufficiency to increase liver size could be tested by exogenously increasing the bile acid pool and observing the change in liver size. Conversely, the necessity of bile acids for liver size increase during pregnancy could also be evaluated. Such an experimental design would establish pregnant mice that are enrolled to either a control or experimental arm where bile acid signaling is perturbed. A few approaches could be used to modulate bile acid signaling. The size of the bile acid pool could be reduced by treating with ursodeoxycholic acid (UDCA), which has been demonstrated to reduce serum bile acids in the context of intrahepatic cholestasis of

pregnancy [239]. Other compounds, referred to as bile acid sequestrants, increase fecal excretion of bile acid and thus reduce the bile acid pool [240]. An alternative experimental approach could prevent hepatocytes from responding to signaling via the ligation of FGFR4, which is a receptor hepatocytes use to respond to shifting bile acid levels [158].

An untested question is whether the hormones of pregnancy and lactation play a role in modulating liver size. One possibility is that hepatocyte proliferation or hypertrophy are directly linked to estrogen, progesterone, and/or prolactin signaling. Alternatively, bile acid synthesis could be under direct or indirect control of these hormones. For example, it is known that estrogen and estrogen receptor contribute to repression of bile export from hepatocytes [241]. One could build rationale for the hypothesis that hormones regulate bile acid synthesis using computation approaches. For example, it is possible to querying for hormone response elements in the promoters of genes that regulate bile acid production. Experimentally, mice could be treated with concentrations of estrogen, progesterone, and prolactin that correspond to pregnancy and lactation concentrations. Then, circulating bile acids and bile acid genes could be evaluated.

Finally, we found some evidence that hypertension of pregnancy may interfere with the liver's ability to increase in size. This observation is limited because of the small sample size. To follow up on this intriguing hypothesis, additional study in humans is required. However, it could also be tested in a mouse model of gestational hypertension with the prediction that mice with hypertension would not have the same increase in liver size as control mice.

Exploration of Breast Cancer Liver Metastasis

Future directions for our study into liver metastasis and the liver metastatic niche in women with breast cancer liver metastasis are described in the "next steps" section of Chapter 4 of this document.

Other: characterization of the mouse involuting liver by RNA-sequencing

Weaning-induced liver involution has – to date – been described in only one published manuscript by Goddard et al [56]. This manuscript utilized approaches such as immunohistochemistry, flow cytometry, metabolomics, and quantitative ECM proteomics to characterize the rodent liver across reproductive stages. Reproductive stages included nulliparous, lactation, various days post-wean, and regressed (4-6 weeks post-wean). To extend this data set and further understand the involuting liver, we sought to perform gene expression analysis via RNA-sequencing on whole liver.

This RNA-sequencing study included tissues from mice in nulliparous, lactation, involution (Inv) day 2, InvD4, InvD6, InvD8, and regressed stages. Whole livers from three historical studies were utilized to build the tissue cohort. Two of the studies (2 and 3) were performed at CU Anschutz campus with mice ordered from Jackson labs; the third study was performed at OHSU with mice ordered from Charles River. All mice were about 12-13 old at time of euthanasia, except for the regressed group which was about 16 weeks old. RNA was extracted from whole liquid nitrogen snap-frozen liver tissues using Trizol and the Fischer Scientific Zymo Direct-zol RNA MicroPrep kit. RNA was analyzed to generate RIN and RNA concentration values to determine if samples were suitable for sequencing. Samples that passed quality control and went on to sequencing, along with the study they came from, are listed in table 1.

Table 5-1 Samples that completed RNA-sequencing

Number	Stage	VPLIR Study	Number	Stage	VPLIR
220	Nullip	2	215	Inv D4	2
221	Nullip	2	211	Inv D4	2
227	Nullip	3	13	Inv D4	3
226	Nullip	3	75	Inv D4	4a (NSAID)
4	Nullip	4a (NSAID)	105	Inv D4	4a (NSAID)
1	Nullip	4a (NSAID)			
13	Nullip	4a (NSAID)	209	Inv D6	2
			201	Inv D6	2
213	Lac D10	2	218	Inv D6	2
200	Lac D10	2	216	Inv D6	2
240	Lac D10	3	230	Inv D6	3
102	Lac D10	4a (NSAID)	232	Inv D6	3
133	Lac D10	4a (NSAID)			
136 (may be labeled "36")	Lac D10	4a (NSAID)	98b	InvD8	3
			101b	InvD8	3
31	InvD2	3	14	InvD8	3
39	InvD2	3			
224	InvD2	3	214	Reg 4wks	2
101	InvD2	4a (NSAID)	203	Reg 4wks	2
120	InvD2	4a (NSAID)	234	Reg 4wks	3
71	InvD2	4a (NSAID)	239	Reg 4wks	3

Because this experiment was launched at the onset of the Covid-19 pandemic in March 2020, the RNA samples were set to an outside (i.e. non-OHSU) resource for sequencing. Library preparation and sequencing was performed by Novogene (Beijingm China). Libraries were prepared using a PolyA enrichment approach using the NEBNext Ultra TM II RNA Libarray Prep Kit. Sequencing was performed with the Illumina

NovaSeq platform. Data alignment, generation of gene counts, normalization and differential gene expression were performed by the laboratory of Dr. Zheng Xia at OHSU. Data analysis is ongoing in collaboration between the Schedin and Zheng Xia labs.

This research will capture a global view of how the liver and its individual cell populations, such as hepatocytes, resident fibroblasts (hepatic stellate cells), macrophages, and adaptive immune cells, change between nulliparous-lactation-involution-regressed reproductive stages. It will also allow us to answer specific questions, such as:

1) Is there a "pro-metastatic signature" in the normal liver during involution, as identified and described previously in the liver [73]?

2) Do hepatic stellate cells from involution hosts resemble physiologically activated fibroblasts identified in mammary gland involution [150]?

3) Are immune checkpoint pathways active during involution (e.g. PD1-PDL1, CTLA4)? Is there evidence for immune suppression?

4) Are cell death signatures (apoptosis, necroptosis, ferroptosis, pyroptosis) enriched in involution stage samples?

These outcomes are expected to not only describe weaning-induced liver involution at the gene expression level, but also yield insight into the liver pre-metastatic niche established by involution.

Chapter 6 Appendix A: NK cells limit liver metastasis in nude hosts

Liver metastases have poor overall survival with only 15-20% of patients eligible for curative-intent surgical resection [223]. Recently clinical trials have assessed the efficacy of new immunotherapeutic agents to treat liver metastasis. Specifically, studies have tested drugs that prevent signaling through the protein PD1, which typically inhibits T cell responses [242]. Unfortunately, liver metastases seem to be poorly responsive to immune checkpoint inhibitors (ICI) [243,244]. A proposed mechanism suggests that tumor-specific cytotoxic T cells accumulate and undergo apoptosis in the liver, thereby hampering the anti-tumor immune response ICI aim to boost [245]. An additional, not mutually exclusive, explanation is that the unique immunological hallmarks of the liver, including resident macrophages and significant numbers of natural killer (NK) and NKT cells [246], constrain T cell responses. These liver resident immune cells may create a tumor microenvironment that is best suited to alternative forms of immunotherapy that do not rely exclusively on ICI. This study investigated how the presence of T, natural killer, and NKT cells impact overt liver metastases using a model in which tumor cells are delivered to the liver via intraportal injection to hosts that were either wiltype, nude, or nude with NK-depletion.

Materials and Methods

Animal Husbandry

Mice were used as described in Bartlett et al[134]. In addition to wildtype Balb/C mice, athymic nude Balb/C mice (CAnN.Cg-Foxn1nu/Crl) were purchased from Charles River Laboratory.

Liver Metastasis Studies

D2.OR mammary tumor cells were washed and suspended in cold (i.e. from the fridge) 1× PBS. Cells were tested in January 2018, were confirmed murine pathogen and Mycoplasma free, and the origin of cells was validated (Idexx Bioresearch, Columbia, MO, USA). Cells used in these studies were within 3 passages of tested vials. Liver metastases were induced by intra-portal vein injection of 50,000 D2OR cells in 10uL PBS, as previously described [64]. Tumor cells were injected into wildtype and nude mice that were either 2 days after weaning, involution day 2 (InvD2), or age-matched never-pregnant (nullip). Six weeks after tumor cell injection, whole liver was dissected, formalin-fixed, and paraffin embedded (FFPE) for histological analyses. Liver metastases were assessed by visual assessment of the liver at time of euthanasia, and by hematoxylin and eosin staining of FFPE liver sections to evaluate for presence of tumors, tumor size, tumor multiplicity, and tumor morphology.

NK Depletion Experiment

Anti-asialo GM1 (Wako Chemicals #986-10001) antibody was used for NK depletion studies according to manufacturer instruction. Control group mice received an isotype control antibody ((BioxCell BE0095 rabbit polyclonal IgG). Antibodies were delivered in 200 µL sterile PBS via intraperitoneal injection, with initial dose given at day 0 and subsequent doses given every 4 days.

Results

In prior studies using the portal vein model in female nulliparous mice, overt liver metastasis incidence was about 30% across 2 different mammary tumor cell lines. The incidence rose to 80-100% when tumor cells were delivered to hosts in the post-wean window (involution day 2) [56,134]. Conversely, when tumor cells were delivered to nude

hosts, either nulliparous or involution stages, the incidence of metastases dropped to 0% (Fig 6-1A). However, tumor cells injected into the mammary gland of nude mice grew robustly with 100% take (Fig 6-1B).

We sought to understand why tumors would grow in the mammary gland of nude mice but not the liver. Nude hosts lack T cells and NKT cells; however, NK cells are present. Furthermore, the liver is enriched for NK cells, whilst the mammary gland has few NK cells[247] . We hypothesized that NK cells, when in the background of T- and NKT-cell depletion (i.e. nude host), restrict outgrowth of mammary tumor cells in the liver. To test this hypothesis, NK cells were depleted from nude hosts prior to portal vein injection of mammary tumor cells. Isotype antibody treated nude mice served as controls. NK cell depletion in the liver was confirmed by flow cytometry (Fig 6-2A). At study endpoint six weeks after tumor cell injection, we found increased incidence of metastasis in the NK-depleted group compared to isotype control (Fig 6-2B), as well as increased number of metastases per mouse (Fig 6-2C).

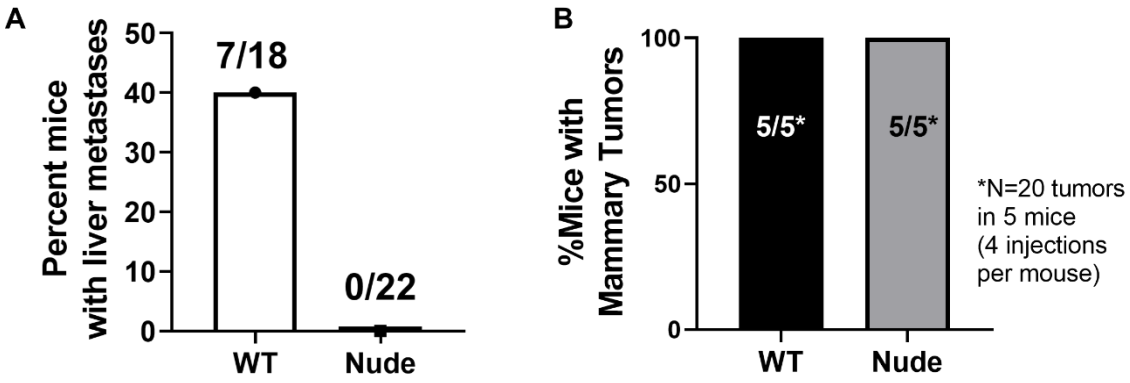

Figure 6-1 Tumor growth in nude mice

A. Incidence of liver metastases 6 weeks after portal vein injection of mouse mammary tumor cells into age-matched wildtype or nude mice. Liver metastases in the wildtype group consisted of 2/11 nulliparous and 5/7 involution stage mice. The nude group contained n = 16 nulliparous and n = 6 involution stage mice. **B.** Incidence of mammary fat pad tumors in wildype and nude hosts following fat pad injection of mouse mammary tumor cells. All mice were nulliparous stage.

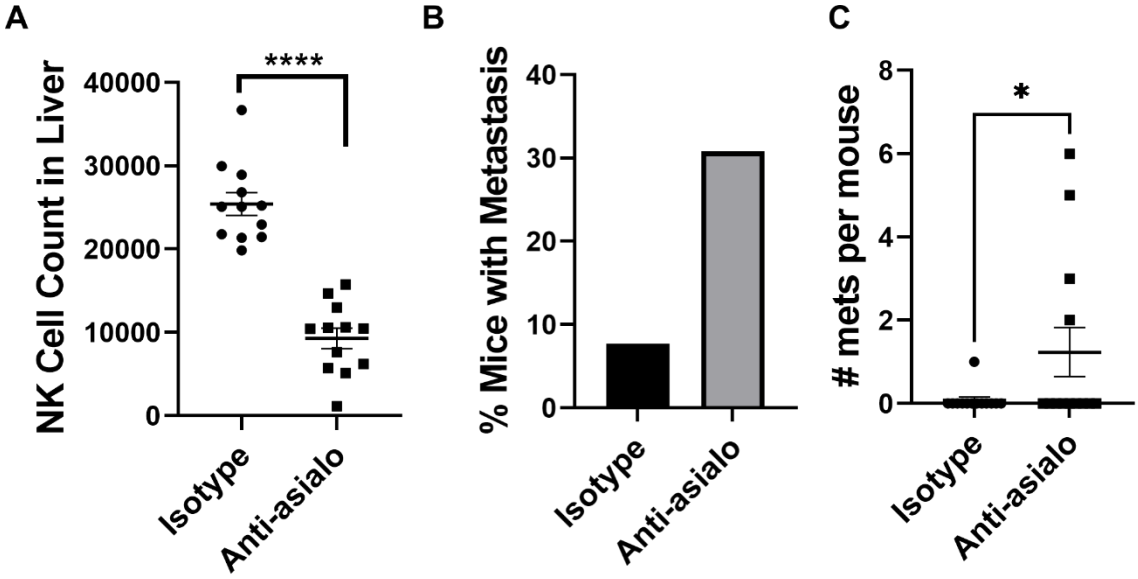

Figure 6-2 NK depletion in nude mice restores liver metastatic growth

A. Flow cytometry quantification of NK cells via surface marker staining for CD49b and NKp46 in whole livers from mice 5 days after intraperitoneal injection with isotype or anti-asialo antibody. Incidence (**B.)** and multiplicity (**C.)** of liver metastasis in nude hosts treated with isotype (n = 13) or anti-asialo (n = 13) antibody; $p<0.05$ by one-tailed Mann-Whitney test.

These data suggest that NK cells play an important role in controlling liver metastases in nude hosts, and that NK activity in wild type hosts is insufficient to control liver metastases. Future studies are required to validate these findings and investigate NK cell functional status in nude versus wild type host livers. Increasing NK cell cytotoxic activity could be an effective immunotherapy strategy to control liver metastases.

Chapter 7 Appendix B: Overt liver metastatic advantage in involution hosts is maintained with injection of 500,000 tumor cells

Prior studies demonstrating overt liver metastatic promotion in the involuting liver with D2OR mouse mammary tumor cells used 50,000 injected cells. To investigate the mechanism of metastatic promotion, additional portal vein injection experiments were performed with shorter time courses: 90 minutes, 1 day, and 3 day endpoints post-injection. These studies required use of 500,000 injected D2OR cells in order to locate and study the tumor cells within the liver. This approach had the assumption that metastatic promotion in the involution liver would be maintained with 10-fold more cells than used for the original experiments, which demonstrated increased overt liver metastasis in the involution host. This study aimed to evaluate that assumption, and directly tested whether portal vein injection of 500,000 tumor cells with a longer time course (6 week endpoint) would replicate the findings that used 50,000 tumor cells.

Approach

500,000 D2OR mouse mammary tumor cells were injected via the portal vein into either nulliparous or involution stage mice, as previously described [64]. Mice were monitored until the 6 week study endpoint, at which mice were euthanized and livers dissected. Livers were washed, photographed, and collected for FFPE. Metastases were evaluated by eye and using measurements from photographs.

Results and conclusions

We found that overt liver metastatic promotion in involution hosts was maintained with injection of 500,000 D2OR cells. In the involution group, 11/12 mice had liver metastases whereas 8/12 nulliparous mice had liver metastases (Fig 7-1A). This

incidence is higher than observed with the 50,000 cell number, as expected. The overall tumor burden in the liver was significantly greater in involution stage hosts compared to nulliparous (Fig 7-1B), although multiplicity did not differ (Fig 7-1C). These data support the assumption that the involution metastatic advantage is maintained with 500,000 tumor cells. Importantly, these data allows us to interpret the early time-course study results (90 minutes, 1 day, and 3 days) knowing that if those studies were allowed to progress to 6 weeks – involution mice would have more liver metastasis.

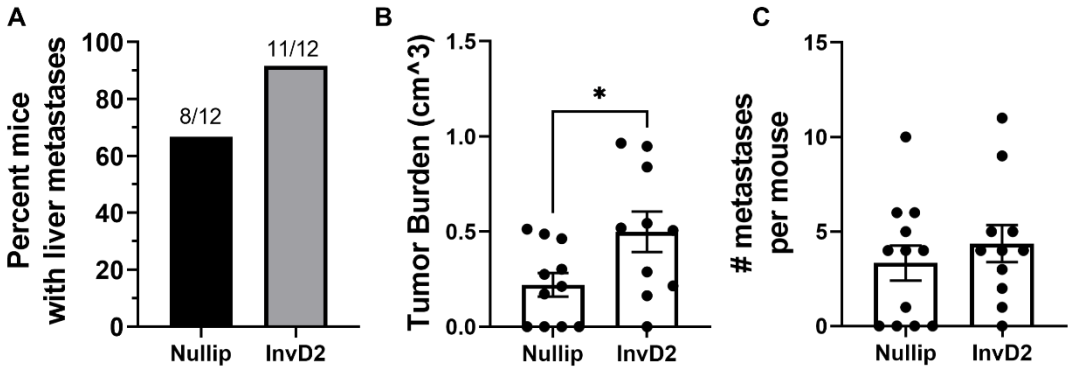

Figure 7-1 Liver metastasis is increased in involution hosts with 500,000 injected tumor cells

A. Incidence of overt liver metastases as called by visual inspection of the liver at time of sacrifice, 6 weeks post-tumor cell injection. Tumor burden (cm^3) (**B.)** and multiplicity (**C.)** of liver metastases. Two-tailed students T test, $p<0.05$.

Chapter 8 Appendix C: Lipid accumulation as a new feature of weaning-induced liver involution

Lipids are a class of hydrophobic macromolecules that include a diverse range of sub-categories from fatty acids to sterols. Lipids affect diverse cellular behaviors and act as signals that induce tissue-level reprogramming [248], including induction of cell death [249–251]. Lipids have also been implicated in monocyte-mediated immune suppression [252,253] and linked to metastatic promotion [254]. In the context of weaning-induced mammary gland involution, oleic acid is critical for induction of mammary epithelial cell death [249,255] and prostaglandins contribute to tumor promotion [53,54]. Arachidonic acid, an eicosanoid, is metabolized by cyclooxygenase (COX) enzymes into prostaglandins or by lipoxygenases into HETEs (Hydroxyicosatetraenoic acid). These downstream molecules potentiate inflammation via increasing platelet aggregation, vascular permeability, and production of chemotactic factors [256]. Given the importance of lipid in the mammary gland during involution and the role in inflammation, we sought to investigate a role of lipids in the liver. Specifically, lipid droplet accumulation, eicosanoid species, and fatty acid composition during weaning were investigated.

Approach

Immunohistochemical staining for adipophilin was used to evaluate lipid droplets in FFPE liver tissues from mice across reproductive stages. Adipophilin, also known as perilipin 2, is a protein embedded in the plasma membrane of lipid droplets and is used to measure lipid accumulation in tissues [257,258]. The primary antibody was perilipin-2 (ADPH, 1:1000, Novus Biologicals #NB110-40878) for 60 minutes; secondary antibody was anti-rabbit (RTU Dako K4003) for 30 minutes. Signal quantification was performed with Aperio ImageScope color deconvolution algorithm.

Lipidomics was performed to measure eicosanoids and free fatty acid species in whole liquid nitrogen flash frozen liver. The Mass Spectrometry Lipidomics Core Facility at UC Denver, headed by Drs. Robert Murphy, carried out targeted LC-MS/MS. The targeted approach quantified selected free fatty acids (lauric, palmitoleic, palmitic, γ-linoleic, α-linoleic, oleic, and arachidonic acid) and arachidonic acid-derived eicosanoids (TXB2, PGD2, PGE2, PGF2α, 6-keto-PGF1α, 5-HETE, 12-HETE, and 15-HETE). Note that leukotrienes were not able to be detected in an optimization experiment, so were not advanced in the full study set. Samples were prepared from whole livers from nulliparous, lactation, involution day 2, and involution day 2 treated with ibuprofen (n = 5/group from Balbc VPLIR NSAID 4a).

Results

Previous IHC staining and quantification on rat livers showed a spike in adipophilin (ADPH) protein at involution day 2 with levels during nulliparous, pregnancy, lactation, InvD4, InvD6, and regressed stages all being similar. The increase was about 2-fold. Here, we observed reproductive-stage dependent changes in adipophilin percent area positive and in localization. Representative ADPH stains in mouse liver are shown in Figure 8-1A. We found an increase in lipid droplets at InvD4 and InvD8, with a return to nulliparous like levels by the fully regressed stage (Fig 8-1B). ADPH appeared reduced at lactation stages, which is consistent with reduced storage of lipid in the liver. Reduced lipid storage in the liver may be attributed to higher metabolic demand for lipid to accommodate milk production. Further, the staining pattern seemed to change by reproductive stage. In particular, it appears that there was a higher density of ADPH around the portal vein in InvD2 host livers (Fig 8-1A, third panel from left). To

determine if there was a measurable increase in lipid droplets around the portal vein, periportal areas were annotated and analyzed (Fig 8-1C). There was a significant increase in ADPH staining in the periportal area at InvD2 compared to lactation (Fig 8-1D). These data are consistent with re-accumulation of lipid droplets from the circulation in early involution, as the portal vein is where blood enters the liver from the gut. Note that blood also enters the liver via the hepatic artery, which is not easily visualized in FFPE mouse liver sections but is immediately adjacent to the portal vein. Such re-accumulation of lipid from the circulation at InvD2 is consistent with the idea that these lipids could act as a signal to initiate involution as the metabolic demand for lipid has ceased.

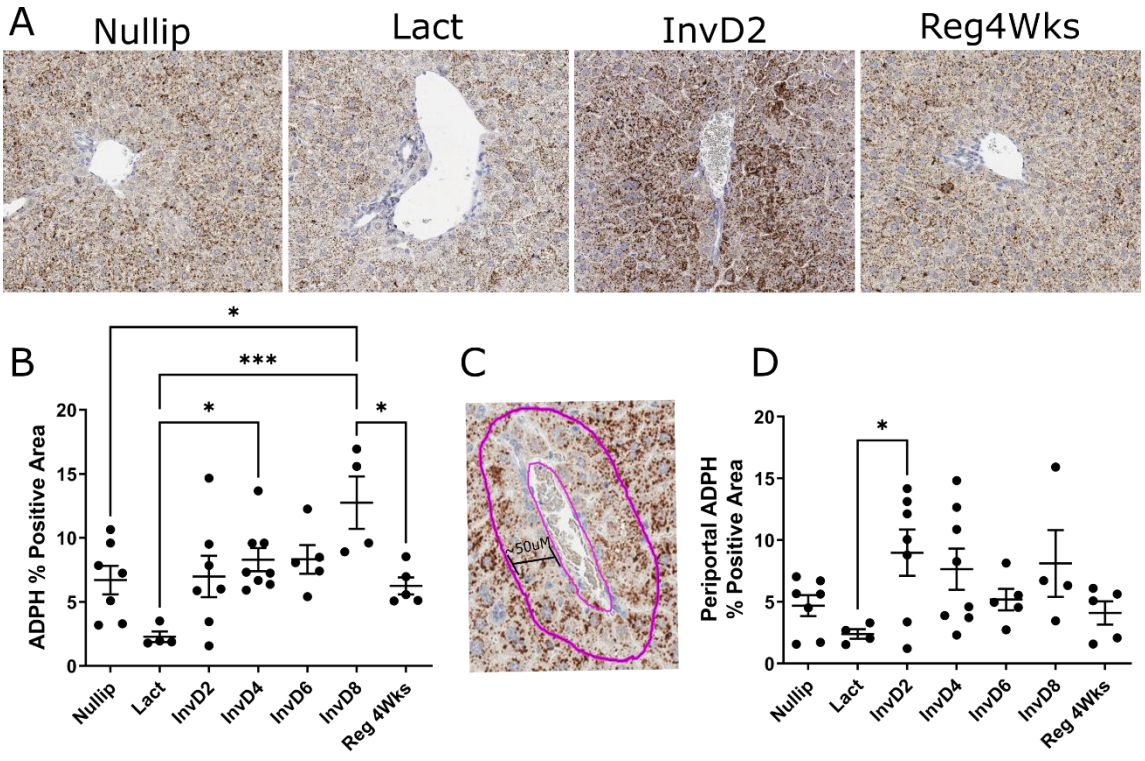

Figure 8-1 Adipophilin protein expression across reproductive stages in mouse liver

A. Representative images of livers stained with adipophilin antibody from nulliparous, lactation, involution day 2, and regressed 4 week reproductive stages. **B.** Quantification of ADPH staining across the whole liver tissue section; One-way ANOVA with multiple

comparisons, *$p<0.05$, *** $p<0.001$. **C**. Example of quantification of ADPH staining in the periportal zone of liver. Three portal veins areas were assessed per case. Vein lumens were negatively annotated to be excluded from analyses. The area between the outer and inner annotation was analyzed. **D.** Quantification of periportal associated ADPH staining; Two-tailed student's T test; $p<0.05$.

We next investigated the composition of eicosanoids in the liver at nulliparous, lactation, and involution day 2 stages +/- IBU treatment via mass spectroscopy on whole liver. Specifically, we were interested in the metabolism of arachidonic acid by lipoxygenase and cyclooxygenase (COX) enzymes into inflammatory mediators HETEs and prostaglandins (Fig 8-2A). We found that arachidonic acid was decreased during lactation compared to nulliparous and InvD2, and that IBU-treatment did not change arachidonic acid levels (Fig 8-2B). The three measured HETE metabolites were increased at InvD2 and effectively reduced with IBU treatment (Fig 8-2C-E). Similarly, prostaglandins were increased at InvD2 and reduced with IBU treatment (Fig 8-2F-H).

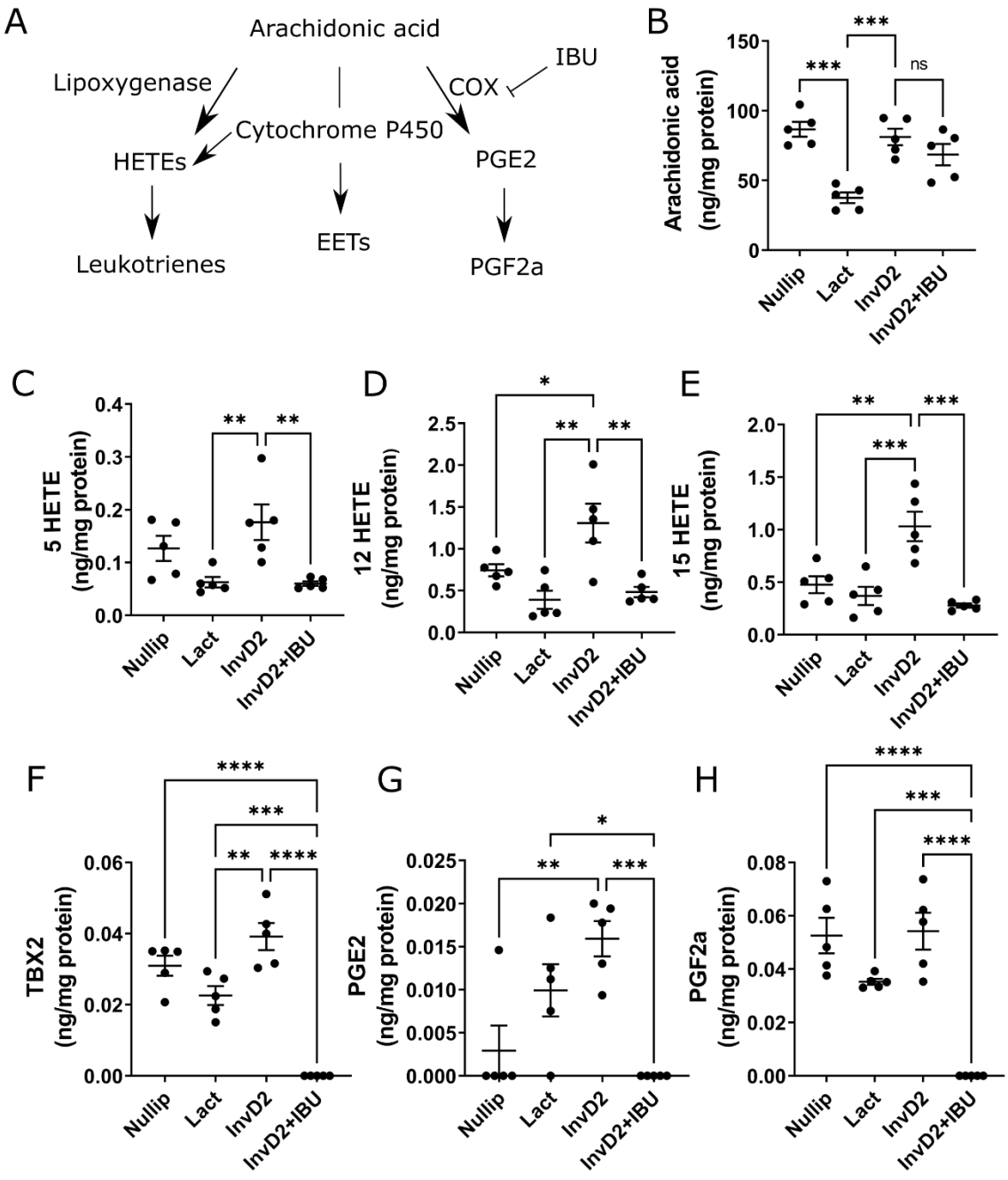

Figure 8-2 Reproductive stage dependent levels of inflammatory mediators

A. Downstream byproducts of arachidonic metabolism by lipoxygenase, cytochrome p450, and cyclooxygenase (COX) enzymes. Note that leukotrienes and EETs were not measured in this study. **B.** Arachidonic acid is reduced during lactation, and not impacted by ibuprofen treatment. **C-E.** Byproducts of lipoxygenase activity on arachidonic acid. **F-H.** Byproducts of COX activity on arachidonic acid. One-way ANOVA *p<0.05, ** p<0.01, *** p<0.001, **** p<0.0001.

We measured select free fatty acids, and sought to use the results to understand fatty acid metabolism in the liver by reproductive stage. The synthesis of fatty acids in the liver is referred to as *de novo* lipogenesis. To assess the rate of fatty acid synthesis, we computed the ratio of palmitic acid (16:0) to linoleic acid (18:2), which is known as the "*de novo* lipogenesis index". We found that *de novo* lipogenesis was significantly increased during lactation compared to nulliparous and InvD2 stages (Fig 8-3A). In contrast, beta-oxidation is the process that breaks down (i.e. catabolizes) free fatty acids into a usable energy source for the cell. Each cycle of beta-oxidation creates one acetyl-CoA molecule and results in a fatty acid chain with two less carbons. The acetyl-CoA is used as input into the citric acid cycle. The ratio of oleic acid (18:1) to stearic acid (18:0) denotes the "desaturation index", which serves as a readout for the rate of beta-oxidation. Desaturation index was increased at InvD2 compared to lactation (Fig 3B). Next, we asked whether the overall profile of fatty acids changed across reproductive stages. Analysis of all measured free fatty acids by principle component analysis (PCA) showed that fatty acid composition is reproductive stage dependent (Fig 8-3C). Free fatty acid profile was distinct at each of the measured reproductive stages, with lactation being most different compared to nulliparous and InvD2 stages (Fig 8-3C).

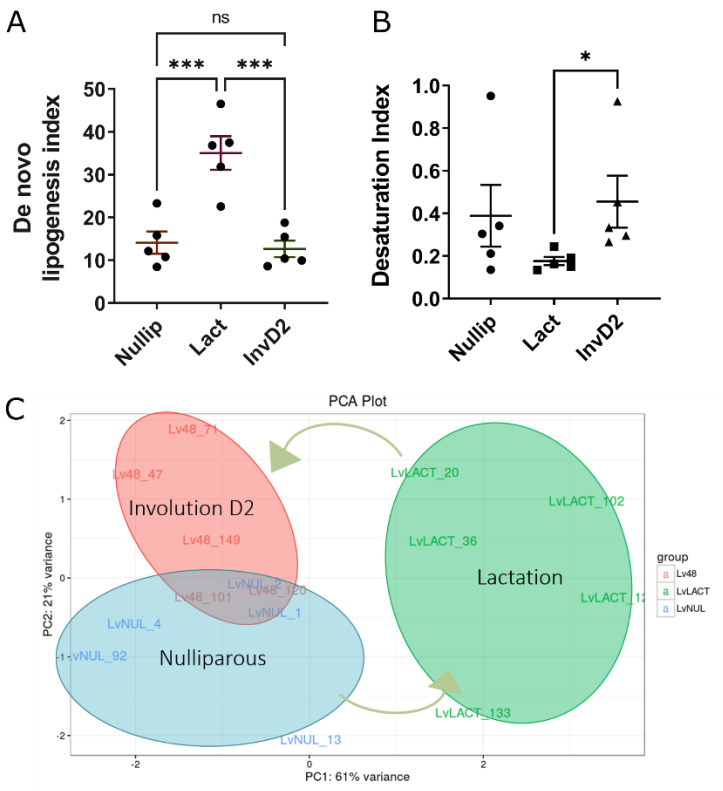

Figure 8-3 Free fatty acid composition is determine by reproductive stage

A. Ratio of palmitic to linoleic acid describes the de novo lipogenesis index, one-way ANOVA with multiple comparisons; **B.** Ratio of oleic to stearic acid denotes desaturation index, one-tailed Student's T test. **C.** Principle component analysis of free fatty acid species. N=5/group. *p<0.05, *** p<0.001.

Conclusions

These data show accumulation of lipid droplets during early involution in both mouse and rat (data not shown, Erica Goddard), which suggest that lipid accumulation is a characteristic of weaning-induced liver involution. Furthermore, the unique eicosanoid and fatty acids profiles at nulliparous, lactation, and involution day 2 stages indicate dynamic regulation of lipid in the liver, potentially coordinated to reproductive stage-specific requirements. For example, increased HETEs and prostaglandins at involution day 2 are consistent with acute inflammation, which is expected given the immune influx that occurs post-wean. Furthermore, the reduction in these inflammatory mediators with ibuprofen treatment is evidence that ibuprofen is effectively "hitting its target" in the liver when given prophylactically at the beginning of weaning. The increased rate of fatty acid synthesis during lactation is expected, given our hypothesis that the liver supports milk production via increased anabolic metabolism. Also consistent with this hypothesis are the reduction in *de novo* lipogenesis and increase in fatty acid breakdown post-wean. Whether the increased lipid in the liver environment following weaning contributes to hepatocyte cell death, myeloid cell-mediated immune suppression, or metastatic promotion is unknown.

Chapter 9 References

1. Chelmow, D. *et al.* Executive Summary of the Early-Onset Breast Cancer Evidence Review Conference. *Obstet. Gynecol.* **135**, 1457–1478 (2020).
2. Surveillance Research Program, National Cancer Institute. SEER*Explorer. *SEER*Explorer: An interactive website for SEER cancer statistics* https://seer.cancer.gov/explorer/.
3. DeSantis, C. E. *et al.* Breast cancer statistics, 2019. *CA Cancer J. Clin.* **69**, 438–451 (2019).
4. Siegel, R. L., Miller, K. D. & Jemal, A. Cancer statistics, 2020. *CA Cancer J. Clin.* **70**, 7–30 (2020).
5. Johnson, R. H., Chien, F. L. & Bleyer, A. Incidence of breast cancer with distant involvement among women in the United States, 1976 to 2009. *JAMA* **309**, 800–805 (2013).
6. Anders, C. K., Johnson, R., Litton, J., Phillips, M. & Bleyer, A. Breast cancer before age 40 years. *Semin. Oncol.* **36**, 237–249 (2009).
7. Gnerlich, J. L. *et al.* Elevated breast cancer mortality in women younger than age 40 years compared with older women is attributed to poorer survival in early-stage disease. *J. Am. Coll. Surg.* **208**, 341–347 (2009).
8. Anders, C. K. *et al.* Young age at diagnosis correlates with worse prognosis and defines a subset of breast cancers with shared patterns of gene expression. *J. Clin. Oncol.* **26**, 3324–3330 (2008).
9. Partridge, A. H. *et al.* Subtype-Dependent Relationship Between Young Age at Diagnosis and Breast Cancer Survival. *J. Clin. Oncol.* **34**, 3308–3314 (2016).

10. Nixon, A. J. *et al.* Relationship of patient age to pathologic features of the tumor and prognosis for patients with stage I or II breast cancer. *J. Clin. Oncol.* **12**, 888–894 (1994).
11. Azim, H. A., Jr *et al.* Elucidating prognosis and biology of breast cancer arising in young women using gene expression profiling. *Clin. Cancer Res.* **18**, 1341–1351 (2012).
12. Ford, D. *et al.* Genetic heterogeneity and penetrance analysis of the BRCA1 and BRCA2 genes in breast cancer families. The Breast Cancer Linkage Consortium. *Am. J. Hum. Genet.* **62**, 676–689 (1998).
13. Copson, E. R. *et al.* Germline BRCA mutation and outcome in young-onset breast cancer (POSH): a prospective cohort study. *Lancet Oncol.* **19**, 169–180 (2018).
14. Rosenberg, S. M. *et al.* BRCA1 and BRCA2 Mutation Testing in Young Women With Breast Cancer. *JAMA Oncol* **2**, 730–736 (2016).
15. Andrieu, N. *et al.* Pregnancies, breast-feeding, and breast cancer risk in the International BRCA1/2 Carrier Cohort Study (IBCCS). *J. Natl. Cancer Inst.* **98**, 535–544 (2006).
16. Scannell Bryan, M. *et al.* Limited influence of germline genetic variation on all-cause mortality in women with early onset breast cancer: evidence from gene-based tests, single-marker regression, and whole-genome prediction. *Breast Cancer Res. Treat.* **164**, 707–717 (2017).
17. Mealey, N. E. *et al.* Mutational landscape differences between young-onset and older-onset breast cancer patients. *BMC Cancer* **20**, 212 (2020).

18. Tan, A. R. *et al.* Molecular profiling comparison of breast cancer subtypes in young women and older women. *J. Clin. Orthod.* **35**, 11581–11581 (2017).
19. Vanharanta, S. & Massagué, J. Origins of metastatic traits. *Cancer Cell* **24**, 410–421 (2013).
20. Paul, M. R. *et al.* Genomic landscape of metastatic breast cancer identifies preferentially dysregulated pathways and targets. *J. Clin. Invest.* **130**, 4252–4265 (2020).
21. Ording, A. G. *et al.* Site of metastasis and breast cancer mortality: a Danish nationwide registry-based cohort study. *Clin. Exp. Metastasis* **34**, 93–101 (2017).
22. Pentheroudakis, G. *et al.* Metastatic breast cancer with liver metastases: a registry analysis of clinicopathologic, management and outcome characteristics of 500 women. *Breast Cancer Res. Treat.* **97**, 237–244 (2006).
23. Adam, R. *et al.* Is liver resection justified for patients with hepatic metastases from breast cancer? *Ann. Surg.* **244**, 897–907; discussion 907-8 (2006).
24. Chen, S. *et al.* Prognostic factors and survival outcomes according to tumor subtype in patients with breast cancer lung metastases. *PeerJ* **7**, e8298 (2019).
25. Niikura, N. *et al.* Treatment outcomes and prognostic factors for patients with brain metastases from breast cancer of each subtype: a multicenter retrospective analysis. *Breast Cancer Res. Treat.* **147**, 103–112 (2014).
26. Wang, R. *et al.* The Clinicopathological features and survival outcomes of patients with different metastatic sites in stage IV breast cancer. *BMC Cancer* **19**, 1091 (2019).

27. Wu, Q. *et al.* Breast cancer subtypes predict the preferential site of distant metastases: a SEER based study. *Oncotarget* **8**, 27990–27996 (2017).

28. Cummings, M. C. *et al.* Metastatic progression of breast cancer: insights from 50 years of autopsies. *J. Pathol.* **232**, 23–31 (2014).

29. Woods, K. L., Smith, S. R. & Morrison, J. M. Parity and breast cancer: evidence of a dual effect. *Br. Med. J.* **281**, 419–421 (1980).

30. Pathak, D. R. Dual effect of first full term pregnancy on breast cancer risk: empirical evidence and postulated underlying biology. *Cancer causes & control: CCC* vol. 13 295–298 (2002).

31. Albrektsen, G., Heuch, I., Hansen, S. & Kvåle, G. Breast cancer risk by age at birth, time since birth and time intervals between births: exploring interaction effects. *Br. J. Cancer* **92**, 167–175 (2005).

32. Schedin, P. Pregnancy-associated breast cancer and metastasis. *Nat. Rev. Cancer* **6**, 281–291 (2006).

33. Bladström, A., Anderson, H. & Olsson, H. Worse survival in breast cancer among women with recent childbirth: results from a Swedish population-based register study. *Clin. Breast Cancer* **4**, 280–285 (2003).

34. Daling, J. R., Malone, K. E., Doody, D. R., Anderson, B. O. & Porter, P. L. The relation of reproductive factors to mortality from breast cancer. *Cancer Epidemiol. Biomarkers Prev.* **11**, 235–241 (2002).

35. Whiteman, M. K. *et al.* Reproductive history and mortality after breast cancer diagnosis. *Obstet. Gynecol.* **104**, 146–154 (2004).

36. Azim, H. A., Jr. *et al.* Prognosis of pregnancy-associated breast cancer: a meta-analysis of 30 studies. *Cancer Treat. Rev.* **38**, 834–842 (2012).

37. Callihan, E. B. *et al.* Postpartum diagnosis demonstrates a high risk for metastasis and merits an expanded definition of pregnancy-associated breast cancer. *Breast Cancer Res. Treat.* **138**, 549–559 (2013).

38. Goddard, E. T. *et al.* Association Between Postpartum Breast Cancer Diagnosis and Metastasis and the Clinical Features Underlying Risk. *JAMA Netw Open* **2**, e186997 (2019).

39. Amant, F. *et al.* Prognosis of women with primary breast cancer diagnosed during pregnancy: results from an international collaborative study. *J. Clin. Oncol.* **31**, 2532–2539 (2013).

40. Stensheim, H., Møller, B., van Dijk, T. & Fosså, S. D. Cause-specific survival for women diagnosed with cancer during pregnancy or lactation: a registry-based cohort study. *J. Clin. Oncol.* **27**, 45–51 (2009).

41. Amant, F. *et al.* The definition of pregnancy-associated breast cancer is outdated and should no longer be used. *Lancet Oncol.* **22**, 753–754 (2021).

42. Phung, M. T., Tin Tin, S. & Elwood, J. M. Prognostic models for breast cancer: a systematic review. *BMC Cancer* **19**, 230 (2019).

43. Strange, R., Li, F., Saurer, S., Burkhardt, A. & Friis, R. R. Apoptotic cell death and tissue remodelling during mouse mammary gland involution. *Development* **115**, 49–58 (1992).

44. Lund, L. R. *et al.* Two distinct phases of apoptosis in mammary gland involution: proteinase-independent and -dependent pathways. *Development* **122**, 181–193 (1996).

45. Stein, T. *et al.* Involution of the mouse mammary gland is associated with an immune cascade and an acute-phase response, involving LBP, CD14 and STAT3. *Breast Cancer Res.* **6**, R75-91 (2004).

46. O'Brien, J. *et al.* Alternatively activated macrophages and collagen remodeling characterize the postpartum involuting mammary gland across species. *Am. J. Pathol.* **176**, 1241–1255 (2010).

47. Wilkinson, H. N. & Hardman, M. J. Wound healing: cellular mechanisms and pathological outcomes. *Open Biol.* **10**, 200223 (2020).

48. Jindal, S. *et al.* Postpartum breast involution reveals regression of secretory lobules mediated by tissue-remodeling. *Breast Cancer Res.* **16**, R31 (2014).

49. Jindal, S., Narasimhan, J., Borges, V. F. & Schedin, P. Characterization of weaning-induced breast involution in women: implications for young women's breast cancer. *NPJ Breast Cancer* **6**, 55 (2020).

50. Rybinski, B., Franco-Barraza, J. & Cukierman, E. The wound healing, chronic fibrosis, and cancer progression triad. *Physiol. Genomics* **46**, 223–244 (2014).

51. Schedin, P., O'Brien, J., Rudolph, M., Stein, T. & Borges, V. Microenvironment of the involuting mammary gland mediates mammary cancer progression. *J. Mammary Gland Biol. Neoplasia* **12**, 71–82 (2007).

52. McDaniel, S. M. *et al.* Remodeling of the mammary microenvironment after lactation promotes breast tumor cell metastasis. *Am. J. Pathol.* **168**, 608–620 (2006).

53. Lyons, T. R. *et al.* Postpartum mammary gland involution drives progression of ductal carcinoma in situ through collagen and COX-2. *Nat. Med.* **17**, 1109–1115 (2011).

54. Pennock, N. D. *et al.* Ibuprofen supports macrophage differentiation, T cell recruitment, and tumor suppression in a model of postpartum breast cancer. *J Immunother Cancer* **6**, 98 (2018).

55. O'Brien, J. *et al.* Non-steroidal anti-inflammatory drugs target the pro-tumorigenic extracellular matrix of the postpartum mammary gland. *Int. J. Dev. Biol.* **55**, 745–755 (2011).

56. Goddard, E. T. *et al.* The Rodent Liver Undergoes Weaning-Induced Involution and Supports Breast Cancer Metastasis. *Cancer Discov.* **7**, 177–187 (2017).

57. Tigas, S., Sunehag, A. & Haymond, M. W. Metabolic Adaptation to Feeding and Fasting during Lactation in Humans. *J. Clin. Endocrinol. Metab.* **87**, 302–307 (2002).

58. Betts, C. B., Quackenbush, A., Anderson, W., Marshall, N. E. & Schedin, P. J. Mucosal Immunity and Liver Metabolism in the Complex Condition of Lactation Insufficiency. *J. Hum. Lact.* **36**, 582–590 (2020).

59. Loisel, F., Farmer, C., Ramaekers, P. & Quesnel, H. Colostrum yield and piglet growth during lactation are related to gilt metabolic and hepatic status prepartum. *J. Anim. Sci.* **92**, 2931–2941 (2014).

60. Rawson, P. *et al.* Metabolic proteomics of the liver and mammary gland during lactation. *J. Proteomics* **75**, 4429–4435 (2012).

61. Rudolph, M. C. *et al.* Metabolic regulation in the lactating mammary gland: a lipid synthesizing machine. *Physiol. Genomics* **28**, 323–336 (2007).

62. Hollister, A., Okubara, P., Watson, J. G. & Chaykin, S. Reproduction in mice: liver enlargement in mice during pregnancy and lactation. *Life Sci.* **40**, 11–18 (1987).

63. Dai, G. *et al.* Maternal hepatic growth response to pregnancy in the mouse. *Exp. Biol. Med.* **236**, 1322–1332 (2011).

64. Goddard, E. T., Fischer, J. & Schedin, P. A Portal Vein Injection Model to Study Liver Metastasis of Breast Cancer. *J. Vis. Exp.* **2017/01/07**, (2016).

65. Ursini-Siegel, J. & Siegel, P. M. The influence of the pre-metastatic niche on breast cancer metastasis. *Cancer Lett.* **380**, 281–288 (2016).

66. Kaplan, R. N. *et al.* VEGFR1-positive haematopoietic bone marrow progenitors initiate the pre-metastatic niche. *Nature* **438**, 820–827 (2005).

67. Peinado, H. *et al.* Pre-metastatic niches: organ-specific homes for metastases. *Nat. Rev. Cancer* **17**, 302–317 (2017).

68. Psaila, B. & Lyden, D. The metastatic niche: adapting the foreign soil. *Nat. Rev. Cancer* **9**, 285–293 (2009).

69. Fidler, I. J. The pathogenesis of cancer metastasis: the “seed and soil” hypothesis revisited. *Nat. Rev. Cancer* **3**, 453–458 (2003).

70. Valastyan, S. & Weinberg, R. A. Tumor metastasis: molecular insights and evolving paradigms. *Cell* **147**, 275–292 (2011).

71. Costa-Silva, B. *et al.* Pancreatic cancer exosomes initiate pre-metastatic niche formation in the liver. *Nat. Cell Biol.* **17**, 816–826 (2015).

72. Nielsen, S. R. *et al.* Macrophage-secreted granulin supports pancreatic cancer metastasis by inducing liver fibrosis. *Nat. Cell Biol.* **18**, 549–560 (2016).

73. Lee, J. W. *et al.* Hepatocytes direct the formation of a pro-metastatic niche in the liver. *Nature* **567**, 249–252 (2019).

74. Kok, S. Y. *et al.* Malignant subclone drives metastasis of genetically and phenotypically heterogenous cell clusters through fibrotic niche generation. *Nat. Commun.* **12**, 863 (2021).

75. Hyatt, H. W., Zhang, Y., Hood, W. R. & Kavazis, A. N. Changes in Metabolism, Mitochondrial Function, and Oxidative Stress Between Female Rats Under Nonreproductive and 3 Reproductive Conditions. *Reprod. Sci.* **26**, 114–127 (2019).

76. Martinson, H. A., Jindal, S., Durand-Rougely, C., Borges, V. F. & Schedin, P. Wound healing-like immune program facilitates postpartum mammary gland involution and tumor progression. *Int. J. Cancer* **136**, 1803–1813 (2015).

77. Morris, V. L., Tuck, A. B., Wilson, S. M., Percy, D. & Chambers, A. F. Tumor progression and metastasis in murine D2 hyperplastic alveolar nodule mammary tumor cell lines. *Clin. Exp. Metastasis* **11**, 103–112 (1993).

78. Day, C. P. *et al.* "Glowing head" mice: a genetic tool enabling reliable preclinical image-based evaluation of cancers in immunocompetent allografts. *PLoS One* **9**, e109956 (2014).

79. van Dam, P. J. *et al.* International consensus guidelines for scoring the histopathological growth patterns of liver metastasis. *Br. J. Cancer* **117**, 1427–1441 (2017).

80. Tsujikawa, T. *et al.* Quantitative Multiplex Immunohistochemistry Reveals Myeloid-Inflamed Tumor-Immune Complexity Associated with Poor Prognosis. *Cell Rep.* **19**, 203–217 (2017).

81. Betts, C. B. *et al.* Mucosal Immunity in the Female Murine Mammary Gland. *J. Immunol.* **201**, 734–746 (2018).

82. Morris, V. L. *et al.* Mammary carcinoma cell lines of high and low metastatic potential differ not in extravasation but in subsequent migration and growth. *Clin. Exp. Metastasis* **12**, 357–367 (1994).

83. Kalluri, R. & Weinberg, R. A. The basics of epithelial-mesenchymal transition. *J. Clin. Invest.* **119**, 1420–1428 (2009).

84. Kaech, S. M., Wherry, E. J. & Ahmed, R. Effector and memory T-cell differentiation: implications for vaccine development. *Nat. Rev. Immunol.* **2**, 251–262 (2002).

85. Blank, C. & Mackensen, A. Contribution of the PD-L1/PD-1 pathway to T-cell exhaustion: an update on implications for chronic infections and tumor evasion. *Cancer Immunol. Immunother.* **56**, 739–745 (2007).

86. Khan, O. *et al.* TOX transcriptionally and epigenetically programs CD8(+) T cell exhaustion. *Nature* **571**, 211–218 (2019).

87. Borst, J., Ahrends, T., Babala, N., Melief, C. J. M. & Kastenmuller, W. CD4(+) T cell help in cancer immunology and immunotherapy. *Nat. Rev. Immunol.* **18**, 635–647 (2018).

88. Sheu, B. C. *et al.* Reversed CD4/CD8 ratios of tumor-infiltrating lymphocytes are correlated with the progression of human cervical carcinoma. *Cancer* **86**, 1537–1543 (1999).

89. Shah, W. *et al.* A reversed CD4/CD8 ratio of tumor-infiltrating lymphocytes and a high percentage of CD4(+)FOXP3(+) regulatory T cells are significantly associated with clinical outcome in squamous cell carcinoma of the cervix. *Cell. Mol. Immunol.* **8**, 59–66 (2011).

90. Steinman, R. M., Turley, S., Mellman, I. & Inaba, K. The induction of tolerance by dendritic cells that have captured apoptotic cells. *J. Exp. Med.* **191**, 411–416 (2000).

91. Erwig, L. P. & Henson, P. M. Immunological consequences of apoptotic cell phagocytosis. *Am. J. Pathol.* **171**, 2–8 (2007).

92. Jacob, L. S. *et al.* Metastatic Competence Can Emerge with Selection of Preexisting Oncogenic Alleles without a Need of New Mutations. *Cancer Res.* **75**, 3713–3719 (2015).

93. Nguyen, D. X. & Massague, J. Genetic determinants of cancer metastasis. *Nat. Rev. Genet.* **8**, 341–352 (2007).

94. Pereira, B. *et al.* The somatic mutation profiles of 2,433 breast cancers refines their genomic and transcriptomic landscapes. *Nat. Commun.* **7**, 11479 (2016).

95. Ursini-Siegel, J., Schade, B., Cardiff, R. D. & Muller, W. J. Insights from transgenic mouse models of ERBB2-induced breast cancer. *Nat. Rev. Cancer* **7**, 389–397 (2007).

96. Kruger, A. Premetastatic niche formation in the liver: emerging mechanisms and mouse models. *J. Mol. Med.* **93**, 1193–1201 (2015).

97. Van den Eynden, G. G. *et al.* The multifaceted role of the microenvironment in liver metastasis: biology and clinical implications. *Cancer Res.* **73**, 2031–2043 (2013).

98. Lee, J. W. & Beatty, G. L. Inflammatory networks cultivate cancer cell metastasis to the liver. *Cell Cycle* **19**, 642–651 (2020).

99. Eefsen, R. L. *et al.* Growth pattern of colorectal liver metastasis as a marker of recurrence risk. *Clin. Exp. Metastasis* **32**, 369–381 (2015).

100. Bohlok, A. *et al.* Histological growth pattern as a potential prognostic factor in patients operated for breast cancer liver metastases. *J. Clin. Oncol.* **37**, e12576–e12576 (2019).

101. Wu, P. H. *et al.* Evolution of cellular morpho-phenotypes in cancer metastasis. *Sci. Rep.* **5**, 18437 (2015).

102. Lyons, S. M. *et al.* Changes in cell shape are correlated with metastatic potential in murine and human osteosarcomas. *Biol. Open* **5**, 289–299 (2016).

103. Anderson, A. R., Weaver, A. M., Cummings, P. T. & Quaranta, V. Tumor morphology and phenotypic evolution driven by selective pressure from the microenvironment. *Cell* **127**, 905–915 (2006).

104. Hanahan, D. & Coussens, L. M. Accessories to the crime: functions of cells recruited to the tumor microenvironment. *Cancer Cell* **21**, 309–322 (2012).

105. Nagaharu, K. *et al.* Tenascin C induces epithelial-mesenchymal transition-like change accompanied by SRC activation and focal adhesion kinase phosphorylation in human breast cancer cells. *Am. J. Pathol.* **178**, 754–763 (2011).

106. Park, J. & Schwarzbauer, J. E. Mammary epithelial cell interactions with fibronectin stimulate epithelial-mesenchymal transition. *Oncogene* **33**, 1649–1657 (2014).

107. Polyak, K. & Weinberg, R. A. Transitions between epithelial and mesenchymal states: acquisition of malignant and stem cell traits. *Nat. Rev. Cancer* **9**, 265–273 (2009).

108. Akalay, I. *et al.* EMT impairs breast carcinoma cell susceptibility to CTL-mediated lysis through autophagy induction. *Autophagy* **9**, 1104–1106 (2013).

109. Kudo-Saito, C., Shirako, H., Takeuchi, T. & Kawakami, Y. Cancer metastasis is accelerated through immunosuppression during Snail-induced EMT of cancer cells. *Cancer Cell* **15**, 195–206 (2009).

110. Soundararajan, R. *et al.* Targeting the Interplay between Epithelial-to-Mesenchymal-Transition and the Immune System for Effective Immunotherapy. *Cancers* **11**, (2019).

111. Dongre, A. *et al.* Direct and Indirect Regulators of Epithelial-Mesenchymal Transition (EMT)-mediated Immunosuppression in Breast Carcinomas. *Cancer Discov.* **2020/12/18**, (2020).

112. Kienast, Y. *et al.* Real-time imaging reveals the single steps of brain metastasis formation. *Nat. Med.* **16**, 116–122 (2010).

113. Luzzi, K. J. *et al.* Multistep nature of metastatic inefficiency: dormancy of solitary cells after successful extravasation and limited survival of early micrometastases. *Am. J. Pathol.* **153**, 865–873 (1998).

114. Goddard, E. T. *et al.* Quantitative extracellular matrix proteomics to study mammary and liver tissue microenvironments. *Int. J. Biochem. Cell Biol.* **81**, 223–232 (2016).

115. Barkan, D. *et al.* Metastatic growth from dormant cells induced by a col-I-enriched fibrotic environment. *Cancer Res.* **70**, 5706–5716 (2010).

116. Høye, A. M. & Erler, J. T. Structural ECM components in the premetastatic and metastatic niche. *Am. J. Physiol. Cell Physiol.* **310**, C955-67 (2016).

117. Oskarsson, T. *et al.* Breast cancer cells produce tenascin C as a metastatic niche component to colonize the lungs. *Nat. Med.* **17**, 867–874 (2011).

118. Winkler, J., Abisoye-Ogunniyan, A., Metcalf, K. J. & Werb, Z. Concepts of extracellular matrix remodelling in tumour progression and metastasis. *Nat. Commun.* **11**, 5120 (2020).

119. Kai, F., Drain, A. P. & Weaver, V. M. The Extracellular Matrix Modulates the Metastatic Journey. *Dev. Cell* **49**, 332–346 (2019).

120. Brodt, P. Role of the Microenvironment in Liver Metastasis: From Pre- to Prometastatic Niches. *Clin. Cancer Res.* **22**, 5971–5982 (2016).

121. Coffelt, S. B. *et al.* IL-17-producing gammadelta T cells and neutrophils conspire to promote breast cancer metastasis. *Nature* **522**, 345–348 (2015).

122. Lee, J. C. *et al.* Regulatory T cell control of systemic immunity and immunotherapy response in liver metastasis. *Sci Immunol* **5**, (2020).

123. Kitamura, T., Qian, B. Z. & Pollard, J. W. Immune cell promotion of metastasis. *Nat. Rev. Immunol.* **15**, 73–86 (2015).

124. Gonzalez N, A. *et al.* Apoptotic cells promote their own clearance and immune tolerance through activation of the nuclear receptor LXR. *Immunity* **31**, 245–258 (2009).

125. Gordon-Weeks, A. & Yuzhalin, A. E. Cancer Extracellular Matrix Proteins Regulate Tumour Immunity. *Cancers* **12**, (2020).

126. Jachetti, E. *et al.* Tenascin-C Protects Cancer Stem-like Cells from Immune Surveillance by Arresting T-cell Activation. *Cancer Res.* **75**, 2095–2108 (2015).

127. Galon, J. *et al.* Type, density, and location of immune cells within human colorectal tumors predict clinical outcome. *Science* **313**, 1960–1964 (2006).

128. Zhang, L. *et al.* Intratumoral T cells, recurrence, and survival in epithelial ovarian cancer. *N. Engl. J. Med.* **348**, 203–213 (2003).

129. Shao, C. *et al.* Prognosis of pregnancy-associated breast cancer: a meta-analysis. *BMC Cancer* **20**, 746 (2020).

130. Bartlett, A. Q. *et al.* Pregnancy and weaning regulate human maternal liver size and function. *bioRxiv* 2021.02.18.431862 (2021).

131. Catalano, P. M. *et al.* Longitudinal changes in basal hepatic glucose production and suppression during insulin infusion in normal pregnant women. *Am. J. Obstet. Gynecol.* **167**, 913–919 (1992).

132. Herrera, E. Metabolic adaptations in pregnancy and their implications for the availability of substrates to the fetus. *Eur. J. Clin. Nutr.* **54 Suppl 1**, S47-51 (2000).

133. Guy, J. & Peters, M. G. Liver disease in women: the influence of gender on epidemiology, natural history, and patient outcomes. *Gastroenterol. Hepatol.* **9**, 633–639 (2013).

134. Bartlett, A. Q., Pennock, N. D., Klug, A. & Schedin, P. Immune Milieu Established by Postpartum Liver Involution Promotes Breast Cancer Liver Metastasis. *Cancers* **13**, 1698 (2021).

135. Perandini, S., Faccioli, N., Inama, M. & Pozzi Mucelli, R. Freehand liver volumetry by using an electromagnetic pen tablet: accuracy, precision, and rapidity. *J. Digit. Imaging* **24**, 360–365 (2011).

136. van Raaij, J. M., Peek, M. E., Vermaat-Miedema, S. H., Schonk, C. M. & Hautvast, J. G. New equations for estimating body fat mass in pregnancy from body density or total body water. *Am. J. Clin. Nutr.* **48**, 24–29 (1988).

137. Marshall, N. E. *et al.* Comparison of multiple methods to measure maternal fat mass in late gestation. *Am. J. Clin. Nutr.* **103**, 1055–1063 (2016).

138. Gorgolewski, K. *et al.* Nipype: a flexible, lightweight and extensible neuroimaging data processing framework in Python 0.13.1. *Zenodo* (2017).

139. Avants, B. B., Tustison, N. & Song, G. *Advanced normalization tools (ANTS)*. (Insight j, 2:1[35], 2009).

140. McCormick, M., Liu, X., Jomier, J., Marion, C. & Ibanez, L. ITK: enabling reproducible research and open science. *Front. Neuroinform.* **8**, 13 (2014).

141. van der Walt, S. *et al.* scikit-image: image processing in Python. *PeerJ* **2**, e453 (2014).

142. Pedregosa, F. *et al.* Scikit-learn: Machine learning in Python. *J. Mach. Learn. Res.* **12**, 2825–2830 (2011).

143. Jones, E., Oliphant, T. & Peterson, P. SciPy: Open Source Scientific Tools for Python. (2001).

144. Alvarez, L., Baumela, L., Henriquez, P. & Marquez-Neila, P. *Morphological snakes*. (2010).

145. Kirwan, J. P., Huston-Presley, L., Kalhan, S. C. & Catalano, P. M. Clinically useful estimates of insulin sensitivity during pregnancy: validation studies in women with normal glucose tolerance and gestational diabetes mellitus. *Diabetes Care* **24**, 1602–1607 (2001).

146. Catalano, P. M. *et al.* Carbohydrate metabolism during pregnancy in control subjects and women with gestational diabetes. *Am. J. Physiol.* **264**, E60-7 (1993).

147. Steele, R. Influences of glucose loading and of injected insulin on hepatic glucose output. *Ann. N. Y. Acad. Sci.* **82**, 420–430 (1959).

148. Black, P. R., Brooks, D. C., Bessey, P. Q., Wolfe, R. R. & Wilmore, D. W. Mechanisms of insulin resistance following injury. *Ann. Surg.* **196**, 420–435 (1982).

149. Calkins, K. L. *et al.* Intravenous Fish Oil and Pediatric Intestinal Failure-Associated Liver Disease: Changes in Plasma Phytosterols, Cytokines, and Bile Acids and Erythrocyte Fatty Acids. *JPEN J. Parenter. Enteral Nutr.* **42**, 633–641 (2018).

150. Guo, Q. *et al.* Physiologically activated mammary fibroblasts promote postpartum mammary cancer. *JCI Insight* **2**, e89206 (2017).

151. Michalopoulos, G. K. Hepatostat: Liver regeneration and normal liver tissue maintenance. *Hepatology* **65**, 1384–1392 (2017).

152. In *Weight Gain During Pregnancy: Reexamining the Guidelines* (eds. Rasmussen, K. M. & Yaktine, A. L.) (2009).

153. Carvalho, J. R. & Verdelho Machado, M. New Insights About Albumin and Liver Disease. *Ann. Hepatol.* **17**, 547–560 (2018).

154. Gerich, J. E. Role of the kidney in normal glucose homeostasis and in the hyperglycaemia of diabetes mellitus: therapeutic implications. *Diabet. Med.* **27**, 136–142 (2010).

155. Hytten, F. Blood volume changes in normal pregnancy. *Clin. Haematol.* **14**, 601–612 (1985).

156. Huang, W. *et al.* Nuclear receptor-dependent bile acid signaling is required for normal liver regeneration. *Science* **312**, 233–236 (2006).

157. Milona, A. *et al.* Raised hepatic bile acid concentrations during pregnancy in mice are associated with reduced farnesoid X receptor function. *Hepatology* **52**, 1341–1349 (2010).

158. Wu, X. *et al.* FGF19-induced hepatocyte proliferation is mediated through FGFR4 activation. *J. Biol. Chem.* **285**, 5165–5170 (2010).

159. Inagaki, T. *et al.* Fibroblast growth factor 15 functions as an enterohepatic signal to regulate bile acid homeostasis. *Cell Metab.* **2**, 217–225 (2005).

160. Galman, C., Arvidsson, I., Angelin, B. & Rudling, M. Monitoring hepatic cholesterol 7alpha-hydroxylase activity by assay of the stable bile acid intermediate 7alpha-hydroxy-4-cholesten-3-one in peripheral blood. *J. Lipid Res.* **44**, 859–866 (2003).

161. Huang, J. & Rudnick, D. A. Elucidating the metabolic regulation of liver regeneration. *Am. J. Pathol.* **184**, 309–321 (2014).

162. Naugler, W. E. *et al.* Fibroblast Growth Factor Signaling Controls Liver Size in Mice With Humanized Livers. *Gastroenterology* **149**, 728–40 e15 (2015).

163. Naugler, W. E. Bile acid flux is necessary for normal liver regeneration. *PLoS One* **9**, e97426 (2014).

164. Westbrook, R. H., Dusheiko, G. & Williamson, C. Pregnancy and liver disease. *J. Hepatol.* **64**, 933–945 (2016).

165. Saudan, P., Brown, M. A., Buddle, M. L. & Jones, M. Does gestational hypertension become pre-eclampsia? *Br. J. Obstet. Gynaecol.* **105**, 1177–1184 (1998).

166. Hutcheon, J. A., Lisonkova, S. & Joseph, K. S. Epidemiology of pre-eclampsia and the other hypertensive disorders of pregnancy. *Best Pract. Res. Clin. Obstet. Gynaecol.* **25**, 391–403 (2011).

167. Barker, D. J. & Thornburg, K. L. The obstetric origins of health for a lifetime. *Clin. Obstet. Gynecol.* **56**, 511–519 (2013).

168. Barker, D. J. The origins of the developmental origins theory. *J. Intern. Med.* **261**, 412–417 (2007).

169. Fleming, T. P. *et al.* Origins of lifetime health around the time of conception: causes and consequences. *Lancet* **391**, 1842–1852 (2018).

170. Stein, T., Salomonis, N. & Gusterson, B. A. Mammary gland involution as a multi-step process. *J. Mammary Gland Biol. Neoplasia* **12**, 25–35 (2007).

171. Janerich, D. T. & Hoff, M. B. Evidence for a crossover in breast cancer risk factors. *Am. J. Epidemiol.* **116**, 737–742 (1982).

172. Lambe, M. *et al.* Transient increase in the risk of breast cancer after giving birth. *N. Engl. J. Med.* **331**, 5–9 (1994).

173. Lonardo, A. *et al.* Sex Differences in Nonalcoholic Fatty Liver Disease: State of the Art and Identification of Research Gaps. *Hepatology* **70**, 1457–1469 (2019).

174. Wagnerberger, S. *et al.* Sex-specific differences in the development of acute alcohol-induced liver steatosis in mice. *Alcohol Alcohol* **48**, 648–656 (2013).

175. Paget, S. THE DISTRIBUTION OF SECONDARY GROWTHS IN CANCER OF THE BREAST. *Lancet* **133**, 571–573 (1889).

176. Redig, A. J. & McAllister, S. S. Breast cancer as a systemic disease: a view of metastasis. *J. Intern. Med.* **274**, 113–126 (2013).

177. Gomis, R. R. & Gawrzak, S. Tumor cell dormancy. *Mol. Oncol.* **11**, 62–78 (2017).

178. Harper, K. L. *et al.* Mechanism of early dissemination and metastasis in Her2+ mammary cancer. *Nature* vol. 540 588–592 (2016).

179. Hüsemann, Y. *et al.* Systemic spread is an early step in breast cancer. *Cancer Cell* **13**, 58–68 (2008).

180. Hosseini, H. *et al.* Early dissemination seeds metastasis in breast cancer. *Nature* **540**, 552–558 (2016).

181. Yang, Y. *et al.* Immunocompetent mouse allograft models for development of therapies to target breast cancer metastasis. *Oncotarget* **8**, 30621–30643 (2017).

182. DeRose, Y. S. *et al.* Tumor grafts derived from women with breast cancer authentically reflect tumor pathology, growth, metastasis and disease outcomes. *Nat. Med.* **17**, 1514–1520 (2011).

183. Fantozzi, A. & Christofori, G. Mouse models of breast cancer metastasis. *Breast Cancer Res.* **8**, 212 (2006).

184. Xiao, W. *et al.* Breast cancer subtypes and the risk of distant metastasis at initial diagnosis: a population-based study. *Cancer Manag. Res.* **10**, 5329–5338 (2018).

185. Soni, A. *et al.* Breast cancer subtypes predispose the site of distant metastases. *Am. J. Clin. Pathol.* **143**, 471–478 (2015).

186. Gong, Y., Liu, Y.-R., Ji, P., Hu, X. & Shao, Z.-M. Impact of molecular subtypes on metastatic breast cancer patients: a SEER population-based study. *Sci. Rep.* **7**, 45411 (2017).

187. Ji, L. *et al.* Risk and prognostic factors of breast cancer with liver metastases. *BMC Cancer* **21**, 238 (2021).

188. Erin, N. *et al.* Altered gene expression in breast cancer liver metastases. *Int. J. Cancer* **124**, 1503–1516 (2009).

189. Tabariès, S. *et al.* Claudin-2 is selectively enriched in and promotes the formation of breast cancer liver metastases through engagement of integrin complexes. *Oncogene* **30**, 1318–1328 (2011).

190. Ma, R. *et al.* Mechanisms involved in breast cancer liver metastasis. *J. Transl. Med.* **13**, 64 (2015).

191. Auguste, P. *et al.* The host inflammatory response promotes liver metastasis by increasing tumor cell arrest and extravasation. *Am. J. Pathol.* **170**, 1781–1792 (2007).

192. Khatib, A.-M., Fallavollita, L., Wancewicz, E. V., Monia, B. P. & Brodt, P. Inhibition of hepatic endothelial E-selectin expression by C-raf antisense oligonucleotides blocks colorectal carcinoma liver metastasis. *Cancer Res.* **62**, 5393–5398 (2002).

193. Tabariès, S. *et al.* Granulocytic immune infiltrates are essential for the efficient formation of breast cancer liver metastases. *Breast Cancer Res.* **17**, 45 (2015).

194. Vaniotis, G. *et al.* Collagen IV-conveyed signals can regulate chemokine production and promote liver metastasis. *Oncogene* **37**, 3790–3805 (2018).

195. Tauriello, D. V. F. *et al.* TGFβ drives immune evasion in genetically reconstituted colon cancer metastasis. *Nature* **554**, 538–543 (2018).

196. Lu, X., Lu, D., Scully, M. & Kakkar, V. The role of integrins in cancer and the development of anti-integrin therapeutic agents for cancer therapy. *Perspect. Medicin. Chem.* **2**, 57–73 (2008).

197. Gilmore, A. P. Anoikis. *Cell Death Differ.* **12 Suppl 2**, 1473–1477 (2005).

198. Guadamillas, M. C., Cerezo, A. & Del Pozo, M. A. Overcoming anoikis--pathways to anchorage-independent growth in cancer. *J. Cell Sci.* **124**, 3189–3197 (2011).

199. Pickup, M. W., Mouw, J. K. & Weaver, V. M. The extracellular matrix modulates the hallmarks of cancer. *EMBO Rep.* **15**, 1243–1253 (2014).

200. Maity, G. *et al.* Culture of human breast cancer cell line (MDA-MB-231) on fibronectin-coated surface induces pro-matrix metalloproteinase-9 expression and activity. *Tumour Biol.* **32**, 129–138 (2011).

201. Barbazán, J. *et al.* Liver Metastasis Is Facilitated by the Adherence of Circulating Tumor Cells to Vascular Fibronectin Deposits. *Cancer Res.* **77**, 3431–3441 (2017).

202. Sun, Z. *et al.* Tenascin-C increases lung metastasis by impacting blood vessel invasions. *Matrix Biol.* **83**, 26–47 (2019).

203. Wennerberg, A. E., Nalesnik, M. A. & Coleman, W. B. Hepatocyte paraffin 1: a monoclonal antibody that reacts with hepatocytes and can be used for differential diagnosis of hepatic tumors. *Am. J. Pathol.* **143**, 1050–1054 (1993).

204. Portincasa, P. *et al.* Water handling and aquaporins in bile formation: recent advances and research trends. *J. Hepatol.* **39**, 864–874 (2003).

205. Kouros-Mehr, H., Slorach, E. M., Sternlicht, M. D. & Werb, Z. GATA-3 maintains the differentiation of the luminal cell fate in the mammary gland. *Cell* **127**, 1041–1055 (2006).

206. Miettinen, M. *et al.* GATA3: a multispecific but potentially useful marker in surgical pathology: a systematic analysis of 2500 epithelial and nonepithelial tumors. *Am. J. Surg. Pathol.* **38**, 13–22 (2014).

207. Asch-Kendrick, R. & Cimino-Mathews, A. The role of GATA3 in breast carcinomas: a review. *Hum. Pathol.* **48**, 37–47 (2016).

208. Tozbikian, G. H. & Zynger, D. L. A combination of GATA3 and SOX10 is useful for the diagnosis of metastatic triple-negative breast cancer. *Hum. Pathol.* **85**, 221–227 (2019).

209. Shaoxian, T. *et al.* Characterisation of GATA3 expression in invasive breast cancer: differences in histological subtypes and immunohistochemically defined molecular subtypes. *J. Clin. Pathol.* **70**, 926–934 (2017).

210. McCleskey, B. C. *et al.* GATA3 expression in advanced breast cancer: prognostic value and organ-specific relapse. *Am. J. Clin. Pathol.* **144**, 756–763 (2015).

211. Böcker, W. *et al.* Common adult stem cells in the human breast give rise to glandular and myoepithelial cell lineages: a new cell biological concept. *Lab. Invest.* **82**, 737–746 (2002).

212. Abd El-Rehim, D. M. *et al.* Expression of luminal and basal cytokeratins in human breast carcinoma. *J. Pathol.* **203**, 661–671 (2004).

213. Kutasovic, J. R. *et al.* Breast cancer metastasis to gynaecological organs: a clinico-pathological and molecular profiling study. *Hip Int.* **5**, 25–39 (2019).

214. De Lara, S., Parris, T. Z., Werner Rönnerman, E., Helou, K. & Kovács, A. GATA3 as a putative marker of breast cancer metastasis-A retrospective immunohistochemical study. *Breast J.* **24**, 184–188 (2018).

215. Schrijver, W. A. M. E. *et al.* Receptor Conversion in Distant Breast Cancer Metastases: A Systematic Review and Meta-analysis. *J. Natl. Cancer Inst.* **110**, 568–580 (2018).

216. Rakha, E. A. *et al.* Breast cancer prognostic classification in the molecular era: the role of histological grade. *Breast Cancer Res.* **12**, 207 (2010).

217. Centeno, B. A. Pathology of liver metastases. *Cancer Control* **13**, 13–26 (2006).

218. Bertucci, F., Finetti, P. & Birnbaum, D. Basal breast cancer: a complex and deadly molecular subtype. *Curr. Mol. Med.* **12**, 96–110 (2012).

219. Alshareeda, A. T. *et al.* Characteristics of basal cytokeratin expression in breast cancer. *Breast Cancer Res. Treat.* **139**, 23–37 (2013).

220. Kimbung, S. *et al.* Claudin-2 is an independent negative prognostic factor in breast cancer and specifically predicts early liver recurrences. *Mol. Oncol.* **8**, 119–128 (2014).

221. Ruiz, A. *et al.* Long-term survival and cure model following liver resection for breast cancer metastases. *Breast Cancer Res. Treat.* **170**, 89–100 (2018).

222. Mariani, P. *et al.* Liver metastases from breast cancer: Surgical resection or not? A case-matched control study in highly selected patients. *Eur. J. Surg. Oncol.* **39**, 1377–1383 (2013).

223. Nordlinger, B. *et al.* Perioperative FOLFOX4 chemotherapy and surgery versus surgery alone for resectable liver metastases from colorectal cancer (EORTC 40983): long-term results of a randomised, controlled, phase 3 trial. *Lancet Oncol.* **14**, 1208–1215 (2013).

224. Vermeulen, P. B. *et al.* Liver metastases from colorectal adenocarcinomas grow in three patterns with different angiogenesis and desmoplasia. *J. Pathol.* **195**, 336–342 (2001).

225. Frentzas, S. *et al.* Vessel co-option mediates resistance to anti-angiogenic therapy in liver metastases. *Nat. Med.* **22**, 1294–1302 (2016).

226. Kimbung, S. *et al.* Transcriptional Profiling of Breast Cancer Metastases Identifies Liver Metastasis-Selective Genes Associated with Adverse Outcome in Luminal A Primary Breast Cancer. *Clin. Cancer Res.* **22**, 146–157 (2016).

227. Conklin, M. W. *et al.* Aligned collagen is a prognostic signature for survival in human breast carcinoma. *Am. J. Pathol.* **178**, 1221–1232 (2011).

228. Ma, C. *et al.* Gut microbiome-mediated bile acid metabolism regulates liver cancer via NKT cells. *Science* **360**, (2018).

229. Wershof, E. *et al.* A FIJI macro for quantifying pattern in extracellular matrix. *Life Sci Alliance* **4**, (2021).

230. Gutcher, I. & Becher, B. APC-derived cytokines and T cell polarization in autoimmune inflammation. *J. Clin. Invest.* **117**, 1119–1127 (2007).

231. Collins, M., Ling, V. & Carreno, B. M. The B7 family of immune-regulatory ligands. *Genome Biol.* **6**, 223 (2005).

232. Björck, P., Beilhack, A., Herman, E. I., Negrin, R. S. & Engleman, E. G. Plasmacytoid dendritic cells take up opsonized antigen leading to CD4+ and CD8+ T cell activation in vivo. *J. Immunol.* **181**, 3811–3817 (2008).

233. Horst, A. K., Neumann, K., Diehl, L. & Tiegs, G. Modulation of liver tolerance by conventional and nonconventional antigen-presenting cells and regulatory immune cells. *Cell. Mol. Immunol.* **13**, 277–292 (2016).

234. Martinez-Sanchez, M. E., Huerta, L., Alvarez-Buylla, E. R. & Villarreal Luján, C. Role of Cytokine Combinations on CD4+ T Cell Differentiation, Partial Polarization, and Plasticity: Continuous Network Modeling Approach. *Front. Physiol.* **9**, 877 (2018).

235. Pennock, N. D. *et al.* T cell responses: naive to memory and everything in between. *Adv. Physiol. Educ.* **37**, 273–283 (2013).

236. Lou, Y. *et al.* Epithelial-Mesenchymal Transition Is Associated with a Distinct Tumor Microenvironment Including Elevation of Inflammatory Signals and Multiple Immune Checkpoints in Lung Adenocarcinoma. *Clin. Cancer Res.* **22**, 3630–3642 (2016).

237. Kubo, H., Mensurado, S., Gonçalves-Sousa, N., Serre, K. & Silva-Santos, B. Primary Tumors Limit Metastasis Formation through Induction of IL15-Mediated Cross-Talk between Patrolling Monocytes and NK Cells. *Cancer Immunol Res* **5**, 812–820 (2017).

238. Wang, W. *et al.* Interleukin-15 suppresses gastric cancer liver metastases by enhancing natural killer cell activity in a murine model. *Oncol. Lett.* **16**, 4839–4846 (2018).

239. Kong, X., Kong, Y., Zhang, F., Wang, T. & Yan, J. Evaluating the effectiveness and safety of ursodeoxycholic acid in treatment of intrahepatic cholestasis of pregnancy: A meta-analysis (a prisma-compliant study). *Medicine* **95**, e4949 (2016).

240. Staels, B. & Kuipers, F. Bile acid sequestrants and the treatment of type 2 diabetes mellitus. *Drugs* **67**, 1383–1392 (2007).

241. Chen, Y. *et al.* Estrogen and Estrogen Receptor-α-Mediated Transrepression of Bile Salt Export Pump. *Mol. Endocrinol.* **29**, 613–626 (2015).

242. Salmaninejad, A. *et al.* PD-1/PD-L1 pathway: Basic biology and role in cancer immunotherapy. *J. Cell. Physiol.* **234**, 16824–16837 (2019).

243. Bilen, M. A. *et al.* Sites of metastasis and association with clinical outcome in advanced stage cancer patients treated with immunotherapy. *BMC Cancer* **19**, 857 (2019).

244. Topalian, S. L. *et al.* Five-Year Survival and Correlates Among Patients With Advanced Melanoma, Renal Cell Carcinoma, or Non-Small Cell Lung Cancer Treated With Nivolumab. *JAMA Oncol* (2019) doi:10.1001/jamaoncol.2019.2187.

245. Yu, J. *et al.* Liver metastasis restrains immunotherapy efficacy via macrophage-mediated T cell elimination. *Nat. Med.* **27**, 152–164 (2021).

246. Gao, B. Basic liver immunology. *Cell. Mol. Immunol.* **13**, 265–266 (2016).

247. Shi, F.-D., Ljunggren, H.-G., La Cava, A. & Van Kaer, L. Organ-specific features of natural killer cells. *Nat. Rev. Immunol.* **11**, 658–671 (2011).

248. Hannun, Y. A. & Obeid, L. M. Principles of bioactive lipid signalling: lessons from sphingolipids. *Nat. Rev. Mol. Cell Biol.* **9**, 139–150 (2008).

249. Sargeant, T. J. *et al.* Stat3 controls cell death during mammary gland involution by regulating uptake of milk fat globules and lysosomal membrane permeabilization. *Nat. Cell Biol.* **16**, 1057–1068 (2014).

250. Magtanong, L., Ko, P. J. & Dixon, S. J. Emerging roles for lipids in non-apoptotic cell death. *Cell Death Differ.* **23**, 1099–1109 (2016).

251. Glass, C. K. & Olefsky, J. M. Inflammation and lipid signaling in the etiology of insulin resistance. *Cell Metab.* **15**, 635–645 (2012).

252. Al-Khami, A. A. *et al.* Exogenous lipid uptake induces metabolic and functional reprogramming of tumor-associated myeloid-derived suppressor cells. *Oncoimmunology* **6**, e1344804 (2017).

253. Veglia, F. *et al.* Fatty acid transport protein 2 reprograms neutrophils in cancer. *Nature* **569**, 73–78 (2019).

254. Zhao, T., Du, H., Blum, J. S. & Yan, C. Critical role of PPARγ in myeloid-derived suppressor cell-stimulated cancer cell proliferation and metastasis. *Oncotarget* **7**, 1529–1543 (2016).

255. Marti, A., Feng, Z., Altermatt, H. J. & Jaggi, R. Milk accumulation triggers apoptosis of mammary epithelial cells. *Eur. J. Cell Biol.* **73**, 158–165 (1997).

256. Ricciotti, E. & FitzGerald, G. A. Prostaglandins and inflammation. *Arterioscler. Thromb. Vasc. Biol.* **31**, 986–1000 (2011).

257. Heid, H. *et al.* Lipid droplets, perilipins and cytokeratins--unravelled liaisons in epithelium-derived cells. *PLoS One* **8**, e63061 (2013).

258. Heid, H. W., Moll, R., Schwetlick, I., Rackwitz, H. R. & Keenan, T. W. Adipophilin is a specific marker of lipid accumulation in diverse cell types and diseases. *Cell Tissue Res.* **294**, 309–321 (1998).